



OTS PRICE

XEROX

\$

10.10 per

MICROFILM

\$

4.04 per

development

components

research

systems

manufacture

instruments

**BARNES ENGINEERING COMPANY**

**30 Commerce Road**

**Stamford, Connecticut**

N 64 12397

Prepared For

JET PROPULSION LABORATORY  
PASADENA, CALIFORNIA

JPL Contract No. 950470  
under NASA NAS 7-100

This work was performed for the Jet Propulsion Laboratory,  
California Institute of Technology, sponsored by the  
National Aeronautics and Space Administration under  
Contract NAS7-100.

FINAL TECHNICAL REPORT

PHASE I

LUNAR AND PLANETARY HORIZON SENSOR

Prepared By:

*Monty M. Merlen*

Monty M. Merlen  
Project Engineer

Approved By:

*Eli Kallet*

Eli Kallet, Manager  
Space Systems

*Norman J. Johnson*

Norman J. Johnson  
Project Consultant

*Robert W. Astheimer*

Robert W. Astheimer, Chief Engineer  
Development Engineering Department

Date: June 25, 1963

## TABLE OF CONTENTS

<u>Section</u>		<u>Page</u>
1.0	INTRODUCTION . . . . .	1-1
2.0	GENERAL DESCRIPTION . . . . .	2-1
	2.1 EXTERNAL CONFIGURATION . . . . .	2-1
	2.2 SCAN GEOMETRY . . . . .	2-1
	2.3 SIGNAL PROCESSING . . . . .	2-4
	2.4 LOGIC FUNCTIONS . . . . .	2-9
	2.5 RADIATION RESPONSE . . . . .	2-11
	2.6 ENVIRONMENTAL CAPABILITY . . . . .	2-15
3.0	SYSTEM OPTICS . . . . .	3-1
	3.1 OPTICAL DESIGN . . . . .	3-1
	3.2 APERTURE . . . . .	3-1
	3.3 WINDOW . . . . .	3-6
	3.4 MIRROR . . . . .	3-6
	3.5 PHOTOCOMMUTATOR . . . . .	3-10
	3.6 THERMOPILE DETECTORS . . . . .	3-10
4.0	MECHANICAL DESIGN . . . . .	4-1
	4.1 SENSOR HEAD . . . . .	4-1
	4.2 OPTICAL ASSEMBLY . . . . .	4-1
	4.3 COMMUTATOR SECTION . . . . .	4-4
	4.4 PRINTED CIRCUIT ASSEMBLIES . . . . .	4-7
	4.5 OFFSET REFERENCE SOURCE . . . . .	4-11
	4.6 THERMAL ANALYSIS . . . . .	4-11
5.0	ELECTRONICS . . . . .	5-1
	5.1 MASTER CLOCK OSCILLATOR . . . . .	5-1
	5.2 RING MULTIVIBRATOR . . . . .	5-1
	5.3 SIGNAL PROCESSING CHANNEL . . . . .	5-4
	5.4 COMMUTATOR . . . . .	5-8
	5.5 SIGNAL AMPLIFIER DESCRIPTION . . . . .	5-15
	5.6 OFFSET SOURCE DRIVE CIRCUIT . . . . .	5-26
	5.7 THRESHOLD CIRCUIT AND ZERO-ONE INPUT . . . . .	5-30
	5.8 ATTITUDE PROCESSING LOGIC . . . . .	5-36
	5.9 ATTITUDE ZEROING DRIVE . . . . .	5-36
	5.10 ATTITUDE READOUT CIRCUIT . . . . .	5-36
	5.11 ALTITUDE PROCESSING LOGIC . . . . .	5-36
	5.12 ALTITUDE RUNUP ZEROING DRIVE MULTIVIBRATOR . . . . .	5-43

<u>Section</u>	<u>Page</u>
5.13 ALTITUDE READOUT CIRCUIT . . . . .	5-43
5.14 ALARM OUTPUT . . . . .	5-43
5.15 ALARM OUTPUT CIRCUIT . . . . .	5-47
5.16 ELECTRONICS RELIABILITY . . . . .	5-47
6.0 CONCLUSION . . . . .	6-1
6.1 GENERAL SPECIFICATION . . . . .	6-1
6.2 SYSTEM TESTING . . . . .	6-4
6.3 ANALOGUE INTERPOLATION . . . . .	6-4
6.4 PROBLEM AREAS . . . . .	6-6
6.5 FEASIBILITY . . . . .	6-7

## APPENDIX I — THERMAL ANALYSIS

## BIBLIOGRAPHY

Section 1.0 INTRODUCTION

This document is the Final Technical Report for Phase I of JPL Contract 950470, as described in Article 1.a.4.i of the Statement of Work. The goal of Phase I was to define optical, mechanical, electronic, and detector parameters of the Lunar and Planetary Horizon Sensor (LPHS) in accordance with JPL Specification 2960.

## Section 2.0 GENERAL DESCRIPTION

### 2.1 EXTERNAL CONFIGURATION

The system consists of four cubical scanning heads and a smaller electronics package. The heads can be mounted separately or in combination, with interconnecting cables between the heads and the electronic module. The mounting configuration will not be worked out until Phase III of the program.

Figure 2-1 shows the external view of a scanning head. On the vehicle, each head must have an unobstructed view through a  $90^\circ$  arc as shown. The heads are aligned to within  $0.05^\circ$  of the vehicle vertical by rotation in the x-y plane. Alignment in the other planes is less critical and should be kept within  $1.0^\circ$  of the vehicle axis.

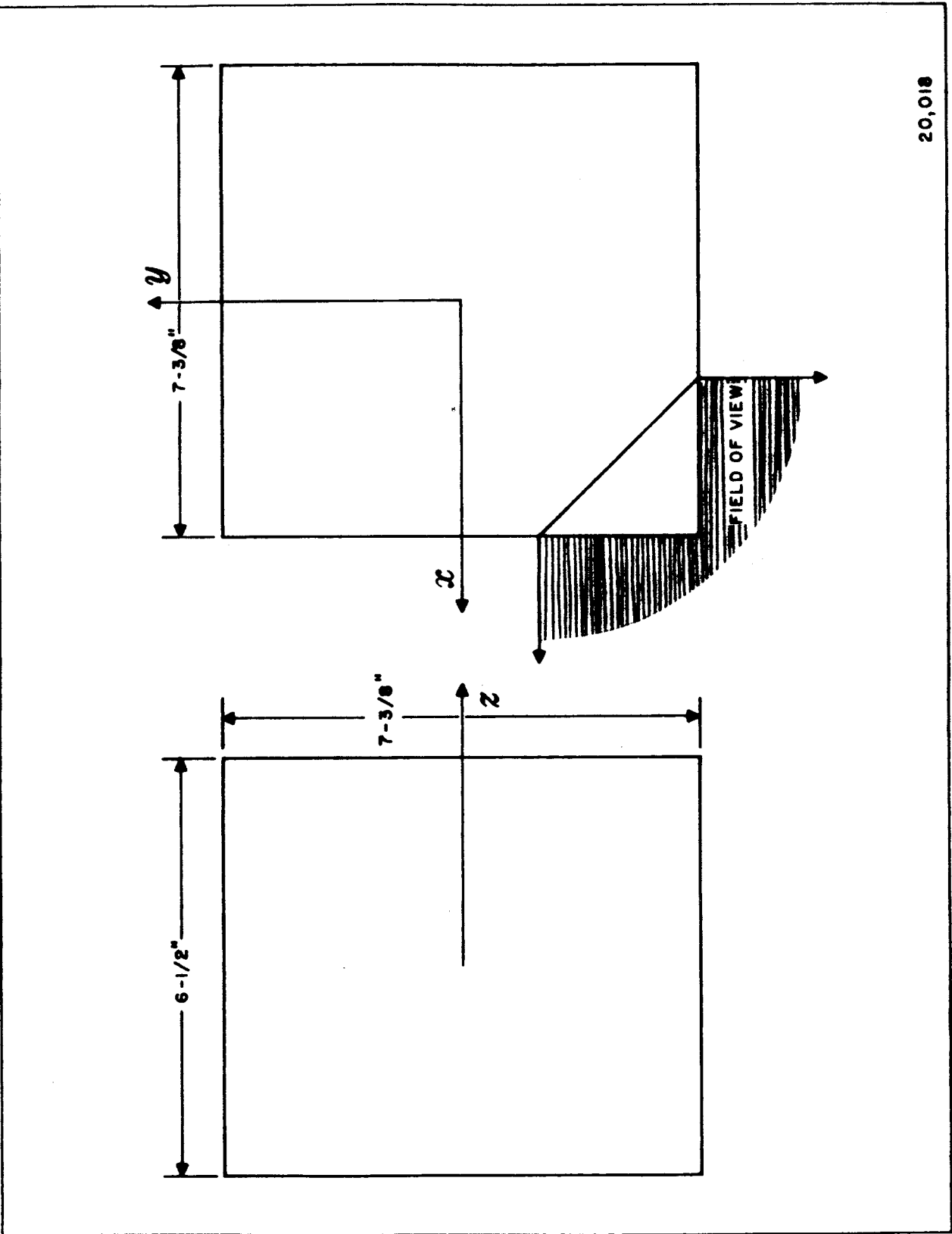
The heads are designed to function correctly with severe thermal gradients present, but low absorptivity external surfaces will insure optimum performance, especially on sunward missions.

Each head weighs about 6 pounds, making the system weigh 25 pounds including the electronic module. Maximum total power required is 3.5 watts of the specified available 104 volt peak to peak, 2400 cycle power and 5.5 watts of the +28 volt power, making a total of 9 watts when operating in space. For laboratory testing in air, the +28 volt power increases to make maximum total power about 15 watts.

### 2.2 SCAN GEOMETRY

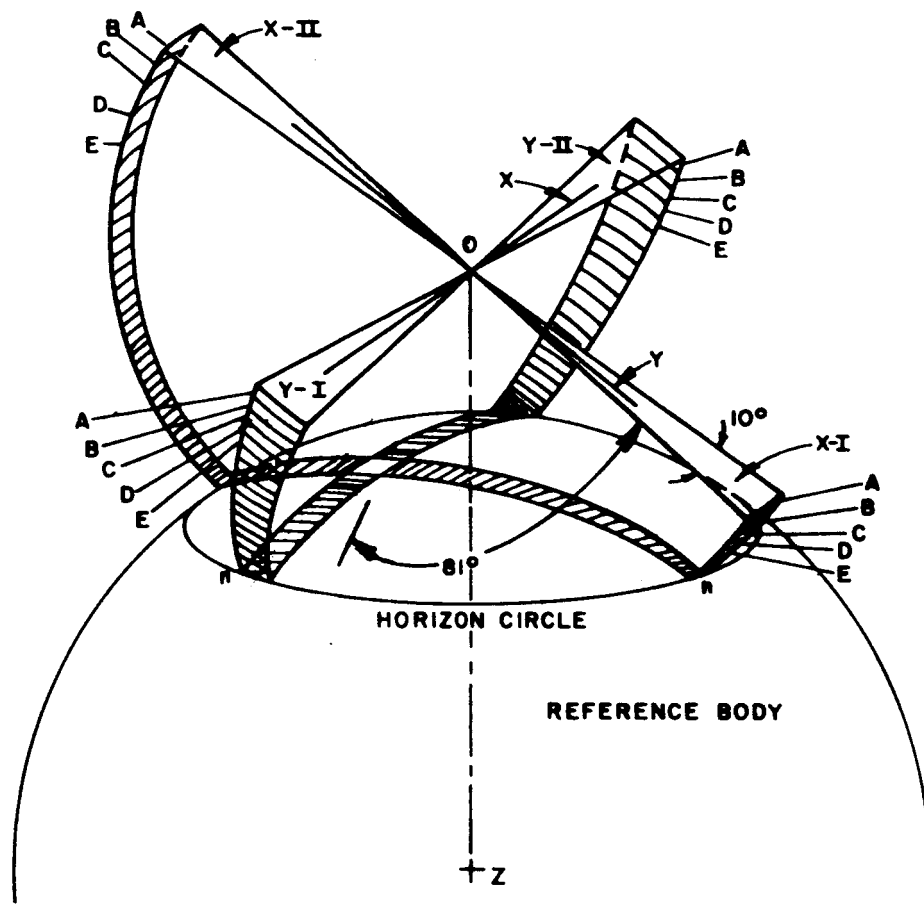
The complete LPHS system utilizes four optical heads arranged orthogonally. The radiation from space and earth passes through a silicon window in each head with a 14 micron turn-on filter coating, and is focused by means of a spherical mirror onto the 90 detector array. The entrance aperture and mirror comprise a Schmidt wide angle optical system. At the focal plane of each collecting mirror is an array of 90 thermopiles, and their fields of view are shown in Figure 2-2.

The LPHS is intended to provide two-axis local vertical position error signals and apparent angular diameter information when used on the following



20,018

Figure 2-1 SENSOR HEAD, OUTLINE DRAWING



20,019

Figure 2-2 SCAN CONFIGURATION



reference bodies: the Moon, Mars, Venus, and the Earth. This is accomplished by electronically scanning the celestial body in the far infrared, proceeding from space to earth. Horizon edge position information is obtained from each of four scanning heads, and is subsequently processed to determine attitude and altitude.

Figure 2-2 shows the scanning configuration in a typical orientation. The rectangular scan segments are sequentially sampled, beginning with segment A and proceeding down toward the local vertical OZ to end at segment n. Each segment sampled is considered as a single count in the processing logic, and corresponds to a  $0.9^\circ$  by  $10^\circ$  field of view. Ninety segments make up a single scan sector. The four scan sectors are commutated simultaneously, completing each cycle in 0.2 seconds. Figure 2-3 shows the acquisition pattern of the complete sensor.

Attitude information is provided by the difference in counts between horizon crossovers in opposite sectors during a single scan cycle. Altitude information is obtained by totaling the counts in opposite sector pairs until horizon crossover is obtained in all sectors. This information also is used to indicate the presence of a foreign body that causes a disturbance of the attitude readout.

The presence of a foreign radiant source such as the sun or the earth seen from the moon will cause no error until the near limb of the disturbing body is within three scan segments (about  $3^\circ$ ) of the reference body. In the worst case, this will produce under three degrees maximum error at the output. An alarm output will be provided while such disturbance is present. The geometry for foreign body interference is shown in Figure 2-4.

### 2.3 SIGNAL PROCESSING

The processing circuit for the LPHS is shown in the system block diagram (Figure 2-5), as presently conceived.

By means of a photocommutator, the detector outputs are sequentially sampled, starting with the uppermost detector, and proceeding down towards the nadir. At the end of each scan, 10 additional sample counts are taken while no detectors are being sampled, and various logic operations occur prior to starting the next scanning period.

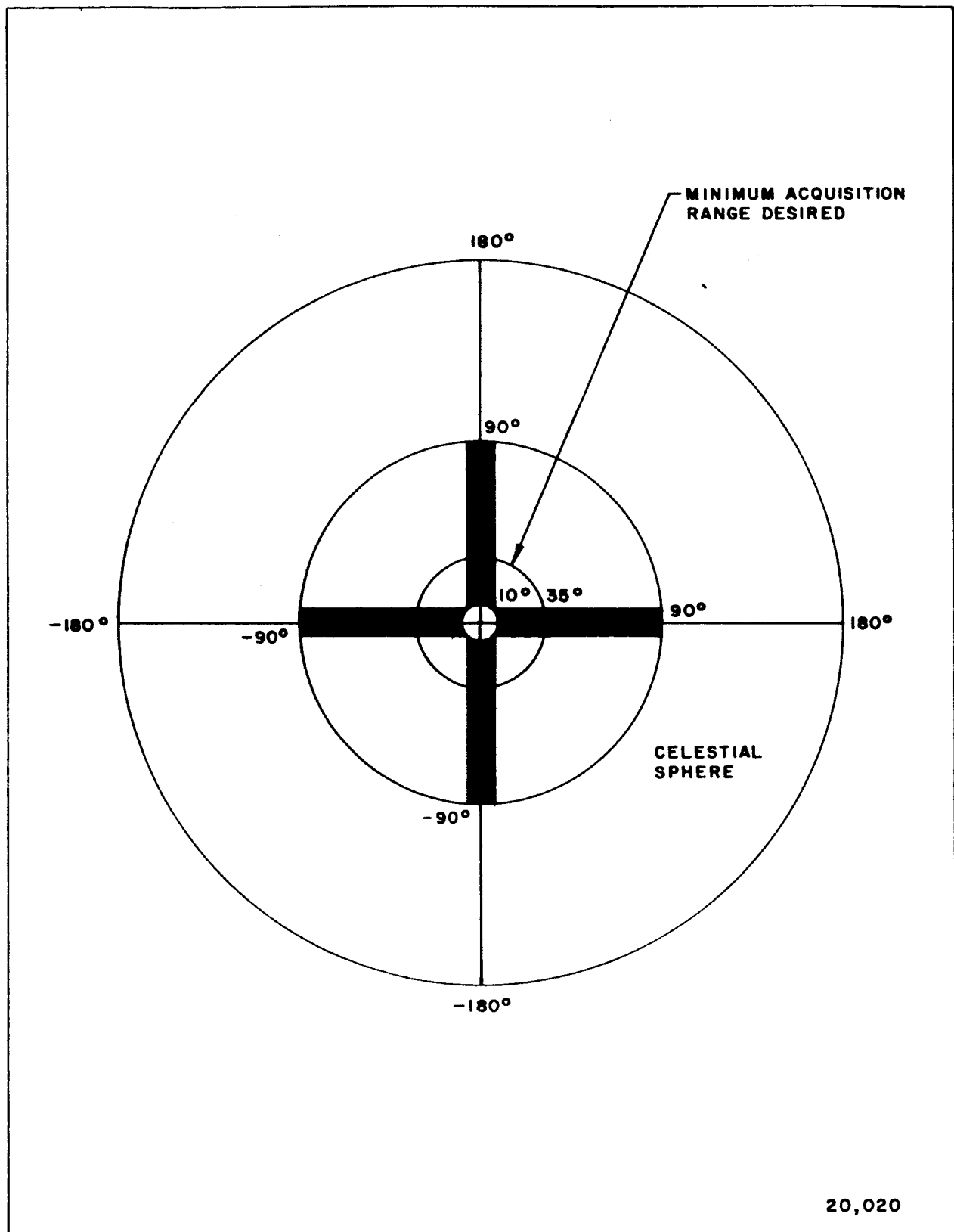


Figure 2 - 3 ACQUISITION PATTERN

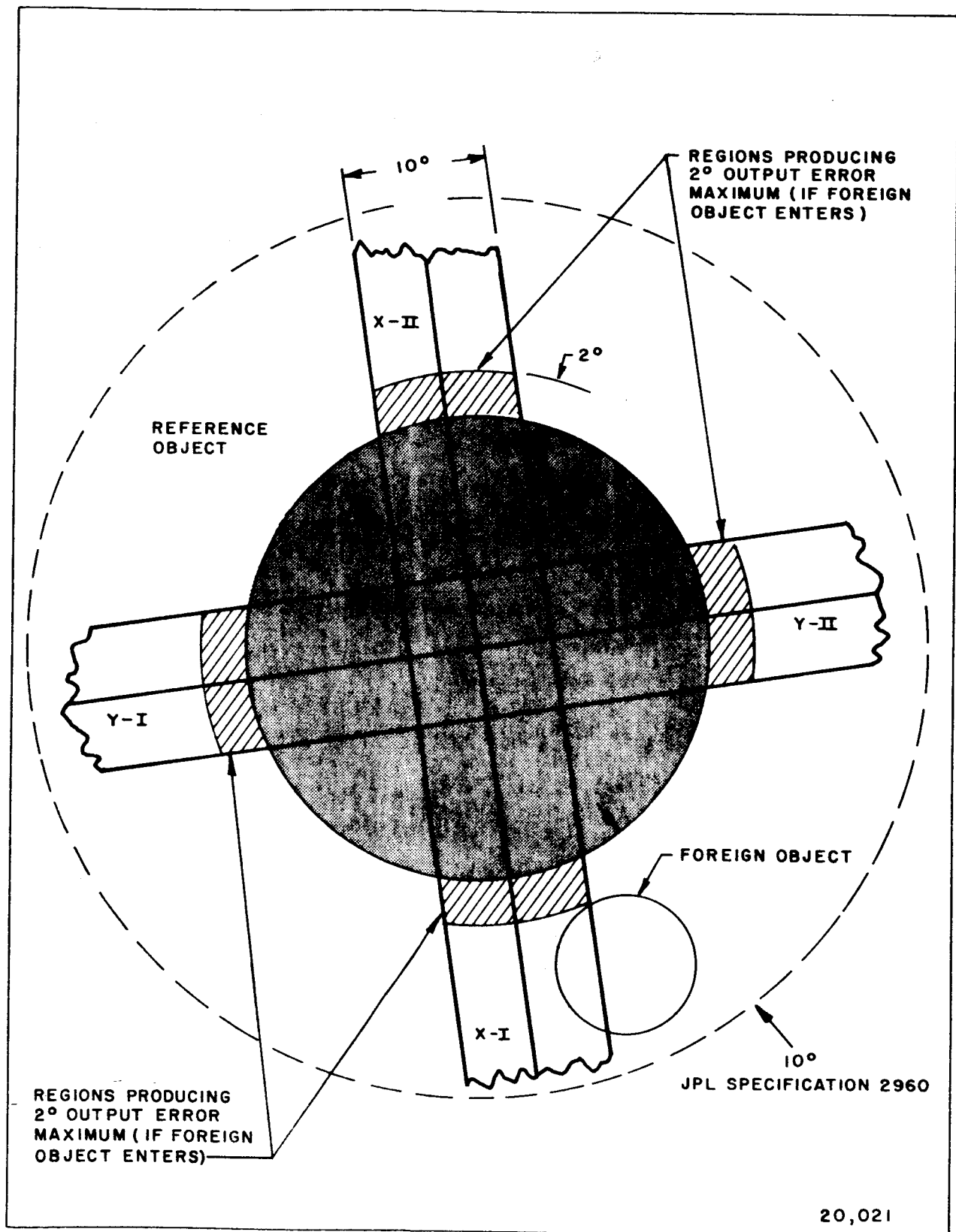


Figure 2-4 FOREIGN RADIANT SOURCE DISTURBANCE GEOMETRY



After commutation, the detector output signals pass through a single pole, double throw switch assembly, called the 0-1 switch. This switch is also photo-activated, and has an appropriate drive for its neon bulbs. Its purpose is to allow commutated signals from the detectors to pass through to the following logarithmic amplifier until determination is made of horizon crossover, at which time the amplifier input is grounded. Then signals are no longer fed into the amplifier until after completion of the scan, at which time the switch is reset. The action is then repeated. The inclusion of this switch in the processing reduces the maximum time duration of the signal to be amplified to a minimum.

The logarithmic signal preamplifier that follows the commutator and switch amplifies the weak detector output signals to usable levels. After amplification, the signal is fed into two circuits. The interrogate switch samples the preamplifier output, and sets the power level into the radiation offset heat source to bring the output signal to zero volts on the space viewing detectors. The other circuit is a time delay threshold circuit, which makes a determination on an amplitude and time duration basis, whether proper horizon crossover has been achieved.

The time determination feature of the threshold circuit enables small spurious targets (such as the sun, or the moon as viewed from the earth, or the earth as viewed from the moon) to be eliminated.

Subsequent to the threshold circuit, the signal is handled on a zero-one basis. Based on the threshold circuit output timing sequences, three determinations must be made: attitude error, altitude and spurious target presence. It is also necessary to provide the proper final system output signals from these determinations.

Attitude error is obtained by integrating a difference signal generated by threshold crossovers of opposite pairs of heads. The polarity of the integrated difference signal is determined by the first threshold crossed and its amplitude is proportional to the difference.

Altitude information is obtained separately from the "X" and "Y" axis heads. The time interval readout from the start of the cycle to horizon threshold crossover for one head is doubled and added to the tilt readout of the pair, giving

the apparent planet subtense angle in that axis. This is compared to a similar determination from the other axis, and the larger is given as the altitude readout. If the difference exceeds two counts, the alarm output is activated, indicating a foreign body or a system malfunction.

## 2.4 LOGIC FUNCTIONS

The following formulations express the interrelationships between the various threshold crossover times and the previously covered descriptions of system output functions.

### Definitions

$X_1$  = count of elements on space of  $X_1$  channel during single scan.

$X_2$  = count of elements on space of  $X_2$  channel during single scan.

$Y_1$  = count of elements on space of  $Y_1$  channel during single scan.

$Y_2$  = count of elements on space of  $Y_2$  channel during single scan.

### Formulas Showing Tilt and Altitude Readout Logic

$$(X_1 - X_2) = \text{tilt readout on "X" axis.} \quad (1)$$

$$(Y_1 - Y_2) = \text{tilt readout on "Y" axis.} \quad (2)$$

$$-7 < (X_1 - X_2) < +7 = \text{linear tilt readout range on "X" axis.} \quad (3)$$

$$-7 < (Y_1 - Y_2) < +7 = \text{linear tilt readout range on "Y" axis.} \quad (4)$$

$$(X_1 + X_2) = \text{altitude readout using "X" axis information.} \quad (5)$$

$$(Y_1 + Y_2) = \text{altitude readout using "Y" axis information.} \quad (6)$$

$$2X_1 - (X_1 - X_2) = (X_1 + X_2) = \text{"X" axis altitude information, when} \quad (7)$$

$$(X_1 - X_2) \text{ is in linear range.}$$

$$2Y_1 - (Y_1 - Y_2) = (Y_1 + Y_2) = \text{"Y" axis altitude information, when} \quad (8)$$

$$(Y_1 - Y_2) \text{ is in linear range.}$$

Note that formulas (7) and (8) obtain altitude by subtracting the small tilt readout signals from the large count readout on only single arms of the respective "X" and "Y" axis. It is simpler to obtain altitude by utilizing the processing implied by this formulation than by formulas (5) and (6). In formulas (5) and (6), each altitude determination is obtained by summing two large numbers, whereas in formulas (7) and (8) only requires accurate generation of one of the large numbers, and summing in the tilt readout required to provide the attitude output.

This method of determining altitude is only accurate while the tilt readouts are in their linear range. However, when the planet attitude is such that its diameter no longer lies within a detector half-width of the "X" and "Y" sensor axis, altitude readout is automatically inaccurate by any method. With the detector sizes that will be used, both methods are equally accurate around null tilt readout.

#### 2.4.1 Spurious Body Determination Logic

When "X" and "Y" axis altitude information agree, the implication is that no spurious body is present to cause the tilt readout error. If they don't agree, however, either a spurious body is present, or a circuit malfunction has occurred, i.e., a timing malfunction in the time delay threshold circuit can produce the equivalent effects of a spurious body signal in the following tilt and altitude circuits. There is no way to separate these two conditions.

Assuming no circuit malfunctions, and both the "X" and "Y" axis tilt readouts within their limited linear range, the following relationships hold when no spurious body is near the true horizon.

$$(X_1 + X_2) = (Y_1 + Y_2), \quad (1)$$

and

$$(X_1 + X_2) - (Y_1 - Y_2) = 0 \quad (2)$$

When a spurious body is near enough to the true horizon on either of the "X" arms to cause error,

$$(X_1 + X_2) < (Y_1 + Y_2), \quad (3)$$

and

$$(X_1 + X_2) - (Y_1 - Y_2) < 0 \quad (4)$$

When a spurious body is present on the "Y" axis close enough to the true horizon to cause error,

$$(X_1 + X_2) > (Y_1 - Y_2), \quad (5)$$

and

$$(X_1 + X_2) - (Y_1 - Y_2) > 0 \quad (6)$$

Therefore, as long as the tilt readouts are not saturated, by providing the larger of the two altitude indications as the system readout, proper altitude will be indicated irrespective of the presence of the spurious foreign body. Also, the polarity indicated by formulas (4) and (6) can be carried through as a final output. In addition to the indication of presence of a spurious body, this also provides means to determine whether the "X" or "Y" axis tilt readouts are in error due to the body's presence.

If the tilt readouts are saturated, and no circuit malfunction exists, both the altitude readout circuit and spurious body indication output may be inaccurate. The saturated tilt readout polarities, however, will still be indicating the direction of tilt correctly.

## 2.5 RADIATION RESPONSE

Of the planetary bodies considered, the Moon experiences the greatest variation in temperature, going from 120°K on the dark side to 400°K fully illuminated. The 120°K signal represents the minimum anticipated signal<sup>1</sup> but processing thresholds will be set to less than one half this level, or 100°K. Figure 2-6 shows



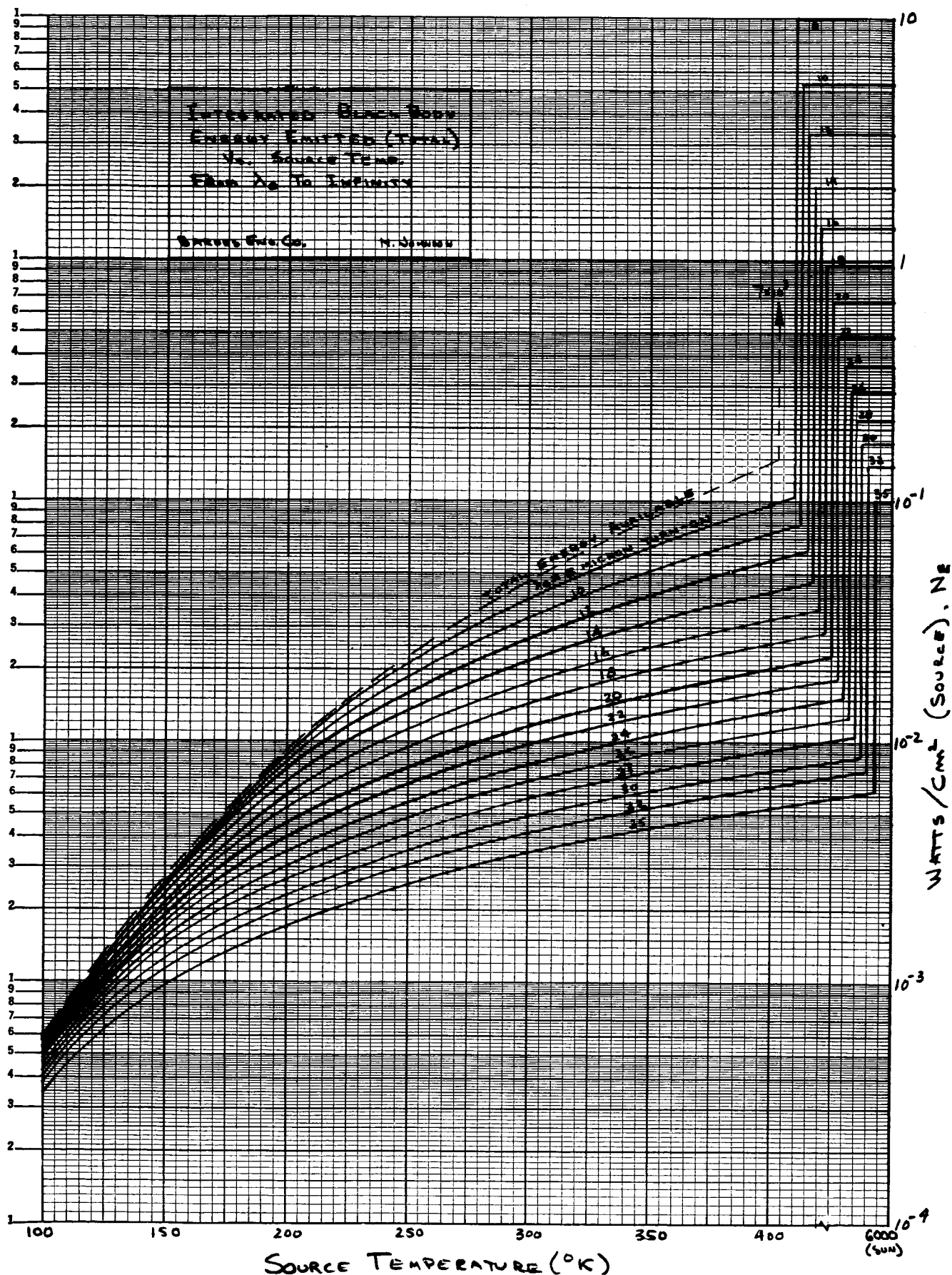
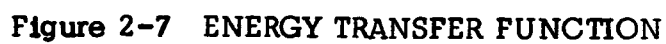


Figure 2-6 INTEGRATED BLACKBODY ENERGY VS. SOURCE TEMPERATURE

emitted radiation vs. source temperature for wavelengths beyond various values of  $\lambda_0$ . Note the reduction in contrast due to longer wavelength turn-on, especially with regard to the sun. Sun signal is further reduced because at most only two active junctions in a single thermopile can receive solar radiation at any time.

Systems using longer wavelength turn-on experience less contrast between hot and cold regions, however, the longest wavelength filter coating of this type is a 19 micron coating made by Optical Coating Laboratories, Inc. This filter achieves 40% average transmission to 35 microns, beyond which it becomes opaque due to coating absorption. With this coating, the system energy transfer function, Figure 2-7, shows a signal of less than 2 microvolts at 120°K, which makes the system barely operable. To gain more energy, the turn-on can be set at a shorter wavelength. This increases contrast, but since the system must be designed to operate with extreme contrast anyway, a moderate increase is tolerable. It is also possible to get higher average transmission with a shorter wavelength turn-on, and since less thickness and fewer layers of coating are required, it may be possible to get increased transmission beyond 35 microns. Because of the atmospheric "window" which ends at 14 microns in a CO<sub>2</sub> absorption band, it would be desirable to turn on at 14 microns. This would minimize contrast on planetary bodies with atmospheres containing CO<sub>2</sub>, although it would have no special significance on the Moon. In the case of Mars and Venus, where extreme variations in surface temperature exist, it is desirable to avoid spectral bands where atmospheric transmission may be high. Both planets appear to have higher CO<sub>2</sub> concentrations than the Earth<sup>2</sup>.

Figure 2-7 also shows the output voltage from a single thermopile as a function of source temperature. A responsivity of .05 volts/watt/cm<sup>2</sup> is anticipated, giving approximately 2 microvolts for a 120°K source. With a 250 cps bandwidth and a maximum detector-photocommutator impedance of 2.0K, the source noise to the preamplifier will be less than 0.5 microvolts peak-to-peak. The preamplifier input impedance will be about 100K, so that the detector-photocommutator impedance can be considered zero ohms to ground. In this condition,



the first stage transistor noise in our bandwidth is close to 2 microvolts peak-to-peak, making the system amplifier-noise limited. For the 120°K case signal to noise ratio, on a peak-to-peak basis, is 4.

## 2.6 ENVIRONMENTAL CAPABILITY

At this time, no difficulty is seen in meeting the anticipated environment, except possibly of temperature. The commutator photoresistors are limited in upper temperature limit to +70°C, due to the manufacturer's claim of chemical deterioration at higher levels. It may prove possible to allow higher temperatures for short periods of time, and further investigation is necessary in this area. An arbitrary lower operational limit for the system of -40°C was used throughout the design, and no difficulty is expected here.

Operation in either vacuum or atmosphere (lab testing) was considered, and no significant difficulties were encountered. Due to convection cooling, somewhat more power is required for the heating of various assemblies during atmospheric operation. The system will be open to vacuum in normal operation in space.

Solar radiation (Venus orbit) provides the worst thermal gradient conditions and also can affect certain optical coatings. Proper design eliminates thermal gradients, and coated silicon provides an ultraviolet-immune optical material.

Redundancy in the neon lamps and photoresistor cells increases the system immunity to micrometeorites, as does the ability of the system to operate satisfactorily if a detector-commutator line opens. The use of double walls also decreases the probability that micrometeorites will damage the system.

The effects of penetrating radiation have been considered in the selection of materials, and only one area is considered questionable. Under very high levels of radiation, such as are found in the Van Allen belts, the neon lamp conduction became lower, and the lamps may appreciably glow even without excitation. Little detailed information has been found regarding this problem.

Other factors, such as vibration, acceleration, shock, input potential variations, radio frequency interference, and magnetic field effects will be considered in detail in Phase II design, although no difficulty is foreseen at this time.

## Section 3.0 SYSTEM OPTICS

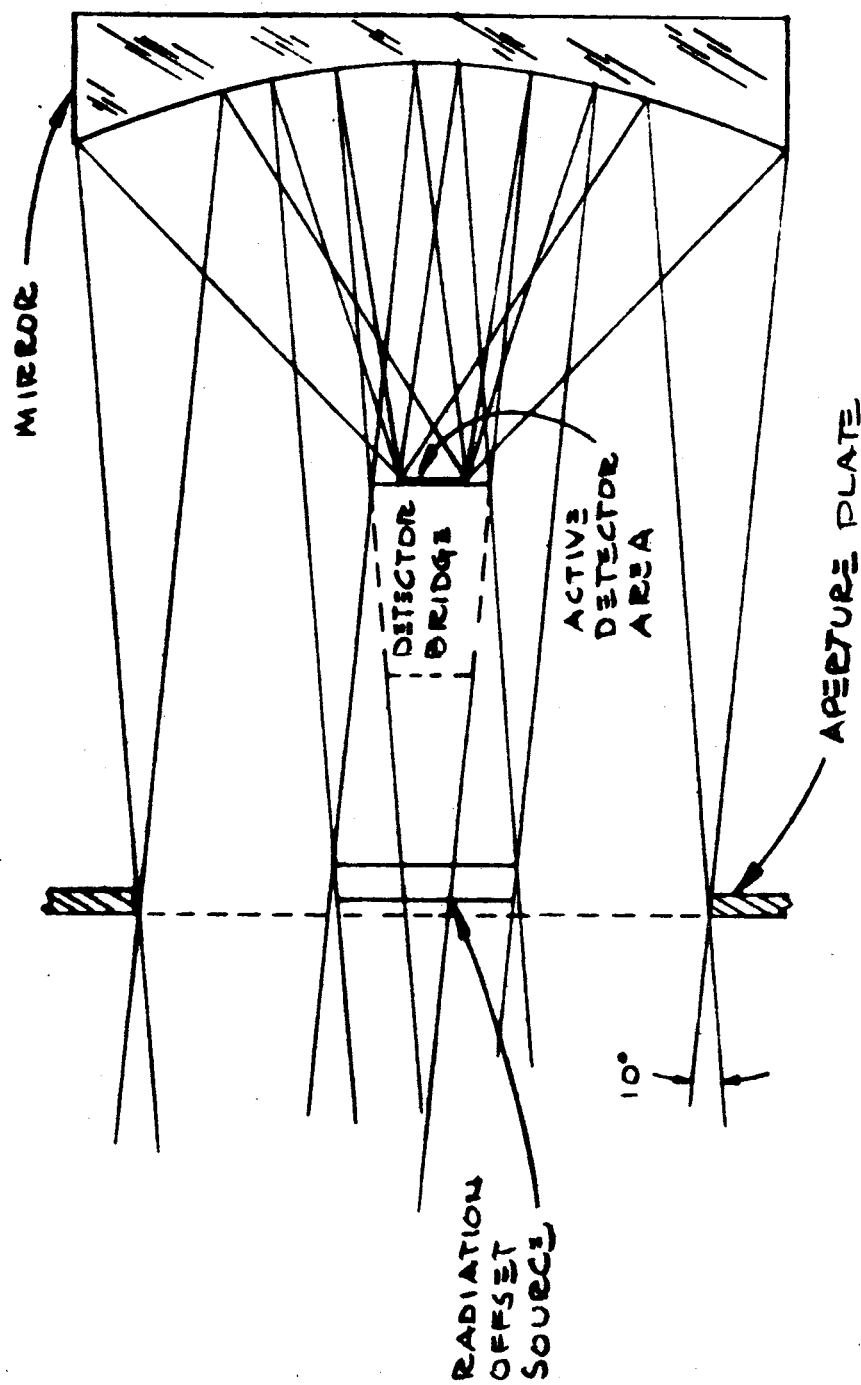
### 3.1 OPTICAL DESIGN

The optical system is basically an uncorrected Schmidt with a  $90^\circ$  by  $10^\circ$  field of view. An optical ray trace is shown in Figure 3-1. Aberrations in the  $90^\circ$  direction are critical and must be kept below  $0.5^\circ$  total, while in the  $10^\circ$  direction they are uncritical up to  $5^\circ$ . Since the active thermopile area is approximately equal to the separation between adjacent thermopiles, a perfectly focused system with no aberration would produce step-like output changes as the horizon passes from detector to detector. Slight defocusing of such a system would produce a linear increase as the horizon moves across the detector and its adjacent gap. Unfortunately, circle of confusion in this system is high enough to produce a blurring of the horizon edge, preventing usage of this technique. This blurring varies sinusoidally (one-half cycle) and does not improve the horizon crossover. In fact, if permitted to become larger than the gap between thermopiles, count error can occur in digital processing when the signal amplitude becomes high enough to activate an adjacent detector with the tail-off of the blurred edge. With an analogue interpolation technique, which will be described later, this condition would produce no appreciable error.

### 3.2 APERTURE

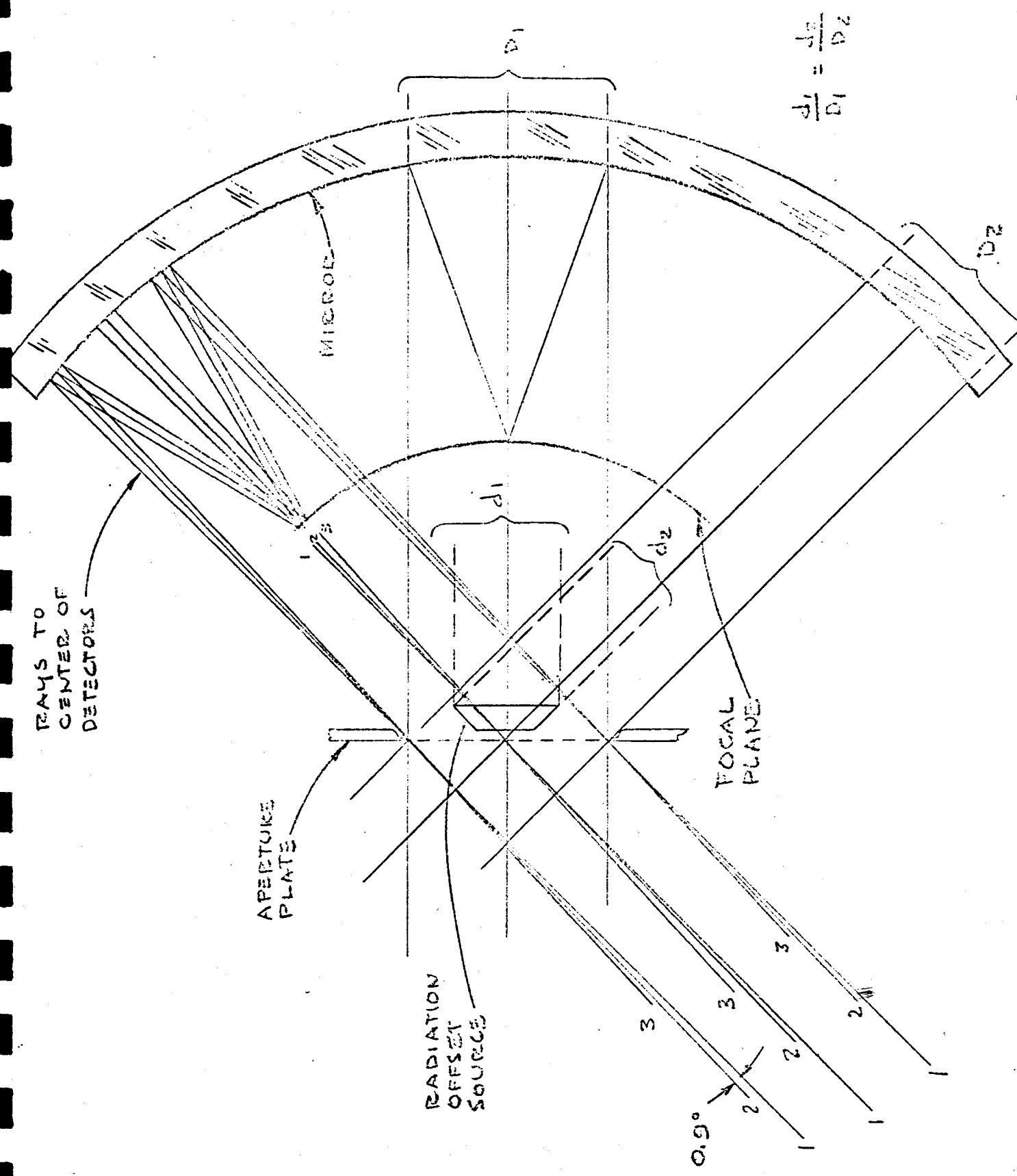
The effective aperture is shown in Figure 2-7. Obscuration occurs because of the detector bridge and the offset heat source. These are shaped so that they present the same percentage of obscuration to all detectors. The bridge is constant width and the offset heat source is in a plane parallel to the window.

A curious problem uncovered concerns the circle of confusion presented by a rectangular aperture. As described before, circle of confusion is critical in the short dimension of the aperture. This type of aberration is proportional to f-number, and consequently to aperture width as measured through its center at any angle. Since the diagonal of a rectangle is its largest dimension, circle of confusion in this direction is maximum. If treated as a vector quantity, we



20,012

Figure 3-1 Optical Ray Trace, Side View - 1 of 2



$$\frac{d_1}{D_1} = \frac{d_2}{D_2}$$

20,023

Figure 3-1 Optical Ray Trace, Top View - 2 of 2

find that the x- component of this circle of confusion exceeds that of the short dimension of the aperture itself. The result is a dog-biscuit shaped circle of confusion which is excessive at the ends; thus the x- component of the aberration must be kept constant, or not larger than a given value.

Referring to Figure 3-2A, the component OX of aberration OB produced by the aperture OI is  $OB \cos \zeta$ . For a spherical mirror of F.L. = +1, ( $R = +2$ ), the longitudinal spherical aberration is given by:

$$\Delta x = \frac{1 - \cos \omega}{\cos \omega} \quad (1)$$

where  $\omega$ , (see Figure 3-2B) is the angle between the radius CI and the axis.

For an object at infinity, the image ray IX' makes an angle  $2\omega$  with the axis, and the lateral spherical aberration is given by:

$$\Delta y = 2 \sin \omega \frac{1 - \cos \omega}{2 \cos^2 \omega - 1} \quad (2)$$

where  $\Delta y = OB$  as shown in Figure 3-2B.

The problem of determining OI as a function of  $\zeta$  yields a fourth order equation, which would be tedious to solve completely. The following procedure, however, provides useful information regarding the shape of the aperture. Let us assume that the extremity I of the radius of aperture OI traces a straight line IA, parallel to axis OY, see Figure 3-2C. In this case we have:

$$OB \cos \zeta = \alpha, \text{ and } OI \cos \zeta = y_0$$

where  $\alpha$  is the largest acceptable value for the aberration and  $y_0$  is the aperture when  $\zeta = 0$ .

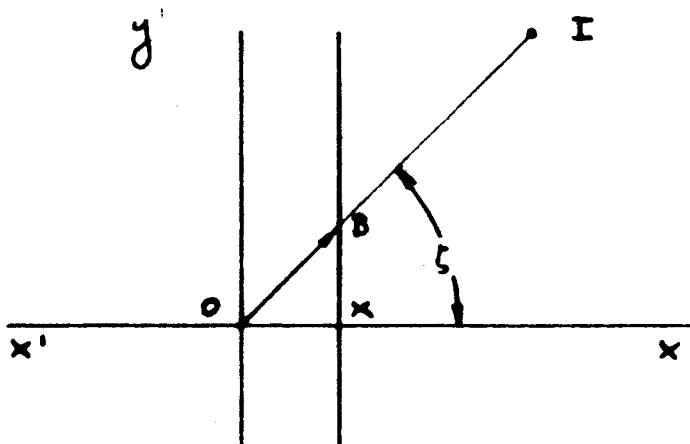
Now, according to relation (2),  $\Delta y$  increases when  $y_0$  increases, consequently the starting aperture  $y$  has to yield an x- component aberration smaller than the acceptable limit.

The following equation derived from relation (2) by assuming that I moved along line IA gives the angle of aperture  $\omega$  as a function of  $\zeta$ ,  $\alpha$ , and  $y_0$ .

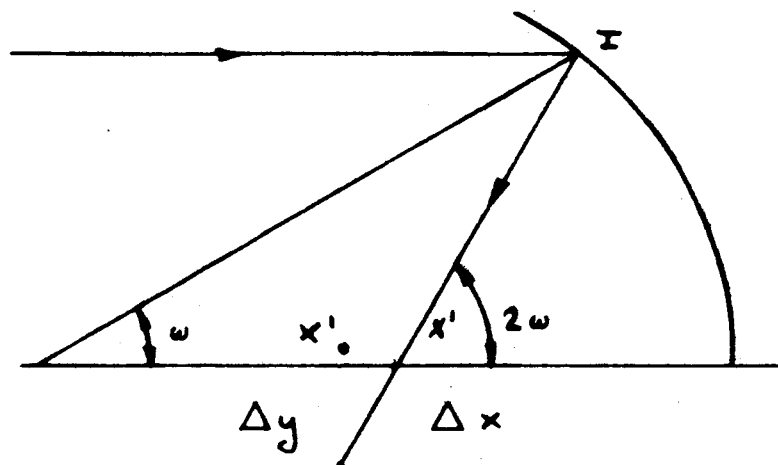
$$2\alpha \cos^2 \omega + 2y_0 \cos \omega - (y_0 + \alpha) = 0 \quad (3)$$



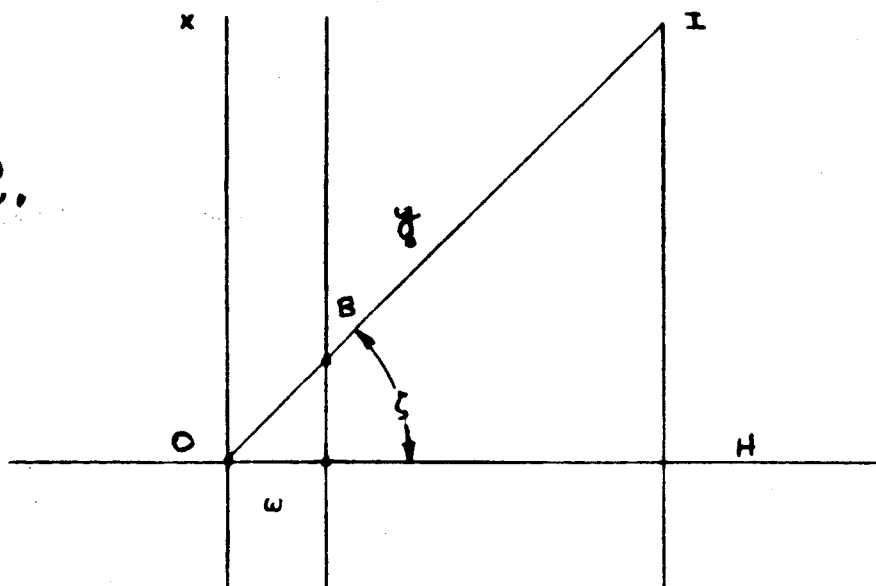
A.



B.



C.



20,024

Figure 3-2 Aperture Determination

In our case  $a = 0.01495$ , corresponding to a radius of aperture 0.17365, and by solving (3) for different  $y_0$  the values of  $\zeta$  yield the shape of the aperture in this system. Thus,

$$+0.0299 \cos^2 \omega + 2 \times 0.19081 \cos \omega - 0.39657 = 0,$$

from which we extract the positive  $\cos \omega = 0.96622$  or  $\omega = 14.934$  to obtain  $\cos \zeta = 0.74041$  or  $\zeta = 47.766$ .

Consequently, to produce a strip shaped circle of confusion, a lip-shaped aperture is necessary. (In polar coordinates, an equation for this aperture shape is:  $r = \sqrt[3]{\text{Csc } \theta}$ . This aperture is theoretically infinite in extent.) It is sufficient to round the corners of the aperture as shown in Figure 2-7 to reduce the aberrations to an acceptable level.

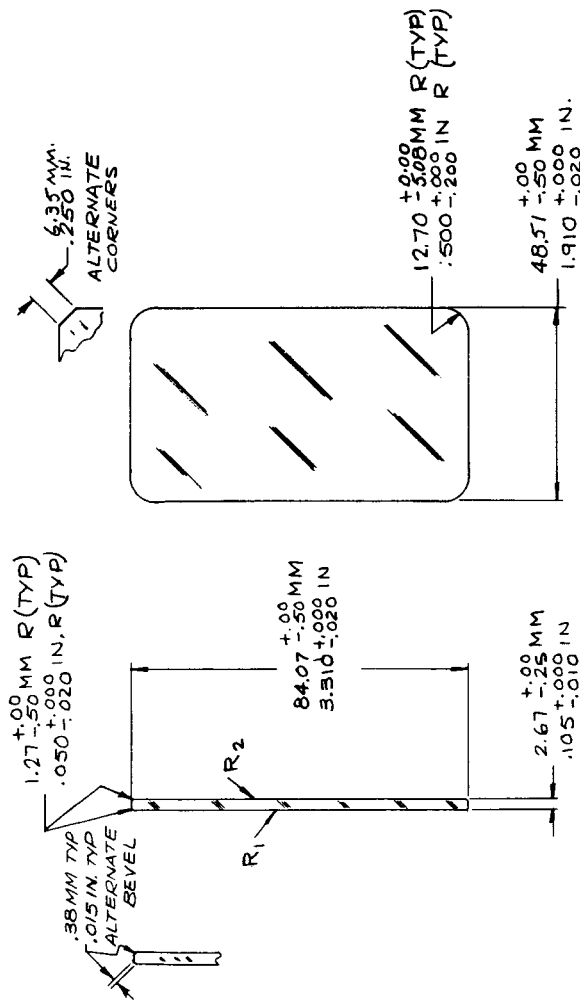
Because the apparent aperture would be spectrally modified if seen through the window material, the actual aperture is located inside the window. To minimize thermal gradients, the aperture should be an inherent part of the housing which includes the detector bridge. Placing the aperture inside the window will further reduce gradients and make assembly easier, as only a simple retainer is required which can be screwed on from the outside.

### 3.3 WINDOW

As previously described, the window will become transmitting at 14 microns and continue as far as possible beyond 35 microns. Figure 3-3 (sheet 1 and 2) is attached, which shows the window and coating characteristics. The substrate will be silicon, although KRS-5 could be considered for laboratory experiments. KRS-5 is more fragile, experiences cold flow, and deteriorates when exposed to solar radiation. Silicon, with its 14 micron coating, is not known to be affected in any way. Optical Coating Laboratories, Inc. will probably fabricate and coat this element.

### 3.4 MIRROR

Figure 3-4, which shows the mirror, is attached. The mirror is made of aluminum to prevent thermal strain when attached to the aluminum housing. The Kanigen



WEIGHTED AVERAGE  
TRANSMISSION =  $\sum T_{\lambda} M_{\lambda}$   
(0.3 MAXIMUM)

$\Delta\lambda$	$M_{\lambda}$
0-.5	27.4
.5-1	43.5
1-2	20.7
2-3	5.51
3-4	1.04
4-5	.406
5-6	.189
6-7	.100
7-8	.058
8-9	.026
9-10	.013
10-11	.016
11-12	.011
12-13	.006

$T_{\lambda}$  = INTEGRATED  
TRANSMISSION OVER  
WAVELENGTH BAND  
 $\Delta\lambda$ . (PERCENT)

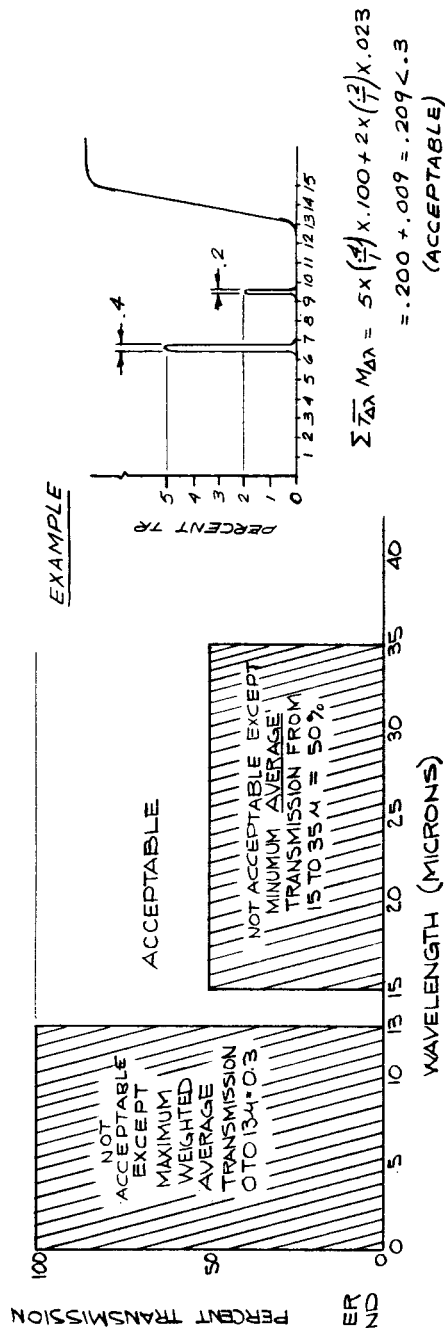


Figure 3-3 WINDOW-LUNAR AND PLANETARY HORIZON SENSOR  
(SHEET 1 OF 2)

Element and coating shall meet the following requirements:

- (1) Transmission to begin at  $14 (\pm 1)$  microns and is to be maximized at longer wavelengths (see sheet 2). Transmission beyond 35 microns is desirable.
- (2) Coating to be spectrally uniform within 5% over entire substrate clear aperture.
- (3) Adherence of coating to be sufficient to withstand normal cleaning procedures and the adherence (cellulose tape) test per MIL-M-13508 as a design goal.
- (4) The solubility of the coating shall pass subsection to running hot (165 F) water for three (3) minutes without resultant degradation in the physical and transmission characteristics as a design goal.
- (5) There shall be no flaking, chipping, peeling, or degradation of transmission characteristics of the coating when exposed by the customer to the following environmental conditions, or natural combination thereof as a design goal:

Temperature:  $-40^{\circ}$  to  $+80^{\circ}$  C

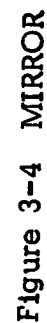
Pressure: Less than  $10^{-12}$  mm.Hg.

Period: 3 years maximum

Radiation: Van Allen belt radiation/solar radiation from orbit of Venus

- (6) Vendor to supply spectral transmission curve for each coated substrate and to notify customer of possible deviation from design goals.

Figure 3-3 WINDOW-LUNAR AND PLANETARY HORIZON SENSOR  
(SHEET 2 OF 2)



process will be used to prepare the ground surface for polishing, and the final surface will be aluminized. The entire fabrication will be performed at Barnes Engineering Company.

### 3.5 PHOTOCOMMUTATOR

In order to maximize resistance change in the cell, it is essential that as much light from each neon lamp reach the active cell surface, and that this light be of the proper spectral composition. When off, it is desirable that no extraneous light reach the cell surface. Figures 3-5 and 3-6 show the spectral match achieved using the AIC type lamp, and the optical arrangement as visualized. Two lamps will be used in parallel redundancy. Their back surfaces will be aluminized to be highly reflecting. Reflecting walls (aluminized mylar) extend to the cell surface. The use of parallel reflecting walls allows every ray coming from the glow region within the  $110^\circ$  angle shown to eventually hit the cell surface. Additional rays will also be reflected by the back surfaces, but the efficiency is much lower. A flat rear surface would not appreciably increase the light transfer, since secondary reflections from it would have to pass through two neon lamps instead of one.

### 3.6 THERMOPILE DETECTORS

#### 3.6.1 Configuration

Barnes Engineering Company is developing a special five thermopile detector block which should be relatively inexpensive. This will permit linearization of the array, allowing a total of one hundred detectors in ninety degrees. This detector will also achieve higher sensitivity than similar types due to intensive research in this area.

These thermopiles are mounted on a pure aluminum substrate (Figure 3-7) which has five channels cut into its surface. A flat mylar insulating film is over the channeled surface and thin layers of bismuth and antimony are deposited using the mask shown in Figure 3-8. These materials appear in alternate sequence, with larger active areas superimposed above the channel (hot junctions) and above

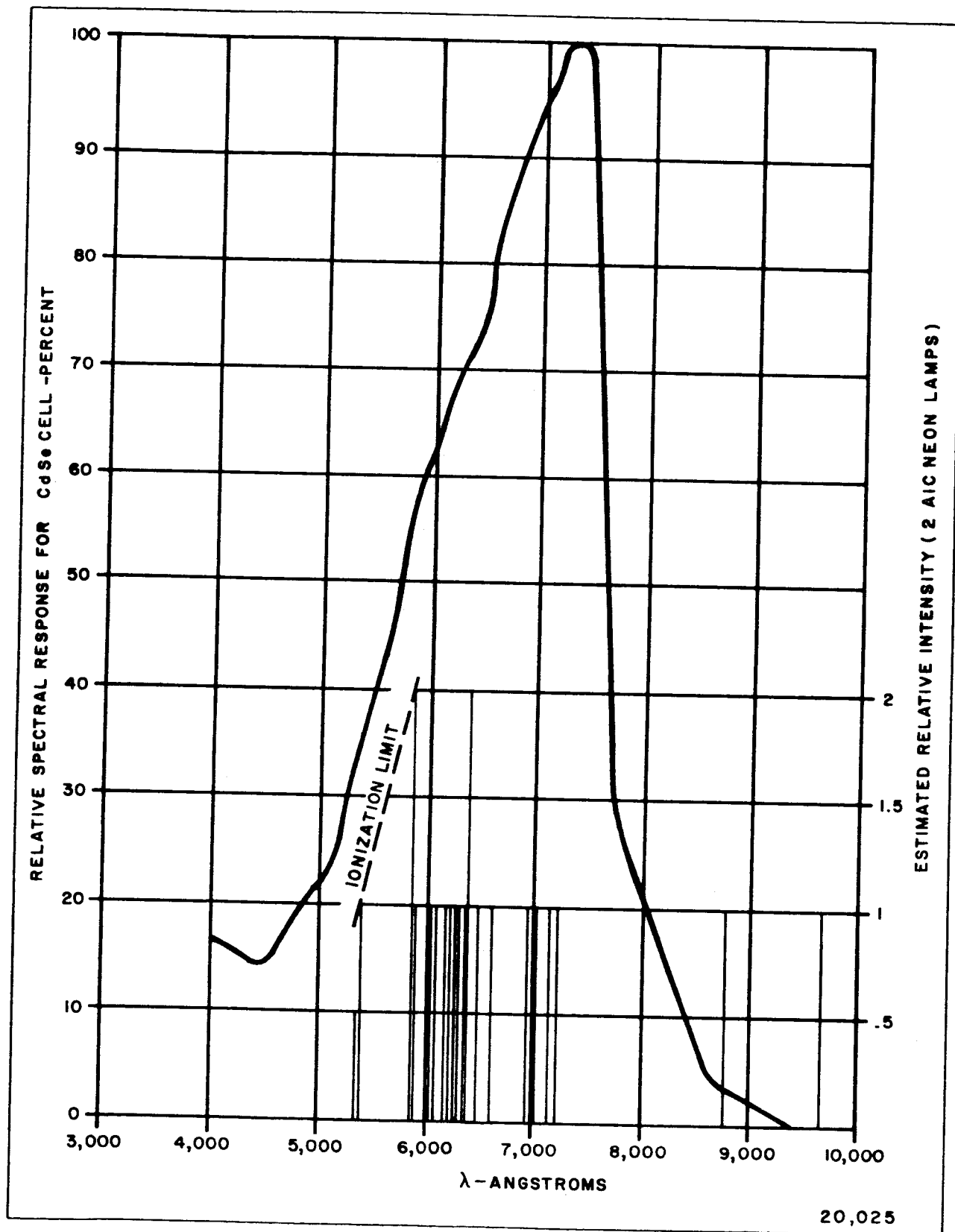


Figure 3-5 SPECTRAL MATCHING OF CELL AND LAMP

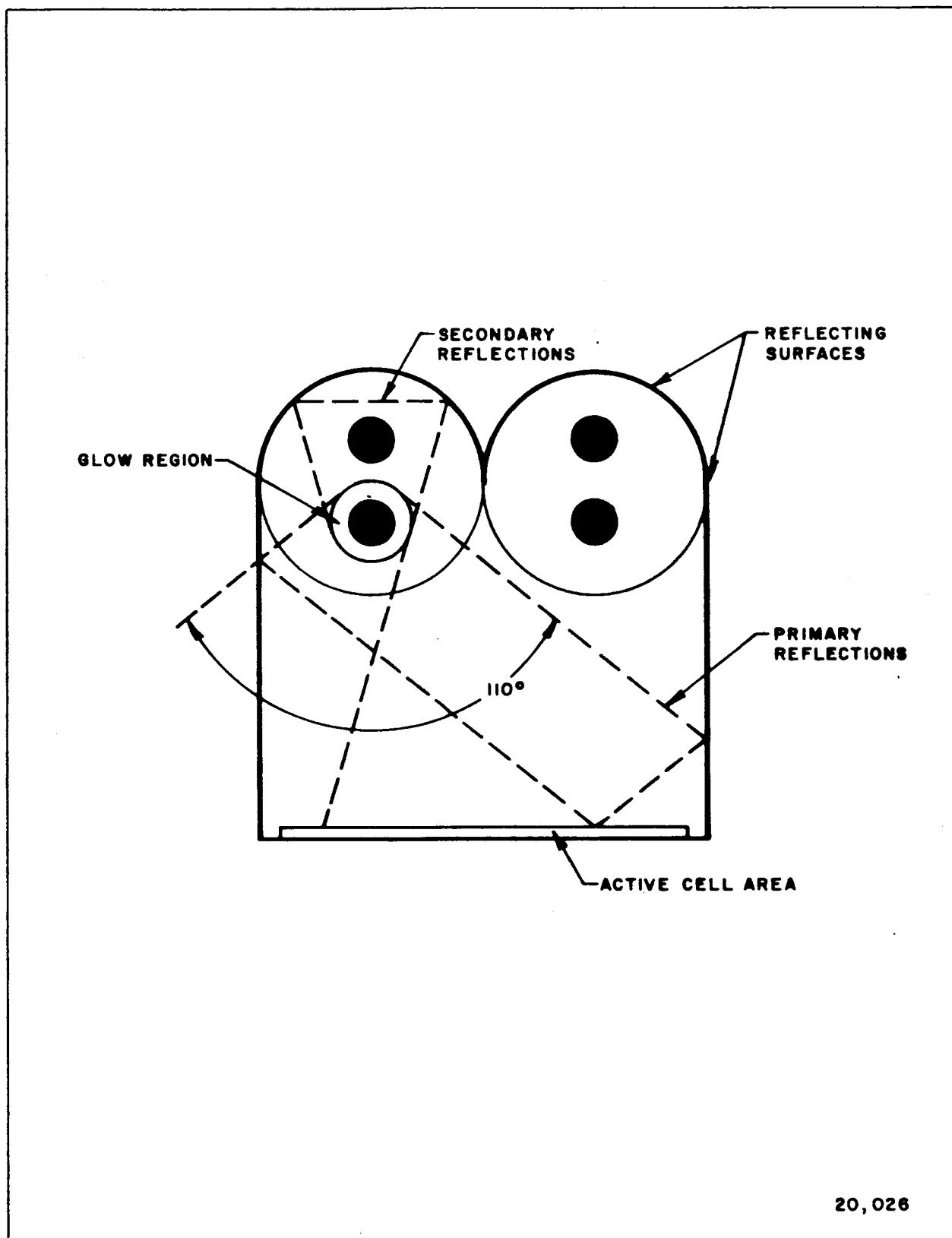
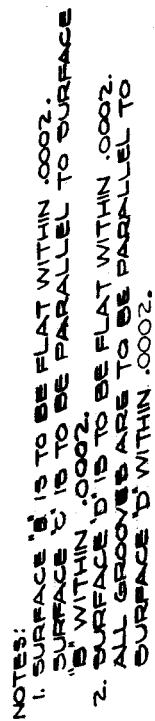


Figure 3-6 PHOTOCOMMUTATOR CELL





**Figure 3-7 SUBSTRATE, 5-CHANNEL THERMOPILE**  
**BARNES ENGINEERING COMPANY 2920**



the ridges supporting the mylar (cold junctions). The hot junctions are then covered with a material that is highly black in the infrared. External leads are attached.

### 3.6.2 Thermal Analysis

The vast improvement obtained with these thermopiles lies in the ratio between active collecting area and the thermal impedance of the leads between hot and cold junctions. Active area has been made as large as possible, while leads have become narrower, thinner, and thermal impedance of bismuth and antimony leads has been equalized. The thinner antimony layer has been placed on top of the bismuth, which results in greater interpenetration of the two materials. The following table gives the relative sizes of the various areas.

TABLE 3-1

	Width*	Length*	Thickness*	Thermal**	
				Conductivity	Capacity
Active Junction					
Bismuth	.008	.012	.0002	—	.03
Antimony	.008	.012	.00008	—	.05
Blackening					
Gold Black	.008	.012	≈ .0002	—	.03
3M/Zapon	.008	.012	≈ .0004	—	~ .4
Bismuth Lead	.0035	.007	.0002	.018	—
Antimony Lead	.0035	.007	.00008	.042	—
Passive Junction					
Bi	.008	.012	.0002	—	—
Sb	.008	.012	.00008	—	—
Mylar	.008	.012	.00025	.00025	—

\* Inches

\*\* Given in c.g.s. units (Handbook of Chemistry & Physics).

The sensitivity of a single junction, based on this is:

$$S = \frac{.008 \times .012 \times 2.54^2}{(4.27 + 4.57) \times 10^{-6} \times 4.186} = 17.1^\circ\text{C}/\text{watt}/\text{cm}^2$$

This neglects losses due to radiation and through the mylar backing, which are trivial. The cold junction coupling is ignored, as its conductivity is fifty times higher than through the leads. The thermoelectric potential generated by a bismuth-antimony pair is about 120 microvolts/ $^\circ\text{C}$ . This produces .043 volts/watt/ $\text{cm}^2$  for twenty-one active junctions. This may be improved as state of the art advances and thinner deposited leads become possible.

The time constant of the detector is relatively uncritical in this application. Gold black and black paint are possible blackening materials having radically different time constants.

$$\begin{aligned} \text{Gold Black: } \tau &= \frac{.008 \times .012 \times (.03 \times .0002 + .05 \times .0008 + .03 \times .0002 \times 2.54^3)}{(4.27 + 4.57) \times 10^{-6}} \\ &= 29 \text{ ms.} \end{aligned}$$

(Speeds of 25 to 50 ms. have been obtained with gold black.)

Black Paint (3M/Zapon):

$$\begin{aligned} \tau &= \frac{.008 \times .012 \times (.03 \times .0002 + .05 \times .00008 + .4 \times .0004) \times 2.54^3}{(4.27 + 4.57) \times 10^{-6}} \\ &= 302 \text{ ms.} \end{aligned}$$

Since the gold blackening is a delicate material and time constant is uncritical, an appropriate paint should be very satisfactory.

## Section 4.0 MECHANICAL DESIGN

### 4.1 SENSOR HEAD

Each sensor head, (Figure 4-1), consists of two sections, the optical assembly and the commutator section. Size is determined by the primary mirror, which is related to the aperture, available infrared signal energy, and detector size. The commutator section is of a sandwich construction fitting between the optical assembly and the mounting flange, actually forming part of the mechanical support for the optical assembly. Both assemblies mount on a central support web, and when the mounting flange and the protective outer cover are removed, all critical components are accessible. The neon lamp matrix can be removed completely, leaving the photoresistors exposed. The cover plate on the optical assembly can also be removed to permit access to the detector bidge.

The most critical part of the mechanical design is related to thermal gradients, particularly on the detector bridge; this problem is further complicated by the need to heat the commutator section. Consequently the commutator section is well insulated from the outer housing to minimize heating power. None of this heat flows through the optical section because it is only attached to the central mounting web at one surface, and through insulation.

Both the optical assembly and the commutator section are electrically insulated from the outer housing and are at circuit ground. This is done with the same insulation which provides the thermal isolation.

Alignment may be done by rotation of the head about a pivot point, as shown in Figure 4-1. The mounting is not determined at this time, and many techniques can be used other than that shown. Another possibility is the use of a circular cut alignment groove, with a mating tongue ring on the vehicle. In this case the sensor head could be aligned and held with the same ring.

### 4.2 OPTICAL ASSEMBLY

This section, shown in Figure 4-2, resembles a 90° wedge with the mirror at the back. Ninety thermopile detectors are mounted on a detector bridge and are at the mirror focal plane. To prevent loss of thermal contact at

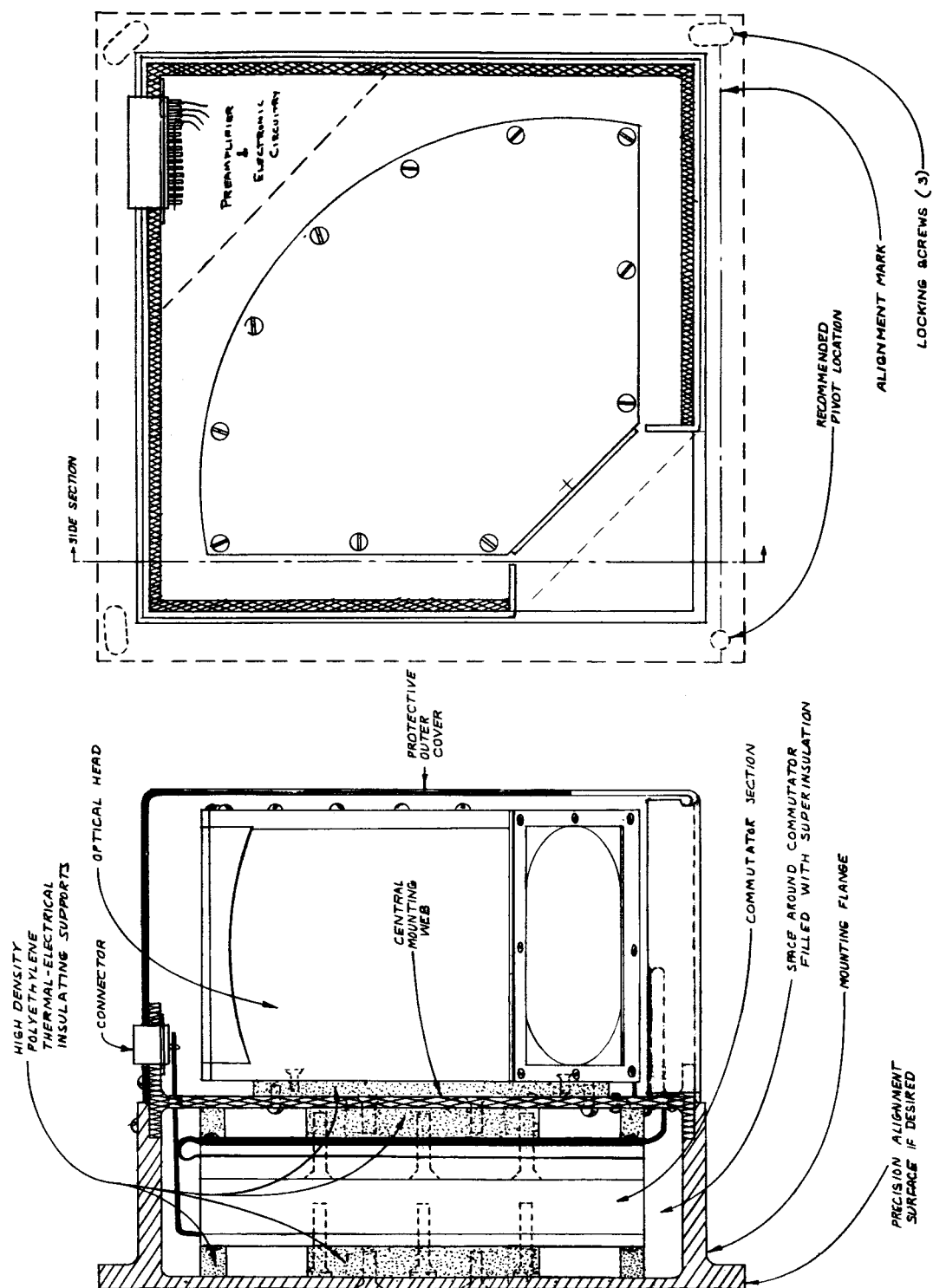


**Figure 4-1 OUTER HOUSING, LUNAR AND PLANETARY HORIZON SENSOR**  
 BARNES ENGINEERING COMPANY  
 2917

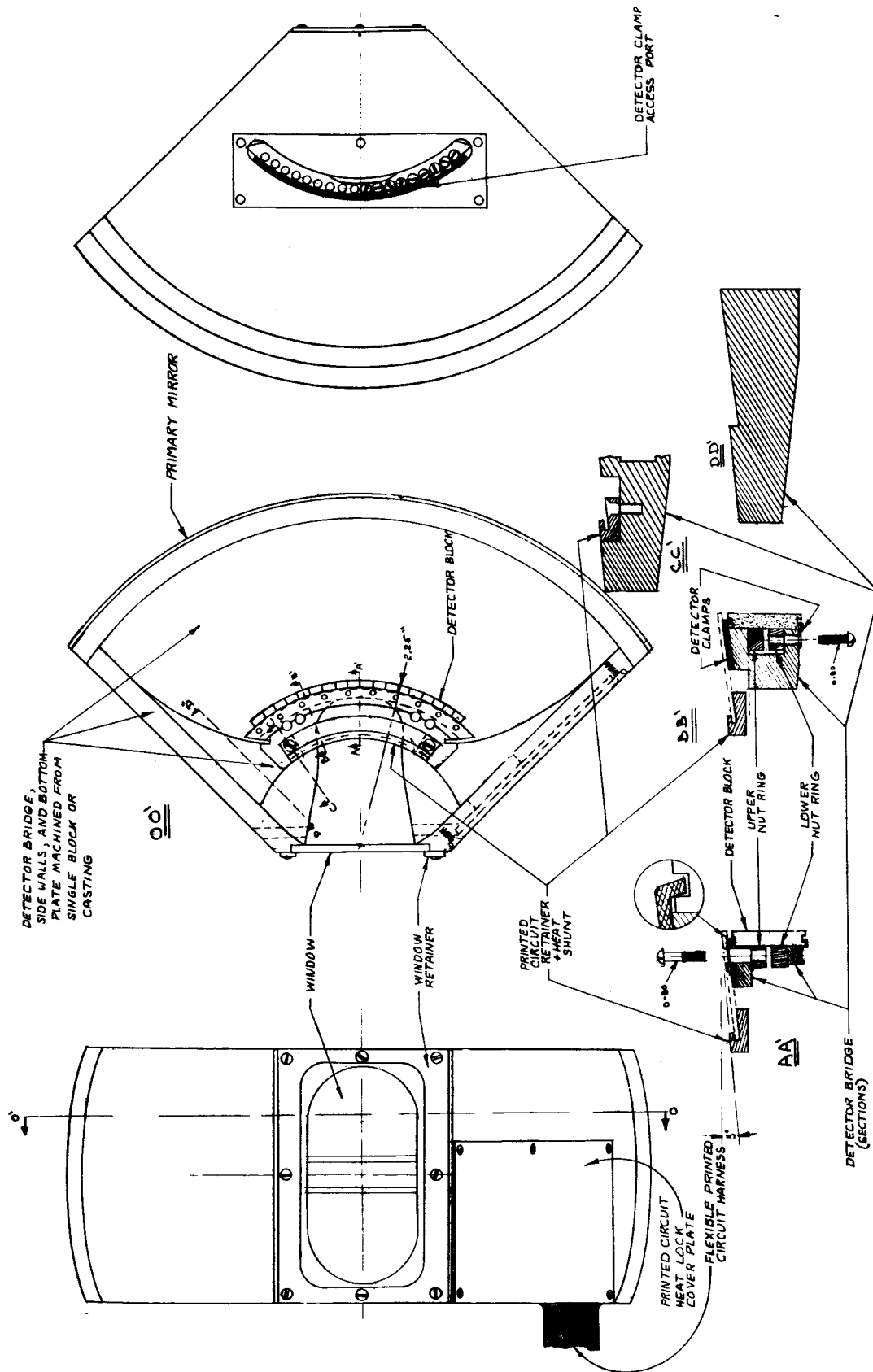


Figure 4-2 OPTICAL HEAD, LUNAR AND PLANETARY HORIZON SENSOR  
 BARNES ENGINEERING COMPANY 2918

joints (in hard vacuum), the bottom plate, the side walls, and the detector bridge are machined from a single piece of aluminum. The detector bridge is shaped so that heat conductivity to a given point is maximum while the heat capacity from that point to the center of the bridge is minimum. This results in a third power curvature which gives minimum gradient for dynamic temperature variations of the side walls. Gradient is also reduced by the narrow cuts which are shown on either end of the detector array. These effectively shorten the bar, and under dynamic temperature variations make the detector array approximate an isothermal. To reduce heat flow through the center of the bridge, the printed circuit retainer also acts as a heat shunt (a bonding material is used at its ends, which are also screwed down).

Five detectors are deposited on a single substrate, which is held in position with clamps secured to the bridge with nut rings, as shown in sections AA and BB. The upper clamp screw also holds down the printed circuit lead assembly. Eighteen substrates comprise the detector array in each head.

#### 4.3 COMMUTATOR SECTION

Potentials produced by the thermopile detectors are very small, and to prevent pickup the commutator section is as close to the optical head as possible. The size of the optical head permits a sandwich structure with 200 neon lamps closely spaced. Since under 100 channels are desired, two-lamp redundancy is possible. Each cell has two lamps above it, and the cell can be as large as the lamps in projected surface area. To minimize electrostatic pickup, the neon lamps are separated from the photocommutator cells by about 0.50 inches. Printed circuits going to the photocommutator cells and to the neon lamps complete the sandwich, which is shown in Figure 4-3.

The egg-crate reflecting walls are attached to the neon lamp assembly and extend down to the surface of the photocommutator cells. The commutator cells, Figure 4-4, are assembled in banks of five, and these assemblies fit into a support frame. The commutator cells are made with two active areas, which are shorted together to give a measure of redundancy.



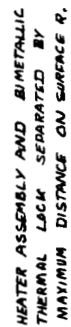


**Figure 4-3 COMMUTATOR SECTION, LUNAR AND PLANETARY HORIZON SENSOR (PRELIMINARY)**

Each cell shall meet the following specifications with both halves in parallel:

- 1) Impedance when excited:  $R < 1000$  ohms. (see note 4)
- 2) Impedance when dark:  $R > 2$  megohms.
- 3) Above impedances to be obtained over an operating temperature range of  $+30^{\circ}\text{C}$  to  $+70^{\circ}\text{C}$ .
- 4) Exposure light source to be high brightness GE type A1C neon lamp with 2 milliamperes excitation current, envelope to come no closer than 0.25" from active cell surface.
- 5) Upon exposure, resistance should decrease from dark value to less than 1000 ohms in less than 1.0 millisecond at any temperature between  $+30^{\circ}\text{C}$  and  $+70^{\circ}\text{C}$ .
- 6) Upon extinction of light source, resistance should reach 100,000 ohms in less than 4.0 milliseconds at any temperature between  $+30^{\circ}\text{C}$  and  $+70^{\circ}\text{C}$ . Resistance should then continue increasing to exceed 2 megohms in less than 10 milliseconds from the instant of extinction.
- 7) As a design goal, it is desirable that the upper and lower operational (or storage) temperature limits be extended to a maximum of  $+80^{\circ}\text{C}$  and a minimum of  $-50^{\circ}\text{C}$ , while maintaining resistances and response speeds within the limits described above.

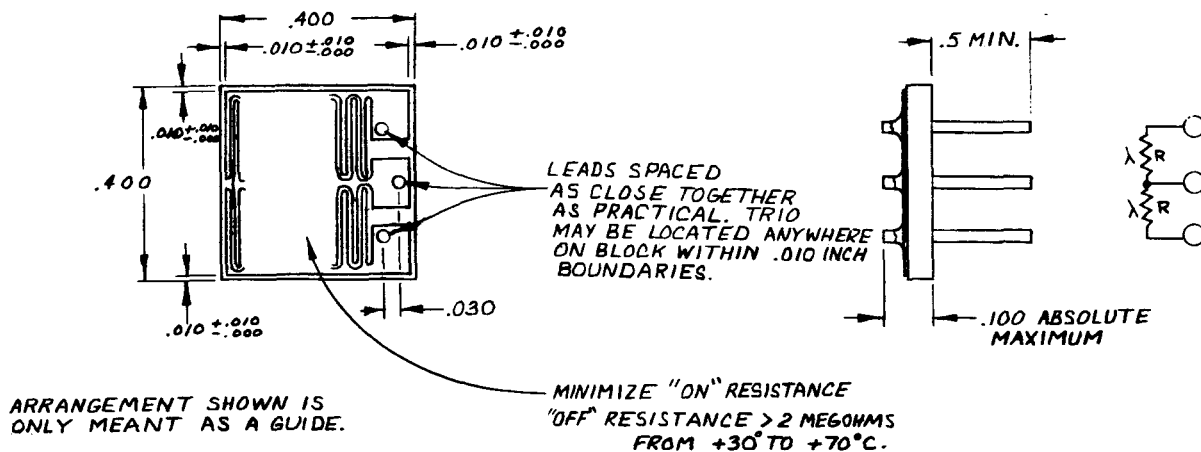


Figure 4-4 COMMUTATOR ELEMENT  
BARNES ENGINEERING COMPANY

The neon lamps are type AIC midget size high brightness lamps, aluminized on their back surfaces. To avoid insulating their leads, the backing plate can be made of glass epoxy board, rather than the aluminum shown.

The temperature limitations of the commutator cells necessitate heating below  $+30^{\circ}\text{C}$ , while the upper limit of  $+70^{\circ}\text{C}$  means that no heat should be dissipated at that temperature. The simplest method for achieving this is the use of positive temperature coefficient resistors, such as those available from Ferroxcube Corporation of America. These resistors serve both as temperature sensors and as heaters. Figure 4-5 shows the power dissipated by an arrangement of these devices as a function of outer housing temperature. Figure 4-5 shows the commutator case temperature vs. outer housing temperature with the positive temperature coefficient resistors and the neon lamp power being dissipated. The neon lamp power (360 milliwatts continuous) would result in overheating at  $+70^{\circ}\text{C}$ , however, a snap action thermal shunt can be used that provides a good thermal conducting path to the outer case at  $+65^{\circ}\text{C}$  to  $+70^{\circ}\text{C}$  and releases at  $+35^{\circ}\text{C}$  to  $+40^{\circ}\text{C}$ . (This shunt must be electrically insulated.)

#### 4.4 PRINTED CIRCUIT ASSEMBLIES

The large number of electrical connections in each sensor head necessitates the use of flexible printed circuit harnessing. Two assemblies are required: the interconnecting harness between the detectors and the photocommutators and the neon lamp matrix connections. Mylar appears to be an excellent base material, having good overall immunity to the space environment. One ounce copper will be used for the detector-commutator harness, and two ounce for the neon matrix.

##### 4.4.1 Detector-Commutator Harness

Figure 4-6 shows this lead assembly. The wires from the detectors lie in notches in the ends of the harness leads, where they are soldered in place. These leads, which are about .010 inches wide, pass through a small heat lock and then narrow down to .004 inches. The heat lock is a region of thermal conduction to the detector bridge designed to shunt heat coming from the commutator



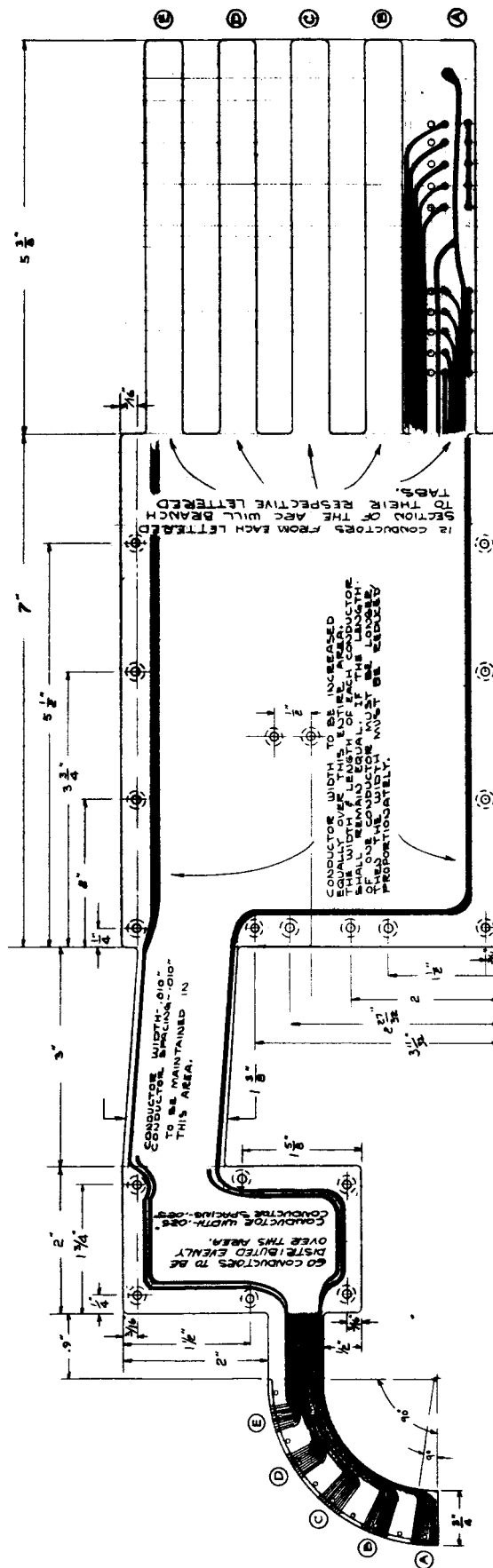


**Figure 4-6 CABLE, FLEXIBLE MYLAR**  
BARNES ENGINEERING COMPANY 2922

section away from the detectors. The narrow leads assist in this action by providing a high thermal impedance to any heat flowing to the detectors. After leaving the detector bridge, the leads widen to .010 inches again in another heat lock to the optical assembly, with the same result as before. The leads narrow to about .006 inches and proceed to the commutator section. Here they widen considerably into a third heat lock on the commutator section. This heat lock keeps the photocommutator cell printed circuit connections at the same temperature, thus eliminating spurious thermoelectric contact potentials. From this heat lock the leads narrow slightly and end at the photocommutator, where they form a single-pole, 95-throw switch (actually only ninety detector sections are used — the remaining ten are for logic processing).

Figure 4-6 indicates only sixty leads; that is, fifty signal leads and ten ground lines, corresponding to nearly half the total number of detectors. The remaining detector leads are on another layer. Each ground line runs close to the five signal leads coming from a single detector block. All ground lines are tied together at the photocommutator. The object of this is to minimize pickup area in the presence of varying magnetic fields (up to 100 gauss/second), and to provide a safeguard against ground line breakage (i.e., an open ground line disables only five detectors, and the system continues to operate with a five detector gap).

The complete harness consists of two circuits, one as shown in Figure 4-6 and the other with detector and commutator terminations slightly shifted. Three layers of mylar or other base material separates and insulates the conductors. On the top and bottom of the imbedded conductors at certain points are large printed copper areas, which form the heat locks. These areas are thermally connected to their appropriate heat sinks by screws, using a bonding agent for good thermal transfer.

#### 4.4.2 Neon Lamp Matrix

The commutation of 95 channels by a line-bar matrix is easily done with two flexible printed circuits, one with ten parallel lines, and the other with ten bars running perpendicular to the lines. Two neon lamps, in parallel, are

connected across each of 95 intersections of the lines and bars. Activation of a single line and a single bar causes a single neon lamp to glow.

The lines and bars run into a cable which goes to the sensor head electrical connector. This cable is insulated and must be physically separated from the detector-commutator harness to prevent electrostatic pickup.

#### 4.5 OFFSET REFERENCE SOURCE

When the detectors are exposed to space ( $0^\circ\text{K}$ ), they tend to radiate out through the aperture, cooling down and producing negative outputs. Since detector responsivities vary as much as 20%, this negative signal is not the same from detector to detector, varying by much more than the minimum expected signal. To avoid these erroneous signals, a small heat source (Figure 4-7) mounted in the aperture (the one spot viewed by all detectors) provides energy to the detectors equivalent to that lost to space. Its radiating surface is parallel to the aperture so that the energy emitted to a detector is always equal to that lost through the aperture, even when viewed at angles up to  $45^\circ$  from the central axis. This surface is blackened for maximum emissivity, while all other surfaces are as reflective as possible.

The unit is supported on a glass-phenolic rod, and the resistors and transistor which provide the heat are mounted in intimate contact with the body of the source. Since silicon transistors are limited to  $200^\circ\text{C}$ , it may prove desirable to remove the transistor if this temperature is attained in practice.

The unit is controlled by a regulator circuit which examines detector outputs and sets the source accordingly. This circuit is described in the electronic section. Figure 4-8 shows the temperature of the source vs. case temperature in vacuum operation. Power required as a function of case temperature is also shown.

#### 4.6 THERMAL ANALYSIS (See Definitions: Appendix I)

##### 4.6.1 Detectors

As has been shown in Section 3.6, the sensitivity of a detector is about  $.05 \text{ volts/watt/cm}^2$ . Using one half the signal threshold level — 0.5 microvolt —

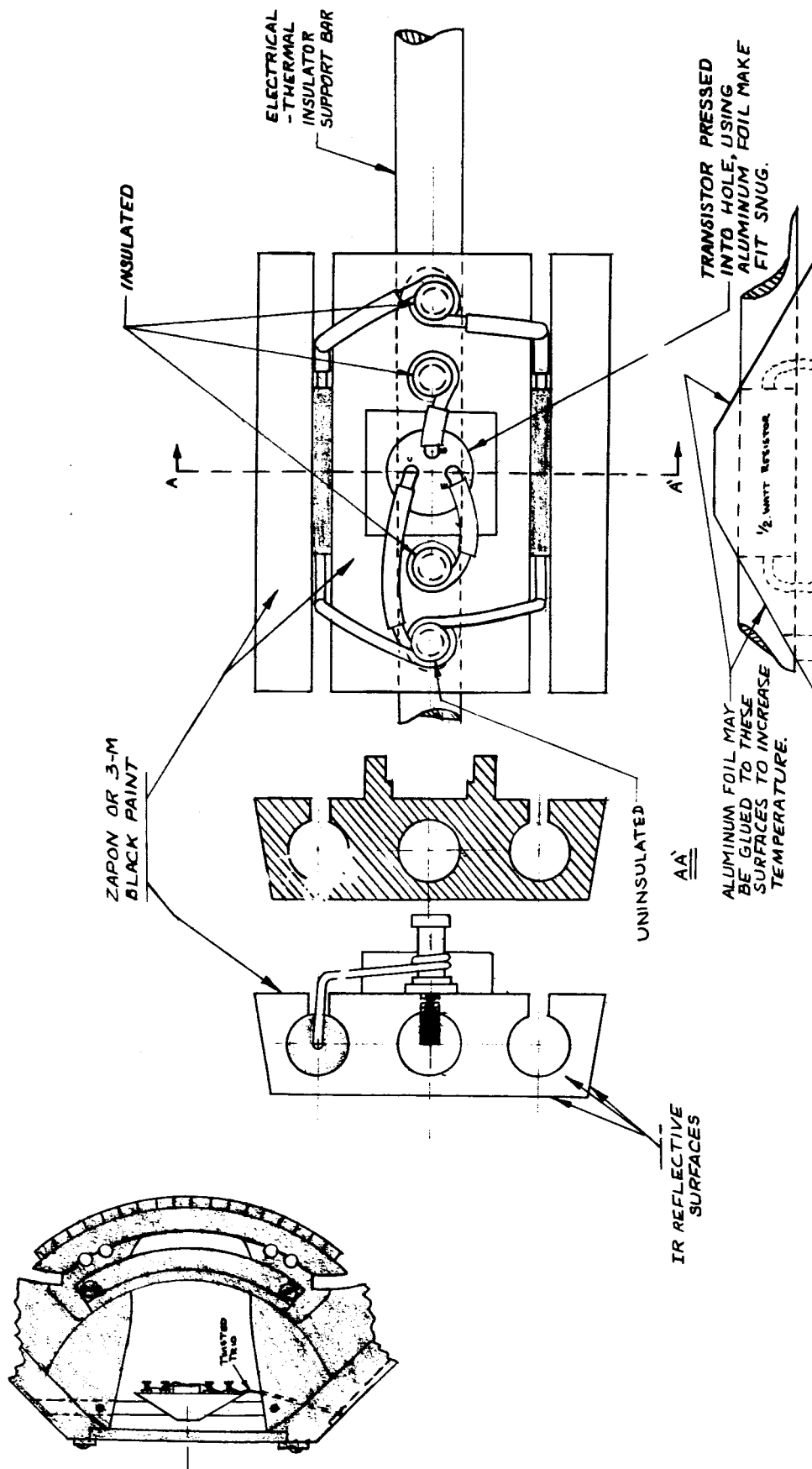


**Figure 4-7 OFFSET HEAT SOURCE, LUNAR AND PLANETARY HORIZON SENSOR**  
 BARNES ENGINEERING COMPANY 2916





as a criteria, the maximum difference between radiation received and radiation emitted is  $10^{-5}$  watts/cm<sup>2</sup>. In the worst case, if a detector is 0.01°C different from another detector, the difference in radiation will be equivalent to a 0.5 microvolt signal. Since the system must be stable over five detectors to eliminate foreign bodies, the maximum temperature difference between these detectors is 0.01°C. The most critical detectors are those in the middle of the bridge, where the thermal gradient is highest for heat conducted from one side of the bridge to the other. Since the system frequency response extends to one cps, there must be less than 0.01°C across the 40 central detectors to avoid gradients that would eventually cross the threshold. This means that the maximum temperature difference across the entire bridge structure is 0.03°C, as shown in calculation (4).

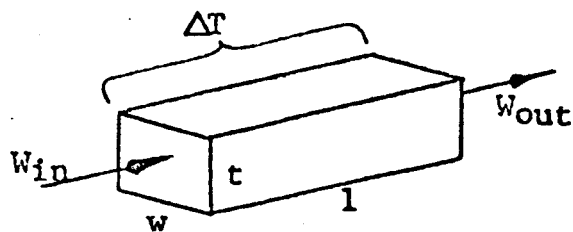
#### 4.6.2 Optical Head

The worst case static gradient occurs if the sun is shining on a side perpendicular to the detector bridge in the Venus orbit (assuming all surfaces are blackbodies, and the radiated side is thermally connected to two other radiating surfaces and to the mounting flange). Calculations (5) through (8) show that this circumstance results in a 0.69°C temperature difference across the bridge. If superinsulation is used, calculations (9) through (12) show that the resulting difference of 0.008°C is considerably less than the 0.03°C maximum difference allowed across the detector bridge. Clearly, an absorptive outer surface is not the most desirable, and higher reflectivity will further reduce solar effect.

Direct solar radiation of the silicon window results in excessive heating (13) unless the window is thermally connected to the optical housing (i.e., with thin mylar tape, shown in calculation (14) and (15). A more conductive thermal connection will further reduce the window temperature. An estimate of gradient across the window (16) shows approximately 1.4°C, which is quite tolerable.

#### 4.6.3 Commutator

The heated commutator is also a critical thermal structure, especially since heat can be transmitted to the detectors through the printed circuit leads.



Static Case:

$$W_{in} = W_{out}$$

$\Delta T$  unvarying with time

$$\text{Thermal Cond.} \times \text{Temp. Difference} \times \text{Width} \times \frac{\text{Thickness}}{\text{Length}} \times 4.186 = \text{Watts Transmitted}$$

$$\frac{\text{cal/cm}}{\text{sec}^\circ\text{C} \times \text{cm}^2} \times ^\circ\text{C} \times \text{cm} \times \frac{\text{cm}}{\text{cm}} \times 4.186 \frac{\text{watts}}{\text{cal/sec}} = \text{watts}$$

FORTY DETECTORS, CENTER BRIDGE				
①	.5	.01	.4 *	1.5 *
				4 x 8
				4.186
				=
				.004 w.
HEAT THROUGH HEAT SHUNT				
③	.5	.019	1.0	.3
				4.0 *
				4.186
				=
				.003 w.
WATTS THROUGH SUPERINSULATION INTO SURFACE X.				
⑪	$2 \times 10^{-6}$	37.8	10	10
				<del>4.186</del>
				=
				.015 watts
WATTS FROM WINDOW THROUGH 0.01 CM. MYLAR STRIP AROUND EDGE				
⑬	$2.5 \times 10^{-4}$	3	21	.3
				4.186
				=
				1.98 watts
THERMAL CONDUCTANCE OF LEADS BETWEEN COMMUTATION AND OPTICAL HEAD				
⑮	.9		120 x .025	.0032
				8
				4.186
				=
				.00452 $\frac{\text{watts}}{^\circ\text{C}}$

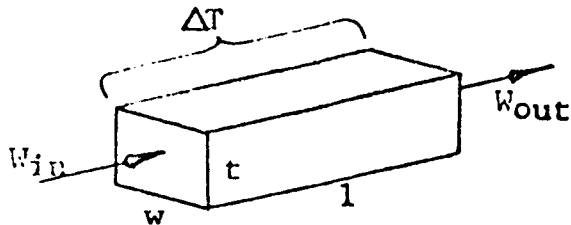
OR 221  $^\circ\text{C}/\text{watt}$

$$\frac{\text{Watts Transmitted} \times \text{Length}}{\text{Thermal Cond.} \times \text{Width} \times \text{Thickness} \times 4.186} = \text{Temp. Difference}$$

BETWEEN HEAT SHUNT SCREWS THROUGH BRIDGE				
②	.01 $^\circ\text{C}$	.5	1.5 *	.5
				4.186
				=
				.019 $^\circ\text{C}$
END TO END OF ENTIRE BRIDGE				
④	.019 $^\circ\text{C}$	.5	3.0 *	.4
				4.186
				=
				.030 $^\circ\text{C}$
WATTS CONDUCTED AWAY FROM SURFACE A TO MOUNTING FLANGE				
⑥		.5	10	.5 *
				4.186
				=
				32.2 $^\circ\text{C}$
TEMP. DIFFERENCE END TO END OF BRIDGE DUE TO SUN RADIATION				
⑧		.5	10	.5 x 2
				4.186
				=
				.69 $^\circ\text{C}$ > .030
WATTS CONDUCTED AWAY FROM SURFACE A TO MOUNTING FLANGE				
⑩		.5	10	.1
				4.186
				=
				37.8 $^\circ\text{C}$

\* APPROXIMATE

# THERMAL WORK SHEET



Static Case:

$$W_{in} = W_{out}$$

$\Delta T$  unvarying with time

Thermal Cond. X Temp. Difference X Width X  $\frac{\text{Thickness}}{\text{Length}}$  X 4.186 = Watts Transmitted

$$\frac{\text{cal/cm}^2 \times \text{sec}^{\circ}\text{C} \times \text{cm}^2}{\text{sec}^{\circ}\text{C} \times \text{cm}^2} \times \text{cm} \times \frac{\text{cm}}{\text{cm}} \times 4.186 \frac{\text{watts}}{\text{cal/sec}} = \text{watts}$$

THERMAL CONDUCTANCE OF LEADS  
BETWEEN COMMUTATOR & PLUG CONNECTOR

(10) .9 20 X .0625

.0064

4.186

.0020  $\frac{\text{WATT}}{^{\circ}\text{C}}$

OR 500  $^{\circ}\text{C/WATT}$

OPTICAL HEAD - MAIN HEAT SHUNT THROUGH  
4 MIL MYLAR TO COPPER LANDS @ -40

(11)  $2.5 \times 10^{-4}$  120 X .030

15

4.186

2.26  $\frac{\text{WATT}}{^{\circ}\text{C}}$

OR .444  $^{\circ}\text{C/WATT}$

OPTICAL HEAD - HEAT SHUNT TO  
DETECTOR HEAT SHUNTS (SHORTEST WIRE)

(21) .9 120 X .010

.0032

4.186

.0058  $\frac{\text{WATT}}{^{\circ}\text{C}}$

OR 173  $^{\circ}\text{C/W}$

OPTICAL HEAD - DETECTOR HEAT SHUNTS  
THROUGH 4 MIL MYLAR TO -40 $^{\circ}\text{C}$  LANDS

(22)  $2.5 \times 10^{-4}$  120 X .015

2.5

4.186

.0941  $\frac{\text{W}}{^{\circ}\text{C}}$

OR 10.6  $^{\circ}\text{C/W}$

OPTICAL HEAD - THERMAL CONDUCTANCE  
THROUGH MAIN SUPPORT

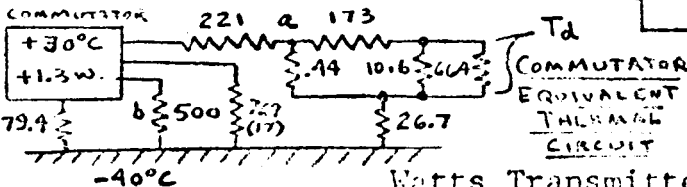
(23)  $2 \times 10^{-4}$  7

.5

4.186

.0375  $\frac{\text{W}}{^{\circ}\text{C}}$

OR 26.7  $^{\circ}\text{C/W}$



a - 120 LEADS SUM  
b - 20 LEADS SUM

Watts Transmitted X Length  
Thermal Cond. X Width X Thickness X 4.186 = Temp. Difference

TEMP. DIFFERENCE END TO END  
OF BRIDGE DUE TO SOLAR  
RADIATION WITH

(12) SUPERINSULATION .5

.015

12

.5 X 2

4.186

.008  $^{\circ}\text{C}$

< .030

TEMP DIFFERENCE FROM  
CENTER TO EDGE OF WINDOW  
ASSUME 1/2 CONDUCTED

(16) WATTS AT CENTER .19

$\frac{2.13}{3}$

2

.3

4.186

.47  $^{\circ}\text{C}$

EQUIVALENT DETECTOR  
IMPEDANCE - TERMINAL AREA

(24)  $2.5 \times 10^{-4}$  .02

$6.3 \times 10^{-4}$

.045

4.186

664  $^{\circ}\text{C/W}$

TEMPERATURE ACROSS  
COMMUTATOR SUPPORTS

(25) (POLYETHYLENE)  $2 \times 10^{-4}$   $6 \times 2.50$

1.30 - .42 = .88 WATTS

1

4.186

70  $^{\circ}\text{C}$

IMPEDANCE = 79.4  $^{\circ}\text{C/W}$

TD RESULTING TEMP.  
ACROSS DETECTOR

(26) 248.1  $^{\circ}\text{C/W}$

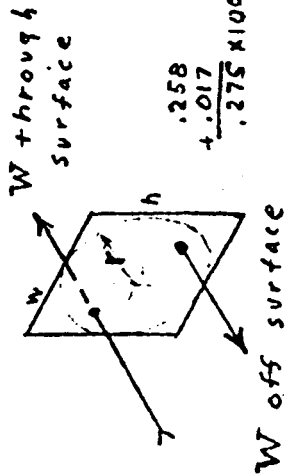
70  $^{\circ}\text{C}$

.442  $^{\circ}\text{C/W}$

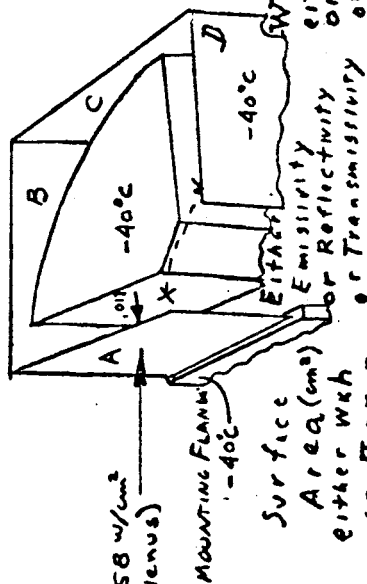
10.4  $^{\circ}\text{C/W}$

.007  $^{\circ}\text{C}$

THERMAL WORK SHEET



ASSUME SURFACE B AND COVER (SHOWING) AT TA AND RADIATING. CONDUCTION LOSS FROM A TO MOUNTING FLANGE.



Additional  
conversions  
or Notations  
(if Any)

Surface #	Apparant Temp. $^{\circ}\text{F}$	Spectral Band	Limits	% of Total
		Turner 2		$\frac{\%}{100}$
		Coltate 2		$\frac{\%}{100}$
		Total		$\frac{\%}{100}$

5	A, B, & COVER (BOTH SIDES)	267°K	<del>0-14</del> <del>14-∞</del> <del>0-∞</del>	<del>REFLECT.</del> <del>STRENGTH</del> <del>ABSORB.</del>	<del>0.029</del> <del>0.029</del> <del>0.017</del> <del>0.012</del>	<del>6 x 10 x 10</del> <del>10 x 10</del> <del>x x</del>	<del>1</del>	<del>17.4 Watts</del> <del>EMITTED</del>	<del>27.5 - (17.4 - 2(1.7)) = 13.4</del> <del>267°K - 31.2° = 234.8</del> <del>OR 235</del>
6	A, B, & COVER (ONE SIDE)	233°K	<del>0-14</del> <del>14-∞</del> <del>0-∞</del>	<del>REFLECT.</del> <del>STRENGTH</del> <del>ABSORB.</del>	<del>0.029</del> <del>0.017</del> <del>0.012</del>	<del>10 x 10</del> <del>x x</del>	<del>1</del>	<del>1.2 Watts</del> <del>RED</del>	<del>USING SUPERINSULATION -10.0</del> <del>BETWEEN A AND X</del> <del>275 - 37.8 = 237.2°K</del> <del>15</del>
7	A, B, & COVER (ONE SIDE)	275°K	<del>0-14</del> <del>14-∞</del> <del>0-∞</del>	<del>REFLECT.</del> <del>STRENGTH</del> <del>ABSORB.</del>	<del>0.033</del>	<del>3 x 10 x 10</del> <del>x x</del>	<del>1</del>	<del>10.0 Watts</del> <del>EMITTED</del>	<del>WINDOW INSULATED, NORMAL TO SUN. HOUSING AT +70°</del>
8	SOLAR RADIATION INTO WINDOW (VENUS)	493°K	0-14 14-∞ 0-∞	.5 REFLECT. .5 STRENGTH .5 ABSORB.	.258 .078 .336 2	3.5 x 7 x x	.5	8.2 Watts EMITTED	ASSUMING .01 CM MYLAR STRIPESOUND EDGE. OTHER SAME AS (3),
9	SOLAR RADIATION INTO WINDOW (VENUS)	346°K		- SAME	.336 -.081 x 2 .174	3.5 x 7 x x	.5	2.13 Watts CONDUCTED	
10	COMBINATION RADIATION (EMITTED ALUMINUM)	303°CON 233° CASE	303 233 ΔT	.048 .020 .028	.028	2 x 18 x 18 x	.1	1.8 Watts	SUPER INSULATION IS NECESSARY.
11				- (17) CONT.	Power Then SUPERINSULATION	2 x 10' x 70" x 2 x 18 x 18 A		.091 Watts	WITH SUPERINSULATION THERMAL CONDUCTANCE = .0013 5.11-23 H <sup>2</sup> IMPEDANCE = 769

In vacuum, the assembly dissipates up to 1.3 watts at  $-40^{\circ}\text{C}$  to maintain  $+30^{\circ}\text{C}$  at the commutator. Superinsulation is used, as thermal losses would be excessive without it (17). The remaining losses occur through the lead assemblies and through the supports, as given in calculations (18) through (25). The temperature difference produced across the detector with a  $70^{\circ}\text{C}$  temperature difference at the commutator is  $.007^{\circ}\text{C}$  maximum (26). This would produce .84 microvolts from the first thermocouple pair if the hot junction were at the housing temperature. The next cold junction (with fifty times the conductance of the leads) creates a temperature divider so that the first pair actually only sees  $.0035^{\circ}\text{C}$ , or a .42 microvolts. In reality the error voltage will be much less, because additional gold lead area will be deposited that has not been considered. Lead terminations and connections will also provide thermal impedance. An equivalent thermal circuit is shown on the third calculation block, giving thermal impedances in proper arrangement.

#### 4.6.4 Dynamic Analysis

The result of temperature variations on the outer housing is to produce thermal gradients on structures having distributed thermal conductivity and heat capacity. The only structure under consideration which is sensitive to small gradients and which may be expected to exhibit them under dynamic conditions is the detector bridge. As shown in Section 4.5.1, a gradient of  $0.01^{\circ}\text{C}$  between any five of the central forty detectors or  $0.02^{\circ}\text{C}$  from center to end is the maximum permissible variation.

Because of the heat mass of the optical case and the mounting arrangement, the detector bridge is considered to be entirely symmetrical. As case temperature rises, heat flows into the bridge from both ends at a rate determined by the thermal conductivity and capacity. No heat flows past the center of the bridge because of the symmetry, and consequently the bridge may be split at the middle, and only a half section considered.

The equation for heat transfer in the one dimensional case is:

$$K \frac{\partial^2 T}{\partial x^2} = \frac{\partial T}{\partial t} \quad (1)$$

where  $K = \frac{\text{Thermal Conductivity}}{\text{Heat Capacity}}$ , both a function of  $x$ .

A constant rate of change is considered, so that:

$$\frac{T}{t} = M \quad (2)$$

For a constant area bar,  $K$  is constant, and the solution of the equation is:

$$T = \frac{M}{K} = \frac{x^2}{2} \quad (3)$$

Using c.g.s. units, the rate necessary to produce a temperature difference of  $.02^\circ\text{C}$  across 5 cm on an aluminum bridge with linear array is:

$$M = \frac{.02 \times .715 \times 2 \times 3600}{5 \times 5} = 4.1^\circ\text{C/hr.} \quad (4)$$

which is not satisfactory.

To simplify the analysis, the equation remained one dimensional, and the variation in area was treated as a variation in  $K$ . Integrating equation (1):

$$\frac{T}{x} = M \int_0^x \frac{dx}{K(x)} \quad (5)$$

Thermal conductivity is proportional to the cross-sectional area,  $Y$ , for any point  $x$ , while heat capacity is proportional to the volume up to point  $x$ . Thus the gradient at a point  $x$  can be described as the calories into volume from zero to  $x$  through the area  $Y$ :

$$\frac{T}{x} = \frac{M}{K} \frac{\int_0^x Y dk}{Y} \quad (6)$$

This equation was solved with boundary conditions:

$$\begin{aligned} T &= 0 \\ \frac{T}{x} &= 0 \quad \text{at } x = 0 \quad Y = 10 \text{ cm}^2 \quad \text{at } x = 10 \text{ cm} \\ Y &= 1 \text{ cm}^2 \end{aligned} \quad (7)$$

Various functions for Y were assumed, and several significant cases are shown in Table 4-1. The resulting temperature variation is shown in Figure 4-9. The best cases were the  $x^3$  (No. 4) and the complex bar (No. 6). The rate necessary to produce maximum temperature difference can be obtained by multiplying the rate given in the table for the linear array by  $(.02^\circ\text{C}/5\text{ cm})$  and dividing by  $(.05^\circ\text{C}/\text{cm})$  to adjust thermal gradient from that assumed in the original calculation. This number is multiplied by four to convert from 10 cm to five cm of length, as temperature gradient are proportional to the square of length. For case No. 4, the rate to produce maximum temperature difference is:

$$M = \frac{39.5 \times .02 \times 4}{.05 \times 5} = 12.6^\circ\text{C}/\text{hr}.$$

For case No. 6, the rate is  $13.5^\circ\text{C}/\text{hr}$ . The actual detector bridge design closely resembles these functions.

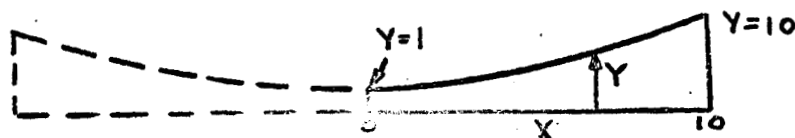
In addition, cuts were made at the end of the detector array which effectively halved the distance from the support to the end detectors, giving a four times increase in allowable rate, or up to  $55^\circ\text{C}/\text{hr}$ . In addition, these cuts tend to place the detector array on an isothermal, giving further insensitivity to housing variations.



TABLE 4-1

## Temperature Distribution Along Detector Support Bar

Heat Transfer Equation:  $\frac{M}{K} \frac{\int Y dX}{Y} = \frac{\partial T}{\partial X}$  where  $M = \frac{\partial T}{\partial t}$ , constant over entire bar.



$K$  = Thermal diffusivity  
(conductivity/capacity)

Detectors distributed linearly or  
with variable spacing along  $X$ .

No.	Y (Area)	T (Temperature)	$T_{10}^*$	$\frac{\partial T^*}{\partial X}_{10}$	$M_{\max} (^{\circ}\text{C/hr})$	
					Linear	Variable
1	C (constant)	$X^2/2$	$50^{\circ}\text{C}$	10	12.9	1.55
2	$.9X + 1$	$X^2/4 + X/1.8 - (1/1.62)$ $(\log(1+.9X))$	29.1	4.5	28.6	3.43
3	$.09X^2 + 1$	$X^2/6 + (1/.27)(\log(\frac{X^2+11.1}{11.1}))$	25.2	4.0	32.2	3.87
4	$.009X^3 + 1$	$X^2/8 + 2.89(\log(\frac{X^2-4.81X+4.81^2}{(X+4.81)^2}))$ $+10.2 \left[ \tan^{-1}(\frac{2X-4.81}{8.45}) + \frac{\pi}{6} \right]$	25.6	3.3	39.5	4.74
5	$e^{.23X}$	$4.34X + 18.88(e^{-.23X} - 1)$	26.4	4.8	26.9	3.23
6	C @ $0 < X < 3$ .371 $e^{.329X}$ @ $3 < X < 10$	$X^2/2$ @ $0 < X < 3$ and the following @ $3 < X < 10$ : $3.04X - .045 e^{-.329X} - 4.49$	25.9	3.0	42.3	5.07

All solutions were obtained with  $T = 0$  and  $\frac{\partial T}{\partial X} = 0$  at  $X = 0$ .

Maximum thermal time rate ( $M_{\max}$ ) is for  $.05^{\circ}\text{C}/\text{unit length}$  for the linear spacing and  $.006^{\circ}\text{C}/\text{unit length}$  for the variable spacing, calculated at  $X = 10$  in all cases (point of maximum gradient). Aluminum appears to be the best practical material, with  $K = .715$ .

\* Assumes  $M/K = 1$ .

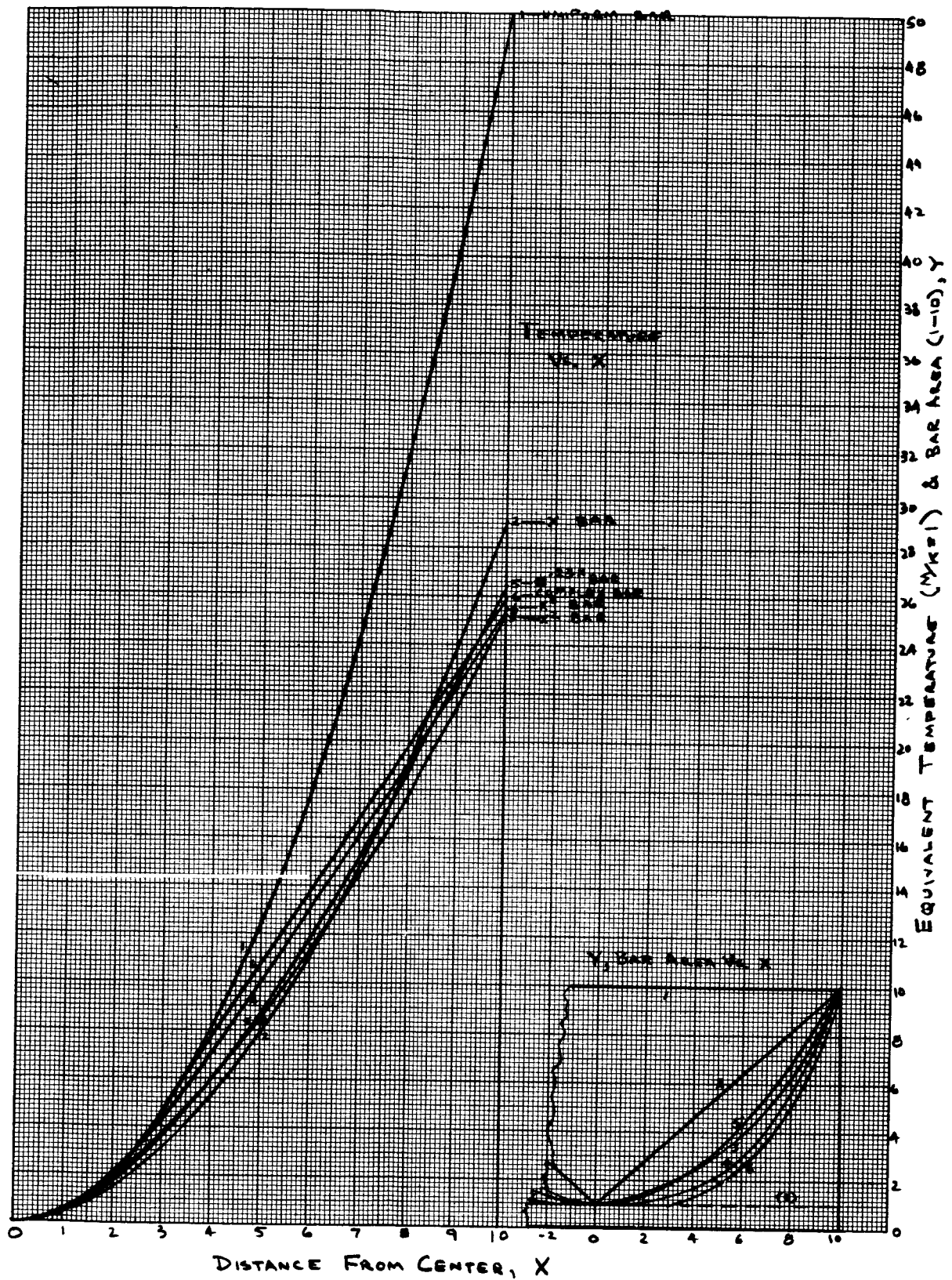


Figure 4-9 TEMPERATURE VS.  $X$

Section 5.0 ELECTRONICS

The various electronic circuits presented in the overall system block diagram (Figure 2-5) are covered in this section. The entire processing is covered, but detailed descriptions are only given for the circuits that are necessary to provide zero-one type inputs to the output attitude, altitude and alarm circuits. These final output processing circuits are included to indicate one method of utilizing the information present at the outputs of the four signal channels to produce the desired final output signals.

Block diagram 5-1 shows the various circuits that are time synchronized. Sections 5-1 and 5-2 describes the circuits shown in this figure. Block diagram 5-5 shows the circuits that comprise a signal channel. The electronic circuits within these blocks are given full coverage in sections 5-4 through 5-7.

Figures 5-19, 5-24, and 5-28 are block diagrams of the attitude, altitude, and alarm output processing. The circuits presented in these figures are briefly covered in sections 5-8 through 5-15.

5.1 MASTER CLOCK OSCILLATOR

The counting techniques used in this system requires precision timing signals (Figure 5-1) which are generated by an asymmetrical multivibrator shown in Figure 5-2. Accuracy of better than 1% is required to maintain altitude readout accuracy to within one count when the processing presently considered is used. A true digital readout in altitude makes this requirement unnecessary, but introduces additional complexity.

5.2 RING MULTIVIBRATOR

One hundred channel commutation is performed by two cascaded ten count ring counters, which directly control the neon lamp commutator elements. The master clock triggers the first (units) counter, which activates the lines. This in turn triggers the second (tens) counter which activates the bars in the 10 x 10 neon matrix. These two counters perform commutation in all four heads simultaneously.

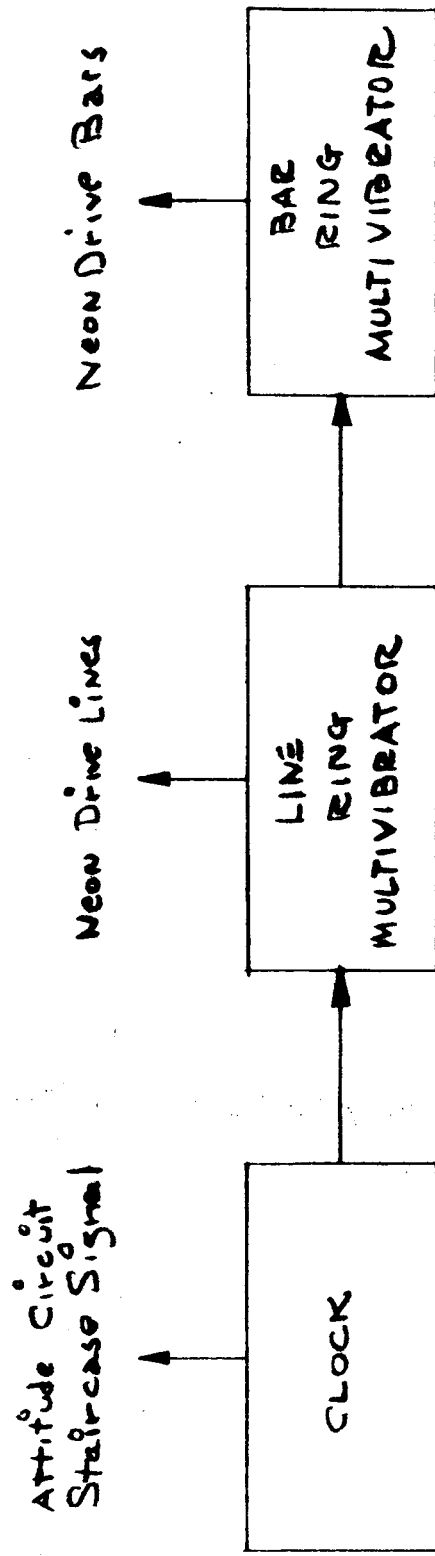


Figure 5-1 Block Diagram: Timing & Commutator Drive Circuits

20,027

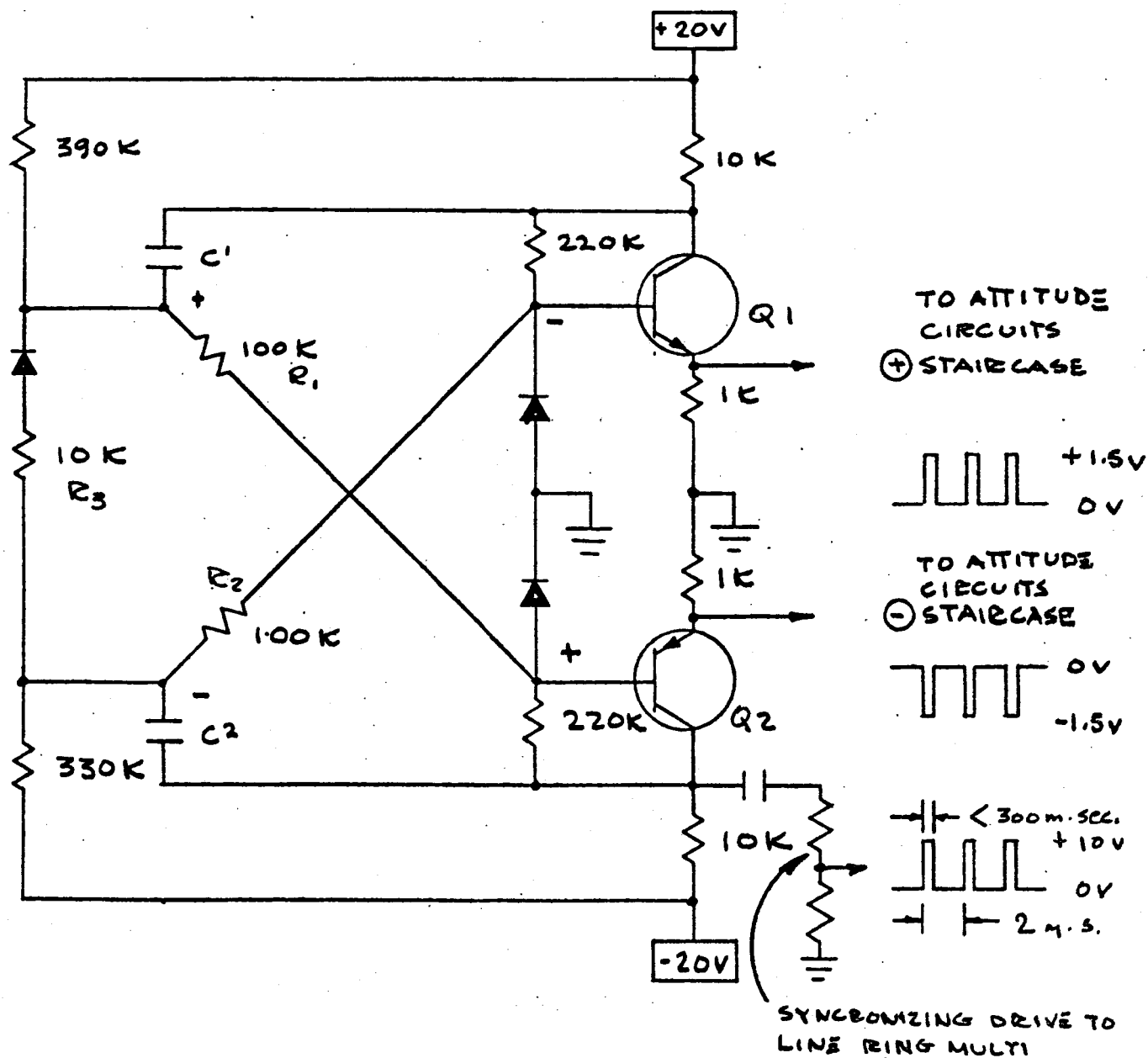


Figure 5-2 MASTER CLOCK OSCILLATOR 20,028

The basic circuit, shown in Figure 5-3, is a ten section multivibrator in which one and only one section is conducting during any sample period. Count proceeds from line 0 to line 9 and repeats. The basic operation can be seen in the waveforms given in Figure 5-4.

When the circuit is first turned on, a transistor will begin conducting, since the bases are connected to ground and the emitters to -20 volts. Assuming this transistor is Q8, current from the +10 volt supply flowing through  $R_f$  brings the emitter potential to a positive voltage, preventing any other transistors from turning on. Signal from the +20 volt supply through its base capacitor keeps Q8 conducting until the synchronizing pulse A forces the transistor off (waveform C1). At this time the collector of Q8 jumps positive from +10 volts, and the voltage at B2 rises abruptly. This causes current to flow into the base of Q9 through capacitor  $C_t$ , turning that transistor on (waveform C2). This current decreases as the capacitor discharges until another synchronizing pulse turns Q9 off. Capacitor  $C_t$  continues to discharge through resistor  $R_t$  until it acquires a 20 volt potential across it. The collector potential of Q9 goes positive, as does the capacitor (B3 and C3) continuing the process. Once the cycle begins, all the capacitor voltages vary in sequence insuring the correct stepping order.

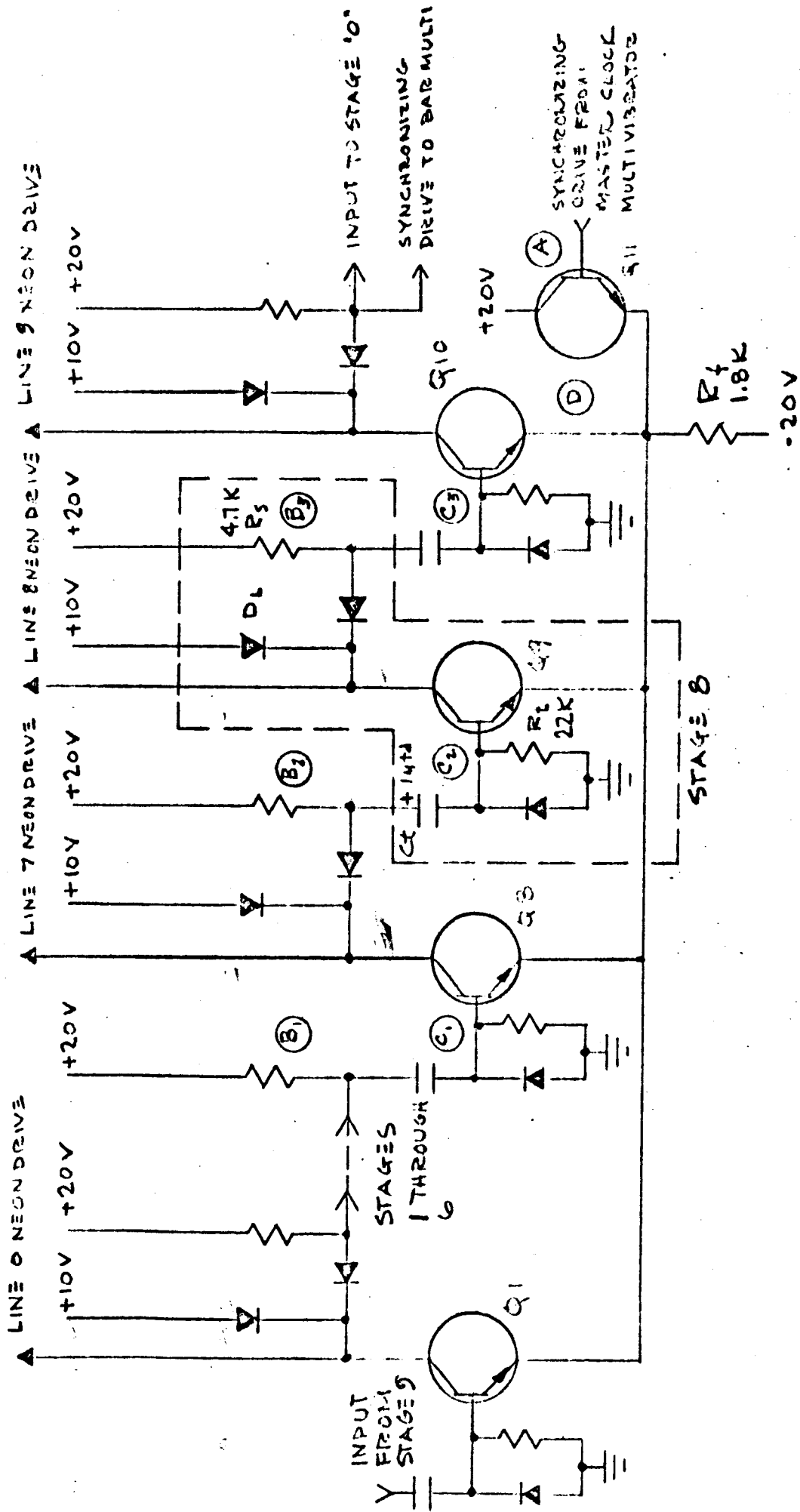
An important point in the design was to insure operation if the current varied from neon to neon, or if the same neon in four heads somehow failed (or a connection opened). This is accomplished by the +10 volt diode coupled supply, which provides the current for the emitter feedback resistor  $R_f$ .

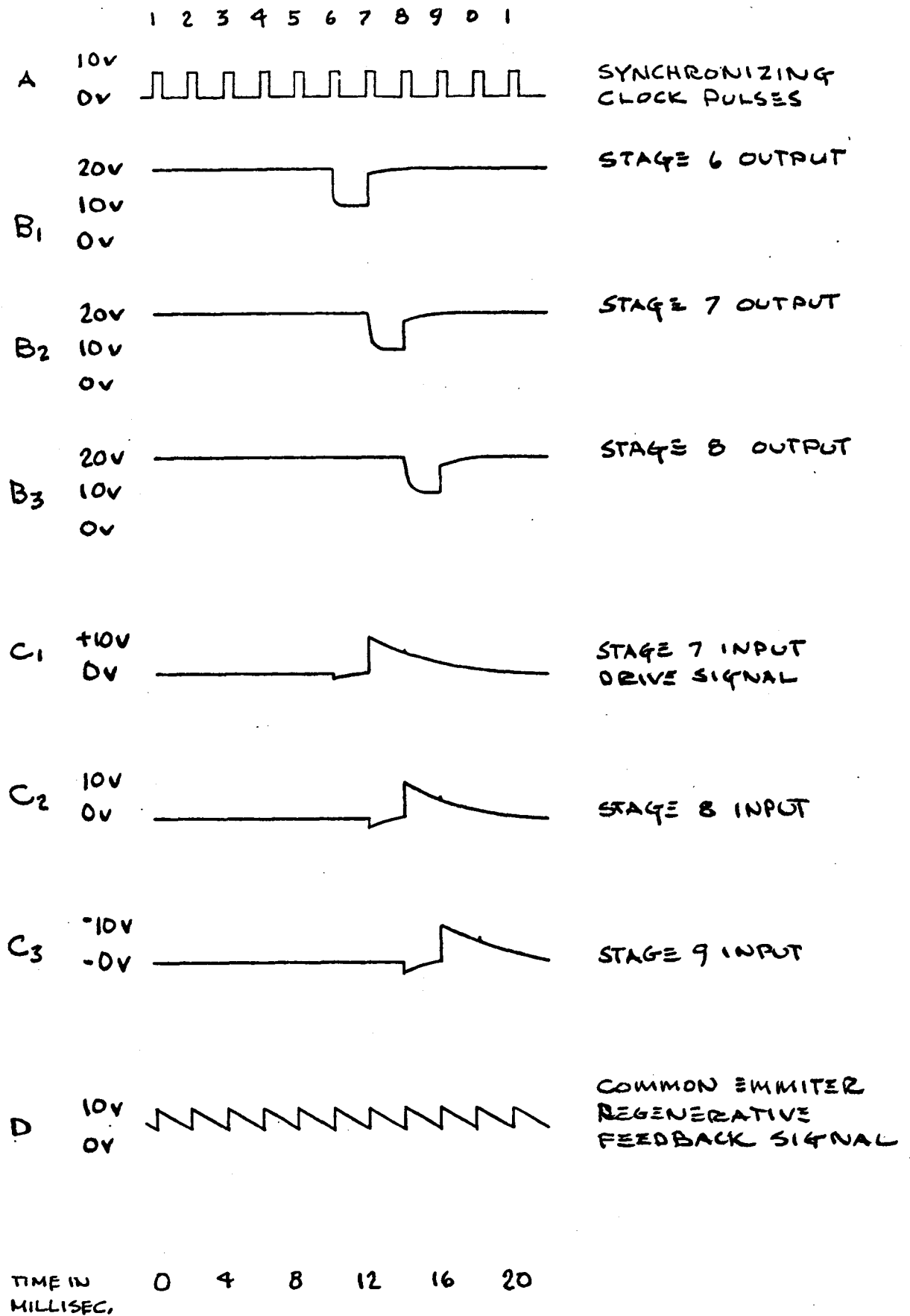
The circuit will also free run at about one third normal speed if no clock drive is present. Timing is much less accurate in this case.

The inverse circuit is used for the bar counter, with PNP transistors in place of NPN's. Other slight modifications necessary are indicated in Figure 5-3.

### 5.3 SIGNAL PROCESSING CHANNEL

Figure 5-5 shows a block diagram of the sensor head with the threshold circuit. Signal flow from detector through to horizon threshold determination and various corresponding feedback links are shown.

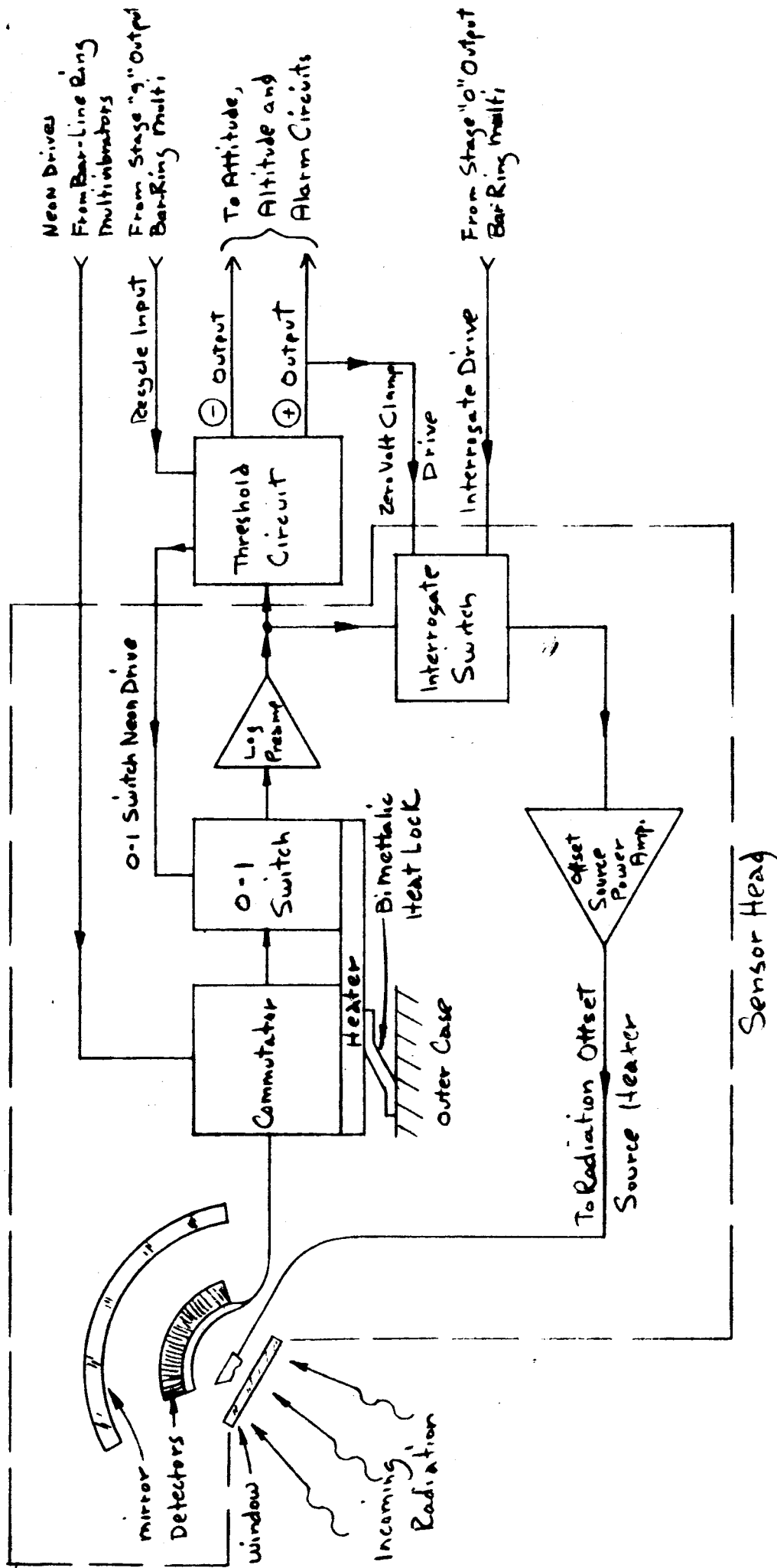




20,030

Figure 5.4 WAVESHAPES, LINE DRIVE RING MULTIVIBRATOR





20,031

Figure 5-5 Single Channel Block Diagram

Commutation and amplification of the detector outputs results in a usable time varying signal. Each apparent horizon crossover is examined on a time basis to determine if it is a spurious foreign body, and reject if it is. Recognition of the time horizon results in output signal from the threshold circuit, which perform various logic functions, including attitude, altitude and spurious body determination. The preamplifier signal also sets the radiation offset heat source.

#### 5.4 COMMUTATOR

Electronically, the commutator is a single pole, ninety-five throw switch which sequentially contacts each of the ninety-five positions, remaining at each position for two milliseconds. Ideally, the switch should make and break simultaneously, exhibiting zero ohms when closed and infinite ohms when open with no contact potentials. The response speed should be practically instantaneous, and very closely follow the switch drive. In addition, capacitive coupling to extraneous varying potentials should be minimized. It should have extremely long life and be minimal in size and power.

Many techniques were considered and abandoned in making this device, including electromechanical switching, fiber optics, electroluminescence, coherent and non-coherent lasing diodes, argon lamps, various neon lamps, and numerous photoresistive materials.

Midget size high brightness lamps (General Electric, Type AIC) were selected to commutate special photoresistive cells made by Opto-Electronic Devices, Inc., using their No. 3 (or possibly No. 4) material. Both cells and lamps will be used in parallel redundancy. Measurements were made on their No. 3 photoresistive material, using the circuit shown in Figure 5-8, which also shows typical waveshapes obtained at temperatures of  $+79^{\circ}\text{C}$ ,  $+25^{\circ}\text{C}$ , and  $-37^{\circ}\text{C}$ . Of significance is the unvarying fast rise (excitation) time and the increasingly slow fall (extinguished) time with low temperatures.

Also of interest is the increase in excited resistance at high temperatures. (The slope of the top of the waveform in Figure 5-8B is a result of the high decay

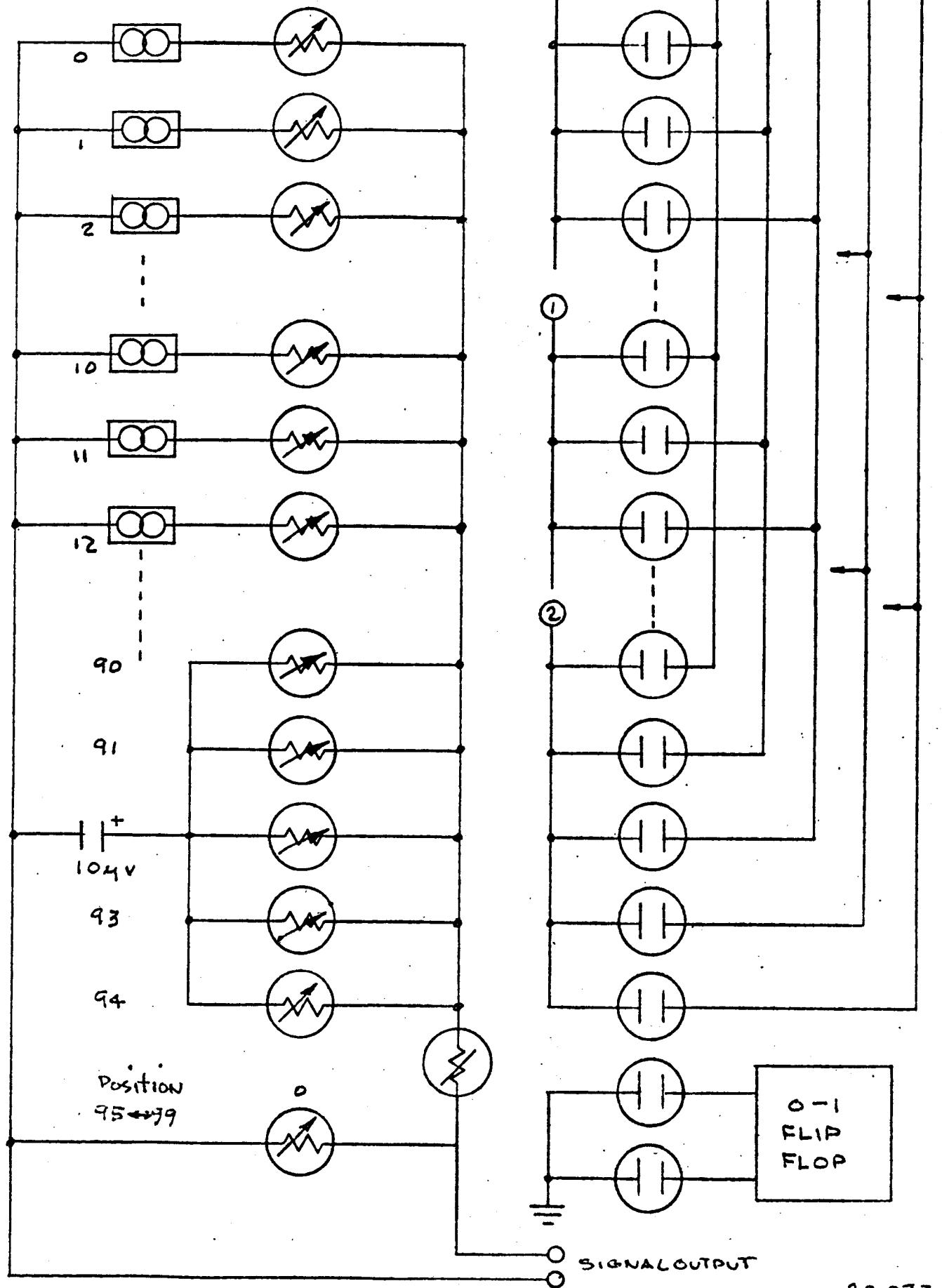
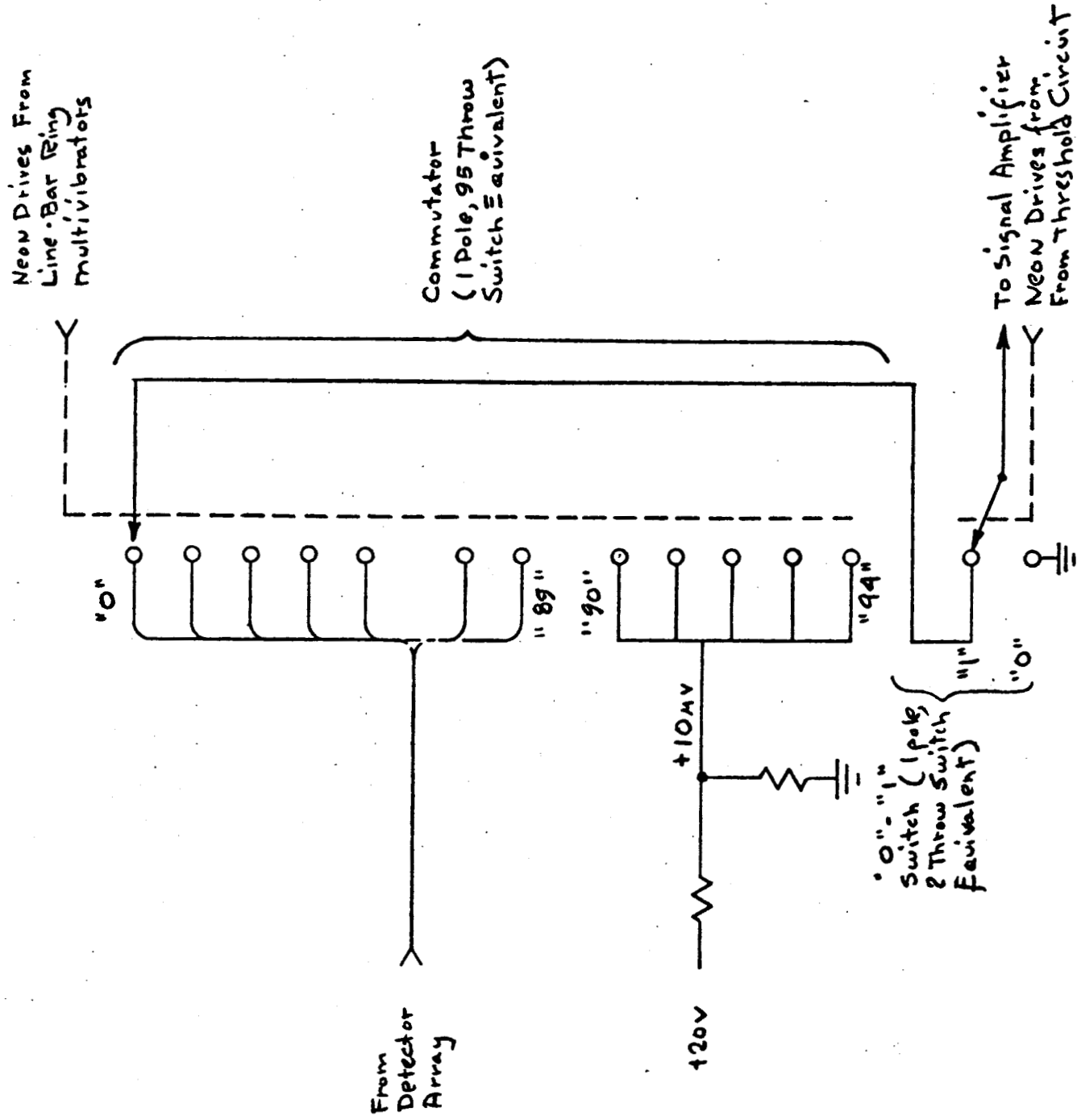


Figure 5-6 Schematic, Detector Switching

20,032



20,033

Figure 5-7 Equivalent Circuit, Detector Switching

# OED-3L5 PHOTO-RESISTOR DATA

Oscilloscope patterns show e in millivolts, t in milliseconds. Right hand scale shows equivalent cell resistance in ohms.

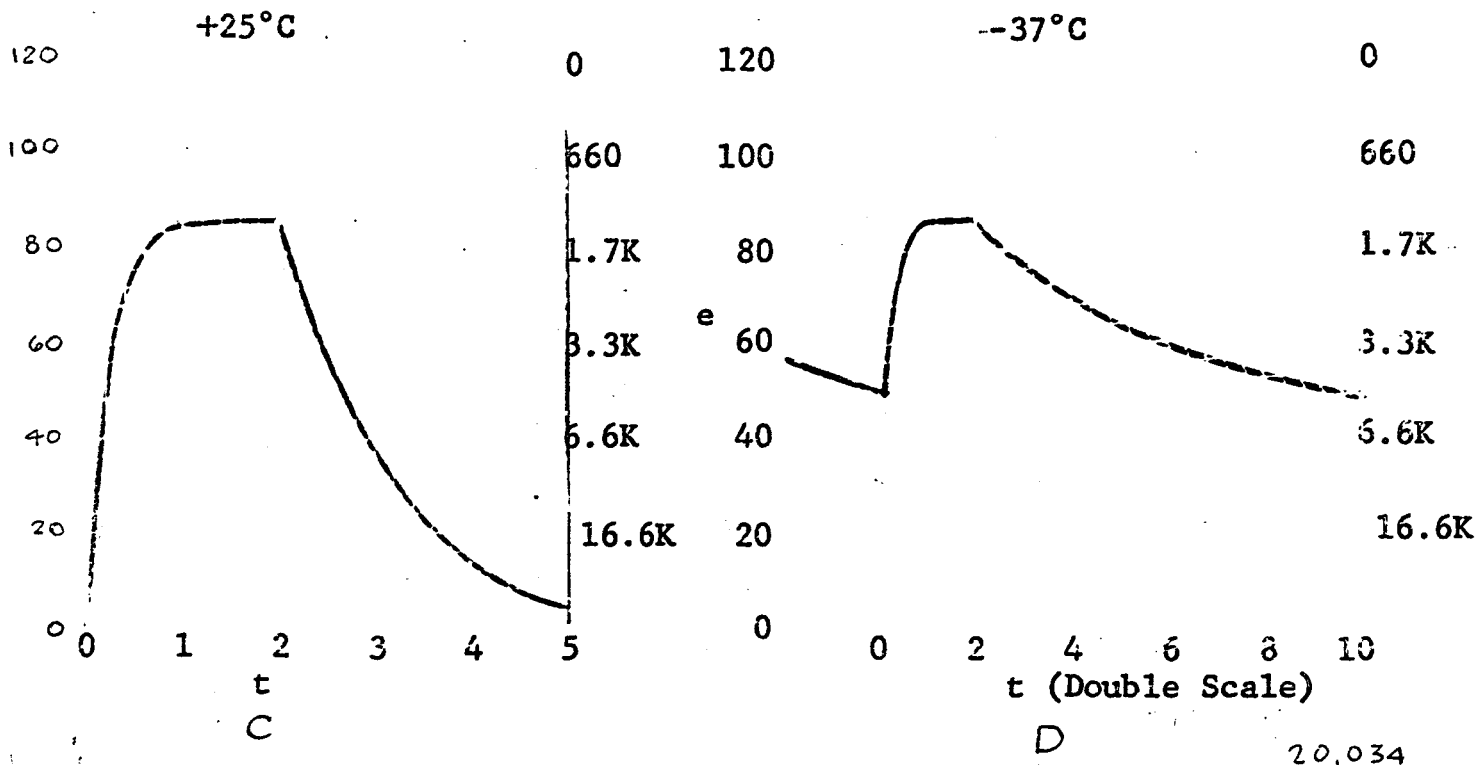
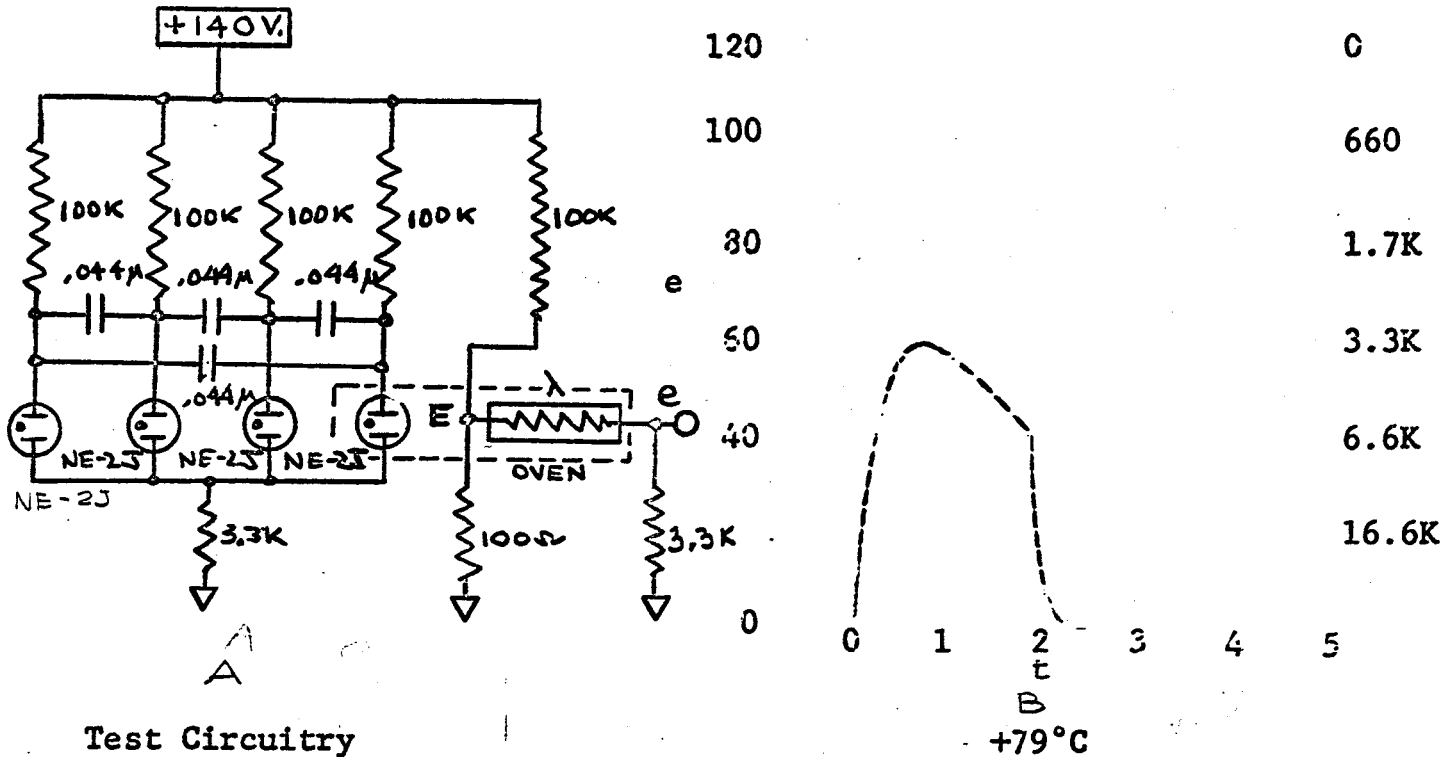


Figure 5-8

response speed, which enables the cell to follow the decrease in neon brightness with current which occurs in the test circuit.)

Figure 5-9 is a summary of the tests performed on these cells, and shows the time variation vs. temperature. When excited the cell responds in less than one millisecond, remaining at the same resistance level (less than 1000 ohms) until the lamp is extinguished. When extinguished, it is essential that the cell reach a high impedance as quickly as possible, since it continues to provide signal while its impedance is low. Assuming a detector viewing the sun and the four adjacent detectors viewing space, the impedance ratio between the sun detector turning off and the fourth space detector turning on must be 1000:1 in the worst case (over 1 megohm). This can be achieved if the photoresistor temperature is not permitted to go below +30°C. Appropriate provisions have been made so that the commutator is heated at temperatures below this temperature.

If the average dark resistance of the cells is over 20 megohms, and the lit resistance cell to cell variations are under 1K ohms, no cross talk problems will occur. The special cells being made for the commutator should easily meet these requirements.

The possibility of non-ohmic terminations producing high resistance junctions for low signal voltages has been investigated. Figure 5-10 shows measurements made on the OED Type 3L5 cell, which shows no appreciable effect. Discussions with OED revealed that they are aware of the problem and will avoid improper terminations.

The cells are excited by neon lamps, which are activated by the line bar ring counter. Voltages up to 180 volts are present at the neon lamps, and electrostatic coupling is reduced by a one half inch separation of the cells from the neons. Further reduction can be achieved if necessary by grounded screening over the cells.

The neons will be activated with 2 milliamps, which brings them well into the high brightness region. The anticipated life of the commutator neons, (based on duty cycle and manufacturers life expectancy figures with 2 milliamps of excitation current) is approximately a million hours.

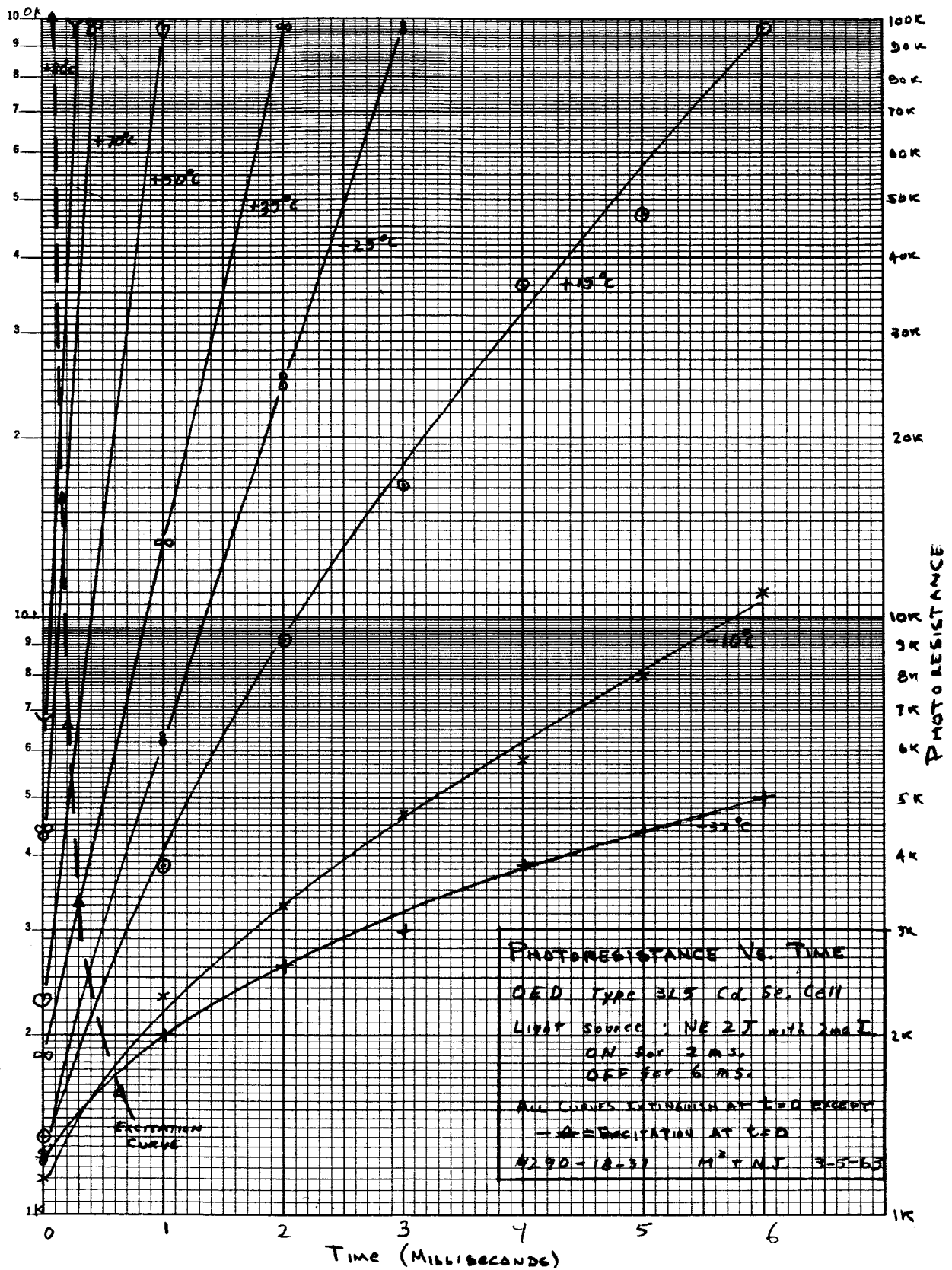


Figure 5-9 PHOTORESISTANCE VS. TIME

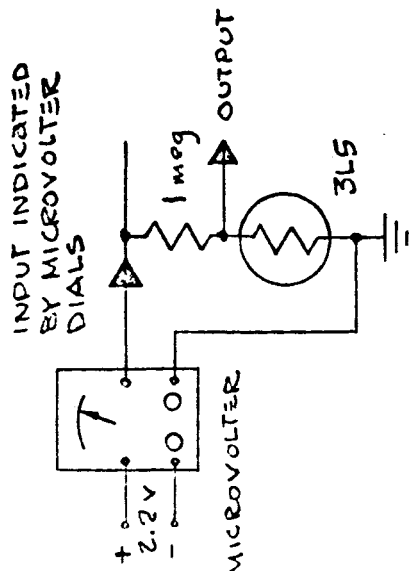
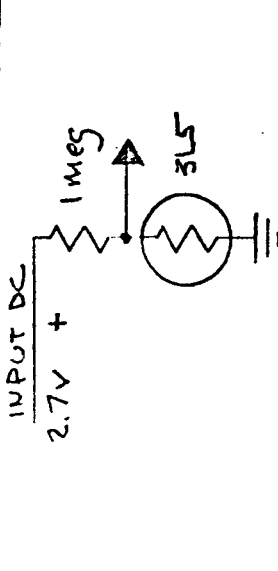
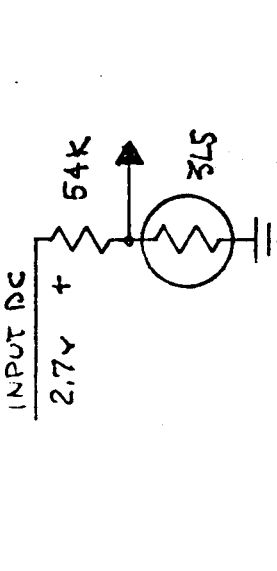
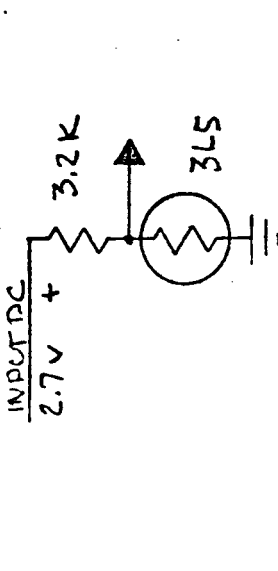
	INPUT INDICATED BY DIALS	OUTPUT (METER)	OUTPUT (SCOPE)	I THROUGH PHOTOCELLS	R OF PHOTOCELLS	
	0	47 $\mu$ v	No Reading Because of Thermal Effect			
	30 mv	100 $\mu$ v				
	524 mv	1 mv				
	1 v	1.8 mv				
	DC Input (Scope)					
	2.7 v	5 mv	5 mv	2.7 $\mu$ a	1.85 k $\Omega$	
		DC Input (Scope)				
	DC Input (Scope)					
	2.7 v	100 mv	100 mv	48 $\mu$ a	2.1 k $\Omega$	
		DC Input (Scope)				
	DC Input (Scope)					
	2.7 v	1 v	1 v	531 $\mu$ a	1.9 k $\Omega$	
		DC Input (Scope)				

Figure 5-10 Cd. Se. Cell Resistance vs. Voltage



## 5.5 SIGNAL AMPLIFIER DESCRIPTION

The signal amplifier shown in Figure 5-11 is designed to produce a logarithmic output response as a function of the input signal (Figure 5-11). In addition, both the low and high frequency cutoffs vary as a function of the instantaneous signal level. These characteristics effectively compress the 500 to 1 anticipated input signal dynamic range to 50 to 1, and produce minimum noise at low signal levels by providing minimum bandwidth when low level signals are being received. With high instantaneous signal levels, the bandwidth is extended to permit rapid return to space level after scanning through the sun without producing excessive overshoot. If excessive overshoot occurred, it would not be possible to tell if the level reached while scanning a cold moon surface immediately subsequent to viewing a hot moon horizon region corresponds to space or the cold moon surface.

### 5.5.1 Gain Considerations

The amplifier configuration shown in Figure 5-11 utilizes both fixed internal and variable overall negative feedback stabilization to control the overall gain and frequency response characteristics. Transistors Q1, Q2, and Q3 provide the forward loop gain, and resistors R6, R7, and R8 set the forward loop gain at a million.

Output transistor Q4 provides phase inversion to drive the field effect transistor Q5. Transistor Q5 acts as a variable resistor to control the overall negative feedback around transistors Q1 through Q3. This varies the overall amplifier gain from  $10^5$  to  $5 \times 10^3$  as the output signal varies from 0 to 5 volts.

The field effect transistor (Q5) is operated in the non-pinchoff region of its characteristics, and therefore acts as a voltage controlled resistive element. The control input is provided to the gate terminal of Q5 from the amplifier's final output through R15. With changes of gate-source potentials from 0 to +5 volts, the drain to source resistance varies from under 1K ohms to over 100K ohms. The speed of response and input-to-output isolation is adequate to cause no difficulties over the amplifier's normal amplitude and frequency range.

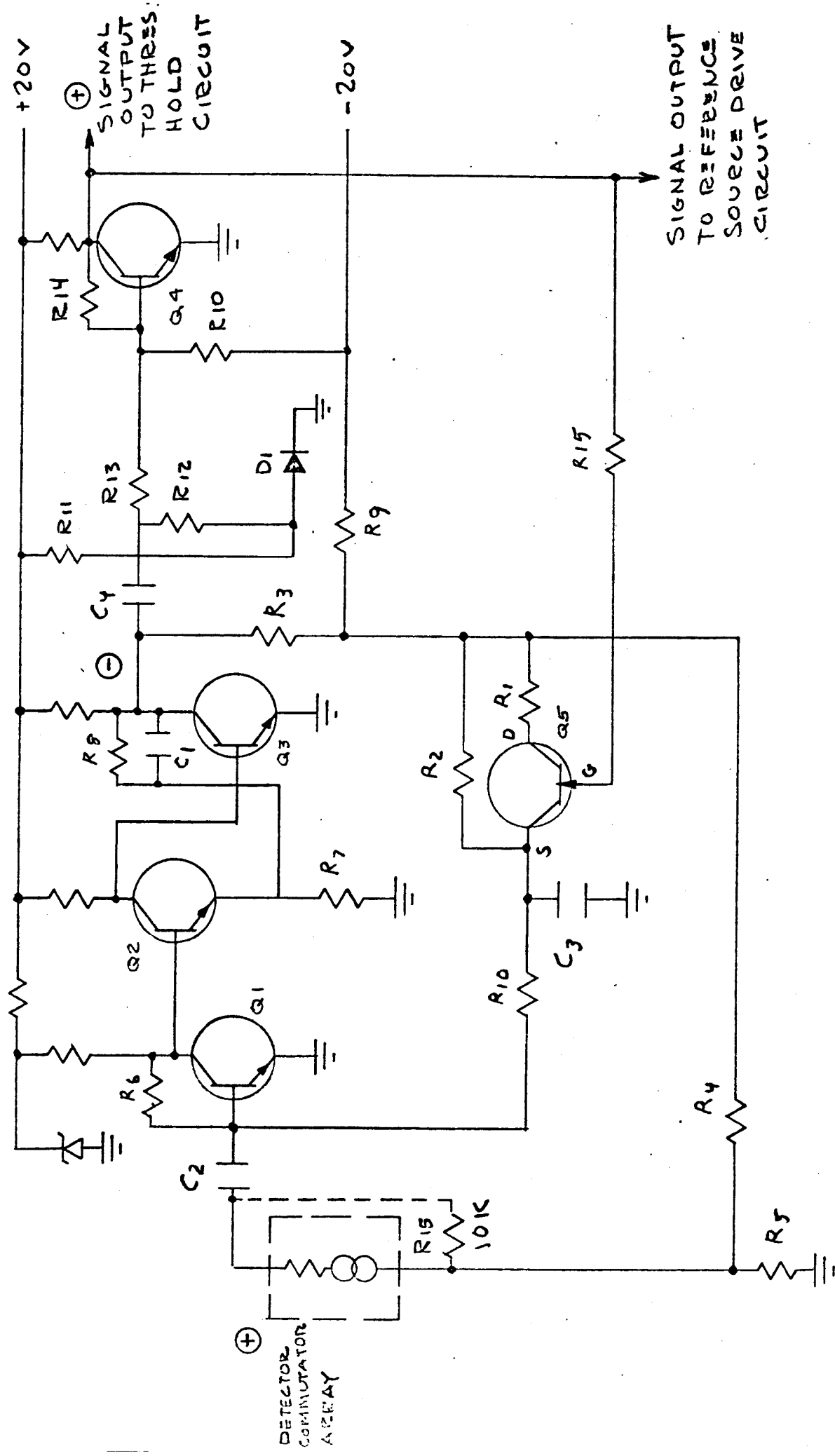


Figure 5-11 Logarithmic Signal Amplifier

20,037

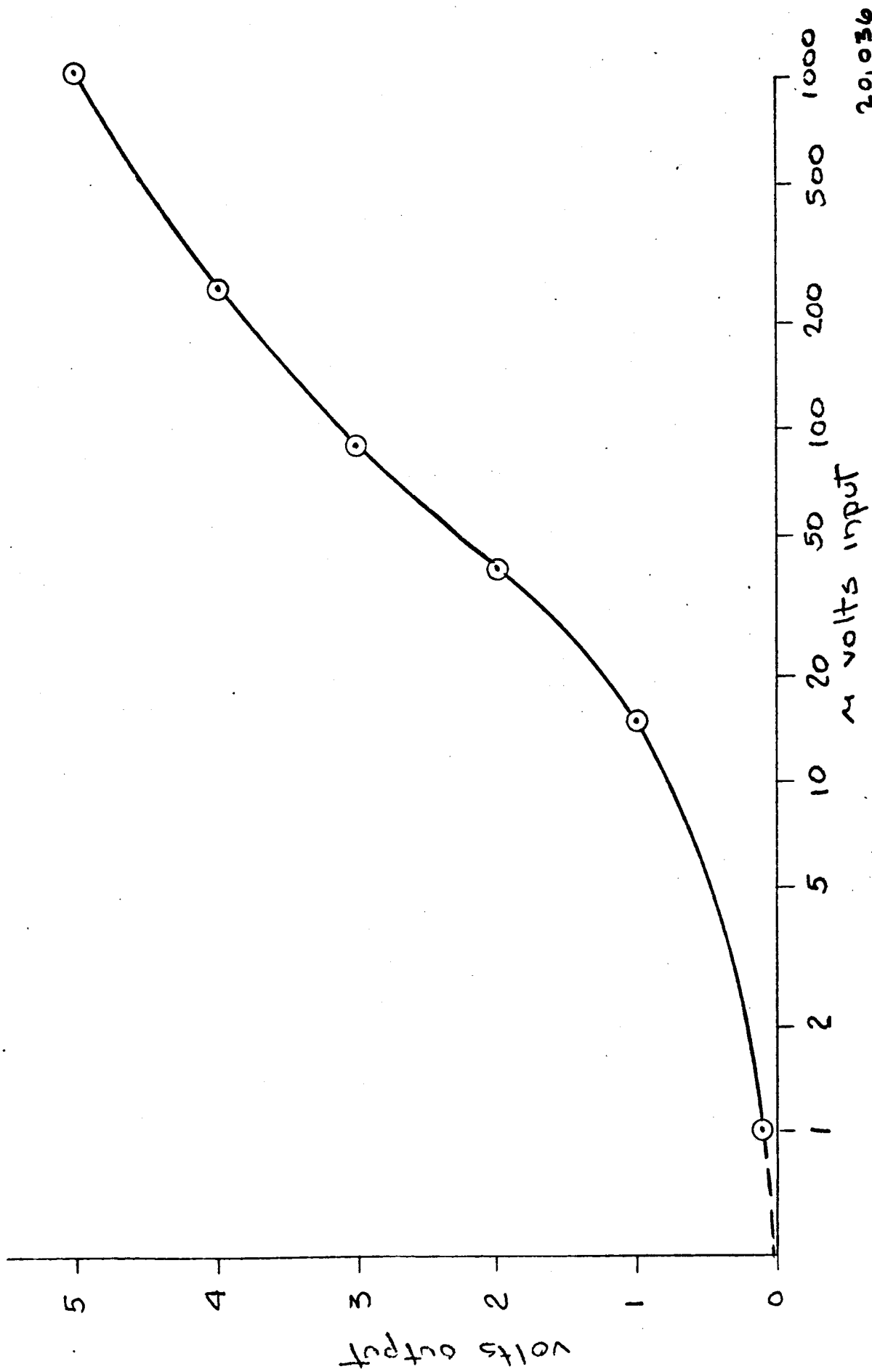


Figure 5.12 Logarithmic Signal Amplifier Output vs. Input. 20,036

To obtain resistive region operation of the field effect transistor, it is necessary to provide proper biasing and phasing of the various signal potentials applied to the device. The following restrictions have to be satisfied:

1. The gate terminal should be close to 0 volts or positive in respect to the source terminal.
2. The drain terminal should be close to 0 volts or negative in respect to the source terminal.

Condition "1" is met by choosing resistor R10 in conjunction with R14 to set the collector of Q4 to the proper zero signal voltage level. R13, R14 and Q4 then comprise a feedback stabilized unity gain phase inverter with D.C. stabilization of the output quiescent potential. In addition, because input signals are normally positive, and the output of Q4 is in phase with the input polarity, the input drive to the gate of Q5 is also positive.

Condition "2" is satisfied because the output of Q3 goes normally negative when input signals are present. Also, resistor R9 in conjunction with R3 and R10 provides overall bias stabilization around transistors Q1, Q2 and Q3, thereby satisfying the remaining restrictions of condition "2".

#### 5.5.2 Overall Feedback Amplifier Design Formulations

$$G = \frac{E \text{ output}}{E \text{ input}} = \frac{A}{1-AB} \quad (1)$$

E output = Signal Amplifier Output

E input = Signal Amplifier Input

A = Amplifier forward loop gain

$$B = -\left(\frac{R_G}{R_3} \times \frac{R_5}{R_4}\right), \text{ with } R_G \ll R_3 \text{ and } R_6 \ll (R_4 + R_5) \quad (2)$$

$$R_G = \frac{R_2 (R_1 + R_{Q5})}{R_2 + (R_1 + R_{Q5})}, \text{ where } R_{Q5} \text{ bears the following relationship to} \quad (3)$$

E output:

TABLE 1

$E_{\text{Output}}$ (Volts)	0	1	2	3	4	5
$R_{Q5}$ (Ohms)	1K	2K	3K	6K	15K	100K

If:  $(R_1 + R_{Q5} \text{ Min.}) \ll R_2 \leq R_{Q5} \text{ Max.}$ ,

then:

$(R_1 + R_{Q5} \text{ Min.})$  determines  $G_{\text{max.}}$  (4)

$\frac{R_2 R_{Q5} \text{ Max.}}{R_2 + R_{Q5} \text{ Max.}}$  determines  $G_{\text{min.}}$  (5)

The desired output vs. input transfer function is such that:

A. With  $G_{\text{max.}}$ ,  $1\mu\text{V}$  input produces 0.1 volt output

therefore,  $G_{\text{max.}} = 10^5$

B. With  $G_{\text{min.}}$ , 1 mv input produces 5 volts output

therefore,  $G_{\text{min.}} = 5000$ .

To achieve the desired gain variation, the following relationship has to be satisfied:

$$20 (R_1 + R_{Q5} \text{ min.}) = \frac{R_2 (R_{Q5} \text{ max.})}{R_2 + (R_{Q5} \text{ max.})} \quad (6)$$

If  $R_1 = 1\text{K}\Omega$  and  $R_2 = 80\text{K}\Omega$

Then (6) is satisfied, and  $R_G$  vs.  $E_{\text{output}}$  has the following relationship:

TABLE 2

$E_{\text{Output}}$ (Volts)	0	1	2	3	4	5
$R_G$ (Ohms)	2K	3K	4K	6.5K	13K	40K

In the signal amplifier,  $R_6$ ,  $R_7$ , and  $R_8$  provide negative feedback stabilization around the individual transistors. This controls the amplifier's forward loop gain and sets it to be approximately one million, irrespective of the transistors' normal gain variation and differences.

Because the controlled forward loop gain is 10 times the maximum desired gain, and 200 times the minimum desired gain, the "A" term in formula (1) can be considered infinite.

The approximate gain can then be expressed as:

$$G \sim \frac{1}{-B} \sim \frac{1}{R_G} \left( \frac{R_3 \times R_4}{R_5} \right) \quad (7)$$

and  $R_3$ ,  $R_4$ ,  $R_5$  can be determined (keeping within the restrictions of Formula 2) to produce the desired maximum and minimum overall amplifier gains.

The amplifiers overall output to input transfer characteristics can now be computed by means of Table 2 and Formula 7, and Figure 5-12 is a plot of the overall response.

### 5.5.3 Frequency Response Considerations

The frequency response of an amplifier without feedback is extended when negative feedback is applied around the amplifier. If the open loop amplifier gain falls off at 6 db per octave at both the high and low frequency ends of the passband, the extension of response at each passband edge is directly proportional to the open to closed loop amplifier gain ratio when overall negative feedback is applied.

When combined internal and overall feedback is used in a transistor amplifier, the internal feedback determines the open loop gain and frequency response irrespective of the individual transistor characteristics. Then the overall Amplifier parameters can be determined by design, rather than by empirical trimming or selection of critical components.

**5.5.3.1 High Frequency Cutoff** - As previously covered, transistors Q1 through Q3 have individual feedback paths which fix their overall gain at 1 million. Capacitor C1 in conjunction with R8 set the frequency response cutoff of the

three transistors to 25 cycles per second. This determines the open (or forward) loop high frequency cutoff. The overall negative feedback loop, enclosing these internally feedback-stabilized stages, sets the open (forward) to closed (overall feedback applied) loop gain ratio. As the amplifier closed loop gain varies with signal level from  $10^5$  to  $5 \times 10^3$ , the open loop to closed loop gain ratio is changed from 10:1 to 200:1. This causes the instantaneous high frequency cut-off of the overall amplifier to vary from 250 cycles to 5000 cycles per second.

Note that in Figure 5-11, C1 (which determines the forward loop amplifier cutoff) receives its drive only from the compressed signal output. For this reason, an equivalent circuit can be generated that greatly simplifies the amplifier high frequency response characteristics. The entire amplifier is considered as having no internal high frequency restrictions. It is then followed by an RC low pass filter with a time constant of 0.7 milliseconds. By means of the amplifier amplitude transfer function (Figure 5-12) the input signal waveshape is transformed into the generated amplifier output signal. This signal then passes through the 0.7 millisecond low pass output filter. The resultant is the final amplifier output waveshape for the input under consideration.

**5.5.3.2 Low Frequency Response Characteristics** - The various low frequency cutoffs in the signal amplifier and subsequent coupling networks produce overshoots at the trailing edges of input pulses. As originally mentioned, excessive overshoots would produce confusion as to whether space or cold moon was being viewed after receiving a large input signal from the sun or a hot moon limb region. In addition, transistors produce predominately low frequency noise, and it is desirable to restrict the amplifier low frequency response to what is actually required to minimize this noise.

The predominant low frequency response limiting network consists of C4, D1, R11 and R12. The values of R11 and R12 are so chosen that when the voltage out of C2 goes minus one volt due to signal drive, diode D1 stops conducting. Between zero and -1 volt, the resistance affecting C4 is R12; with signals that produce greater than -1 volt, the resistance affecting C4 is (R12 + R13) in parallel with R11.

The resistance values are related as indicated below,

$$R_{12} \ll R_{13} \leq R_{11}$$

and are so selected that  $R_{12} \leq 7 \left[ \frac{(R_{11} \times R_{13})}{R_{11} + R_{13}} \right]$

C4 is then determined to produce a time constant of 200 milliseconds in conjunction with R12.

The result is that for output signals whose instantaneous values are less than 1 volt, the low frequency cutoff of the network is 1 cycle per second, and for signals over 1 volt, the low frequency cutoff is approximately 0.15 cycles per second. Consequently, the bandwidth is most restricted when the signal level is low and noise is critical, and is allowed to increase at high signal levels when noise is no longer critical.

With the selected R and C values, the droop produced by the circuit on the top of a 4 millisecond duration input pulse of 5 volt amplitude is .015V. This corresponds to the overshoot at the trailing edge of the pulse produced by this network after scanning the sun.

The 400°K hot moon produces a 200 microvolt input signal, which results in a 3.6 volt signal into the network. An 8 millisecond duration 400°K moon signal would produce an overshoot of .02 volts.

Additional low frequency cutoff networks in the amplifier cause additional overshoot and droop. To get the total overshoot at the preamplifier output for the sun and moon conditions just covered, it is necessary to evaluate these as well. Then, by using superposition, they are all summed, and yield the total overshoot at the amplifier output.

There are two such additional networks. The first includes the input coupling capacitor C2, which is so selected as to minimize any overshoot. The second network includes C3, which does contribute to the output waveshape overshoot. In this amplifier configuration, the negative feedback signal developed across R5 is fed into the low side of the signal source. The feedback then passes through the detector-commutator assembly through input coupling capacitor C2



into the base of Q1, thereby closing the loop. Resistor R15 provides the feedback path in case the detector-commutator continuity breaks.

The effective amplifier input impedance (as seen by the detector-commutator array) is the actual open loop input impedance multiplied by the open loop to closed loop gain ratio. The apparent value of C2 is similarly increased, thereby providing maximum fidelity transfer of the detector-commutator output into the amplifier (the effective input impedance ranges from 50K ohms to 1 Megohm, and the effective series input coupling capacitor varies from 1000  $\mu$ fds to 2000  $\mu$ fds).

The detector commutator output dynamic range of 1000 to 1 necessitates such large time constants at the amplifier input. This effectively eliminates large signal overshoot and droop at the input. Capacitor C2, in conjunction with the amplifier input, responds to this large input signal dynamic range, even though the output is compressed to 50:1.

Capacitor C3, however responds to the more restricted output signal dynamic range. Therefore, the value of C3 (in conjunction with R3, R4, R9, and R10) is used to set the effective low frequency cutoff (as seen at the collector of Q3) and thereby control the overshoot. The capacitor value used provides an effective minimum low frequency cutoff up to the collector of Q3 of 0.16 cycles per second, while the output signal is less than 1 volt (input under 10 microvolts). The low frequency response extends proportionally with the increasing overall negative feedback as the signal level increases to 5 volts at the output (corresponding to 1 millivolt input). At a five volt output level, the effective low frequency cutoff is one-twentieth of 0.16 cycles, or .008 cycles per second.

This low frequency cutoff determines the droop on the top of a pulse. With a 4 millisecond duration, 5 volt output pulse amplitude, the droop is approximately 1 millivolt, which is negligible.

The overshoot at the end of the pulse is determined by the output pulse amplitude and time duration, in conjunction with the amplifier's effective low level signal time constant. It can be expressed by the following relationship:

Volts overshoot at Q3 output\*

$$= \text{Output Pulse Amplitude (Volts)} \times \text{Output Pulse Duration (seconds)}$$

With a 4 millisecond, 5 volt pulse (maximum sun signal), the overshoot would be .02 volts. This corresponds to 0.2 microvolts at the amplifier input.

Correspondingly, an 8 millisecond pulse of 3.6 volt amplitude (maximum moon signal) would produce approximately .03 volts overshoot.

When processing pulses due to sun or moon, the maximum combined overshoots produced by all the amplifier low frequency networks is less than 0.5 microvolts (referred to the input). With a minimum input signal of 2 microvolts from a 120°K moon signal, adequate safety margin is provided to assure whether space or cold moon is being viewed at the termination of these high signal pulses.

#### 5.5.4 Noise Considerations

Noise problems are most significant when signals from either space or the cold side of the moon are being processed. With either of these two conditions, noise peaks of over 1 microvolt (referred to the input) of the proper superimposed polarity and time durations can prevent these two situations from being resolved.

With input signals ranging from slightly negative to +10 microvolts, the effective amplifier bandwidth extends from 1 cycle to 250 cycles per second. The limiting noise sources at the input is a 50 ohm thermopile detector, in series with a pair of light exposed cadmium selenide cells (commutator switch segment and the "1" element of the "0-1" switch). The two Cadmium Selenide cells have a combined series resistance of 2K ohms.

The Johnson noise in a 250 cycle bandwidth of the 50 ohm thermopile is less than 0.1 microvolt peak-to-peak. The Johnson noise of the 2K-ohm resistance cadmium selenide elements is approximately .5 microvolts peak-to-peak, which is sufficiently high to mask the detector noise, and make it negligible.

---

\* Using a one second equivalent time constant.

When the 120°K moon is present, the signal at the input is 2 microvolts. With an earth-space threshold level setting of 1 microvolt referred to the input, a maximum input referred peak-to-peak noise of 2 microvolts is acceptable.

The acceptable noise level when space is being viewed is more difficult to ascertain, and is dependant on the form of processing in the subsequent threshold circuit. There, a clamp circuit is used to set the signal to zero volts while space is being viewed. If the clamp is "soft", (or a programmed transistor is used to provide non-polarity sensitive clamping action) the peak-to-peak noise excursions will be symmetrical around zero volts. Then 2 microvolts of peak-to-peak input-referred noise is again acceptable. However, if a "hard" clamp is used, (i.e.: one that sets to the peak, rather than the average, of negative polarity noise peaks), only 1 microvolt is acceptable.

An additional factor is the amplitude-time interrelationship of the threshold circuit. It's arrangement is such that only positive excursions of over 1 microvolt whose time durations are longer than 8 milliseconds can cause output response. This action tends to eliminate short duration positive excursion noise components, and thereby reduces the weighting of high frequency noise components that lie above 50 cycles per second. Considering the overall performance, the maximum acceptable input-referred peak-to-peak noise is 2 microvolts.

Since the theoretical peak-to-peak noise at the amplifier input is 0.5 microvolts, and the acceptable noise is 2.0 microvolts, the amplifier noise can be 12 db above the theoretical noise limit. With currently available transistors, this is realizable (although the input stage transistor will require empirical selection).

It should be noted that inherent transistor noise, and not the input impedance value determines the limiting noise. Tests conducted on low noise transistors show no appreciable noise increase at transistor outputs when the input impedance is varied from 0 ohms to 5K ohms. Less than 6 db of output noise increase occurs when the input impedance is further raised to 30K ohms. Therefore, reducing the series impedance of the commutator to under 2K ohms will not reduce the effective input noise.

It has been found that by using 100K-ohm input impedances, a transistor noise can approach 3 db of the 100K-ohm theoretical noise limit in a 2 cycle to 250 cycle band. To achieve a 100K-ohms input impedance in this system, a very large transformer would be required to couple the commutator output to the amplifier input. Even if a very extended low frequency response transformer were available which did not have pickup or microphonic problems, it still would not be usable. Because of the large primary inductance required, any residual primary currents due to signal excitation would produce voltage fluctuations at the commutator output when different resistance commutator cells are exposed. These voltage fluctuations would appear as spurious levels at the amplifier input. The required resistance match of the 95 cadmium selenide cells used in each commutator is not realizable.

The utilization of a field effect transistor as the input stage was also considered as a possible means of obtaining a better noise figure. However, this device requires an input impedance of over 1 megohm at very low frequencies to achieve its low noise operational capability. This would require using an even more impossible coupling transformer, and therefore had to be ruled out as a practical means of realizing lower system noise figures.

To achieve lower noise, some new state of the art device will be required. One such possibility is a recently developed parametric amplifier, which obtains very good low frequency noise figures with input impedances around 2 thousand ohms. This device, along with any others that may be developed, will be considered in further detail as possible means to obtain better overall system performance in the future.

#### 5.6 OFFSET SOURCE DRIVE CIRCUIT

The radiant offset heat source is adjusted in temperature to counterbalance detector radiation through the window to space. The criteria for proper balance is that the radiating detector produces zero microvolts output. If this voltage becomes negative, power into the offset heat source is increased; if positive, the power decreases.

The gain of the preamplifier is utilized to obtain a high level signal which contains the offset information. This signal is suitable for processing when reference d-c levels have been restored. Referring to Figures 5-13 and 5-14, the preamplifier signal (waveform A) appears at the coupling capacitor. If the visual horizon is seen, five elements later horizon crossover is verified and the zero volt clamp drive signal causes the input to be shorted. (In waveform A, the horizon signal is the synthetic signal which causes crossover if no visual horizon crossover has occurred over the 90 detectors.) After five sample periods the shorting ceases and the cycle begins again at the first detector (0). The interrogate signal (D) allows the signal to appear at the error amplifiers input (E) for ten sample periods.

The diode D2 passes negative going signals during the interrogate period, and the offset heat source is adjusted by the average of the negative going signal, if it goes negative at all.

If the signal is negative with respect to ground, as shown in waveforms A1 and D1, the error amplifier output may increase to 19 or 20 volts (waveform F1) from the nominal 4 to 5 volt level.

If it is positive with respect to ground, the error amplifier is turned off, and no power is supplied to the offset heat source (A2, D2, and F2).

The error amplifier has a gain of approximately 2000 (or 200 with a 10:1 duty cycle), and performs the function of maintaining the error amplifier output for the period between negative going interrogation samples. The time constant during this period is 2.2 seconds, while the charge time constant is .01 seconds during the 0-9 period.

The null tolerance will be 0 to -1 microvolts, referred to the input. This means at 0 or positive microvolts input, the power output is zero, and at -1 microvolt, the power output is maximum. If during the 0-9 period, only five elements view space, the gain drops to 100 and the null tolerance is correspondingly 0 to -2 microvolts.

Of significance is the diode D1, which prevents interrogation from occurring when the threshold has been crossed and the input is grounded. The coupling

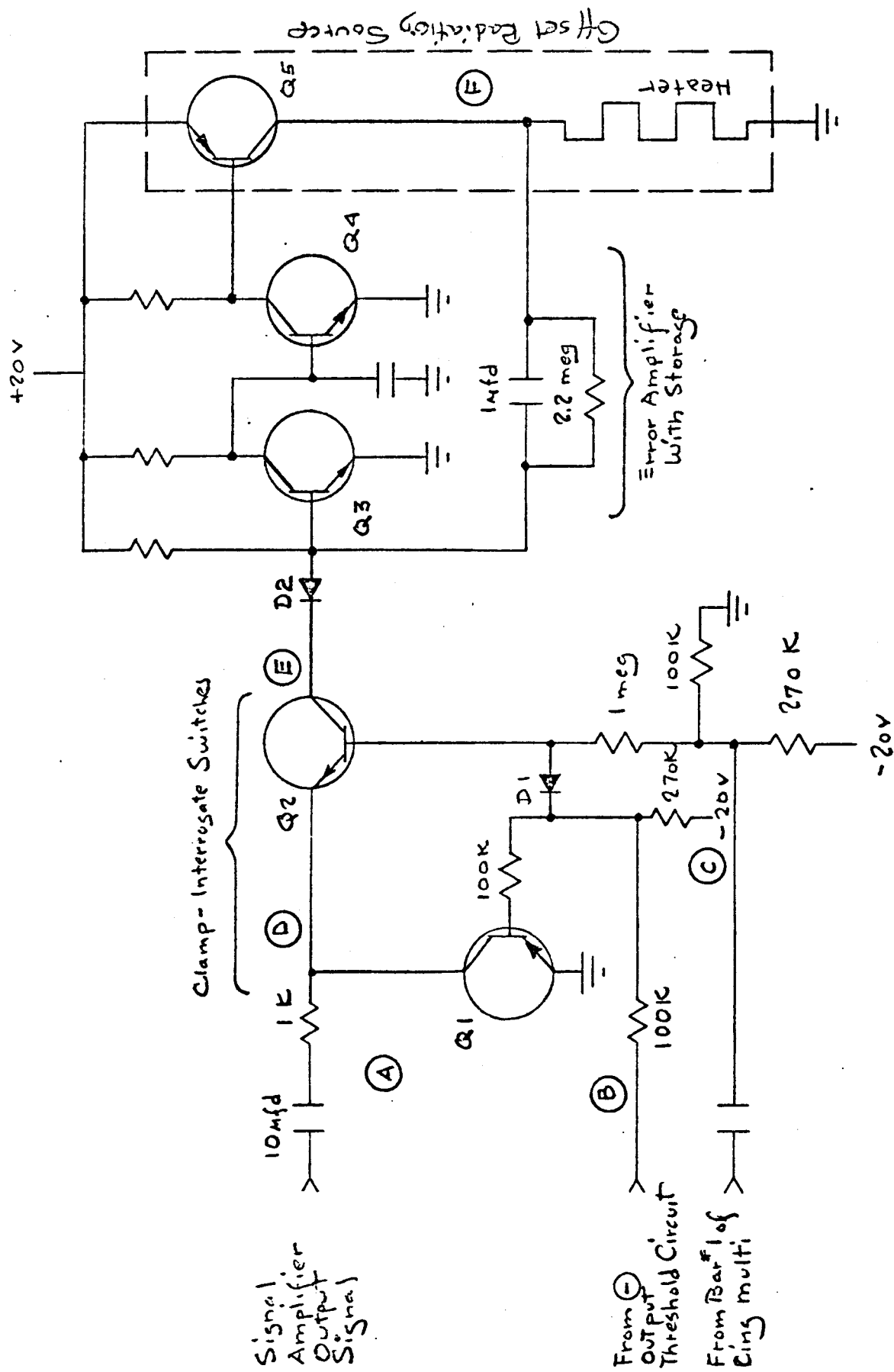


Figure 5.13 Offset Source Drive Circuit

20,045

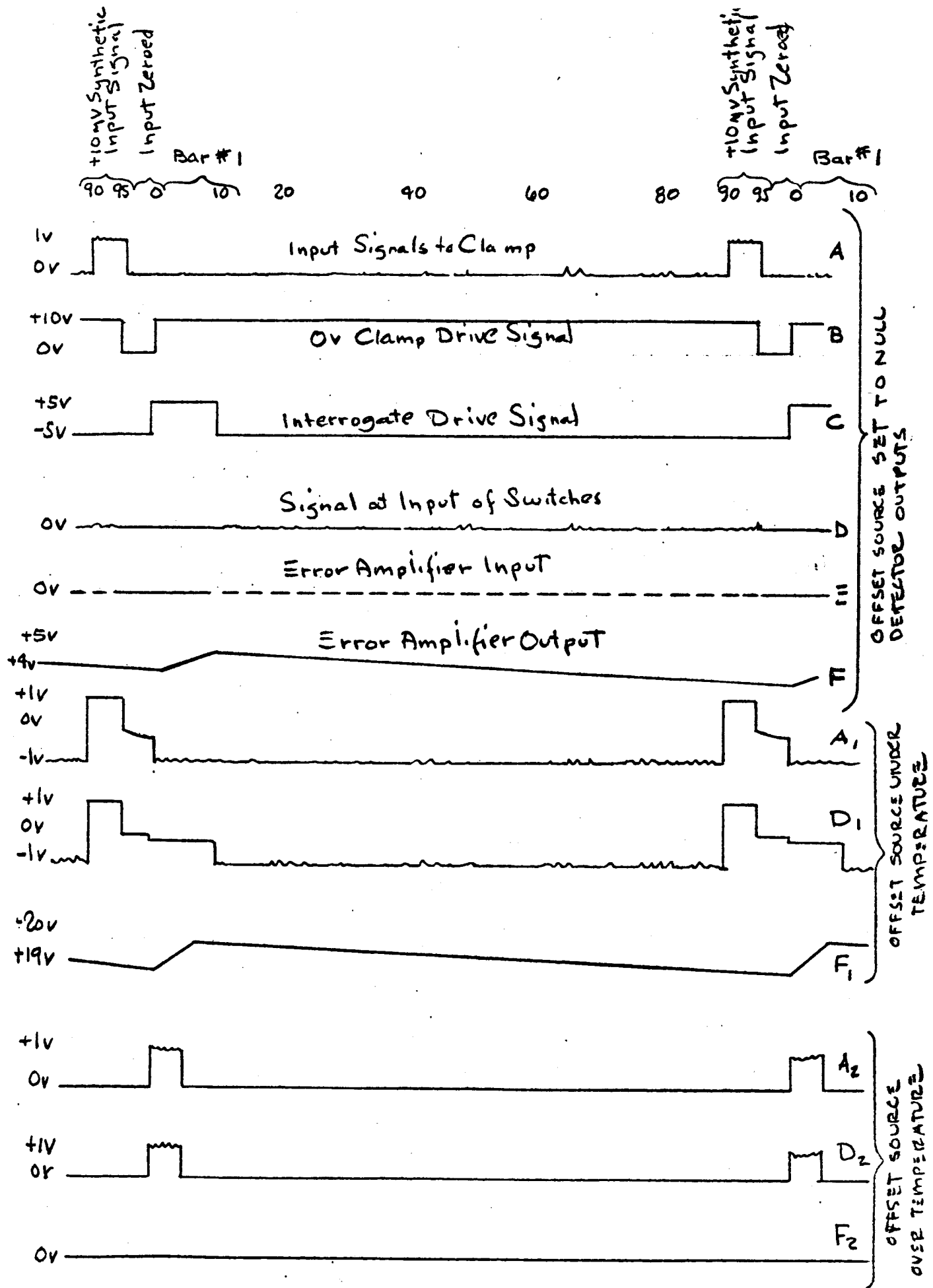


Figure 5-14 Waveshapes, Offset Source Drive Circuit

capacitor is set during this period through transistor Q1, which is conducting. At the first detector, transistor Q1 is turned off, and remains off while foreign body and planet signals are present, allowing the input capacitor to follow such signals without losing its ground referred voltage and preventing serious pre-amplifier loading. Also, if positive signal occurs during the 0-9 interrogation, diode D2 disconnects and again no current flows through the input capacitor. If the space signal is very negative, some loading does occur. However, since signal processing cannot continue properly until the offset heat source is set, this causes no operational problem.

### 5.7 THRESHOLD CIRCUIT AND ZERO-ONE INPUT

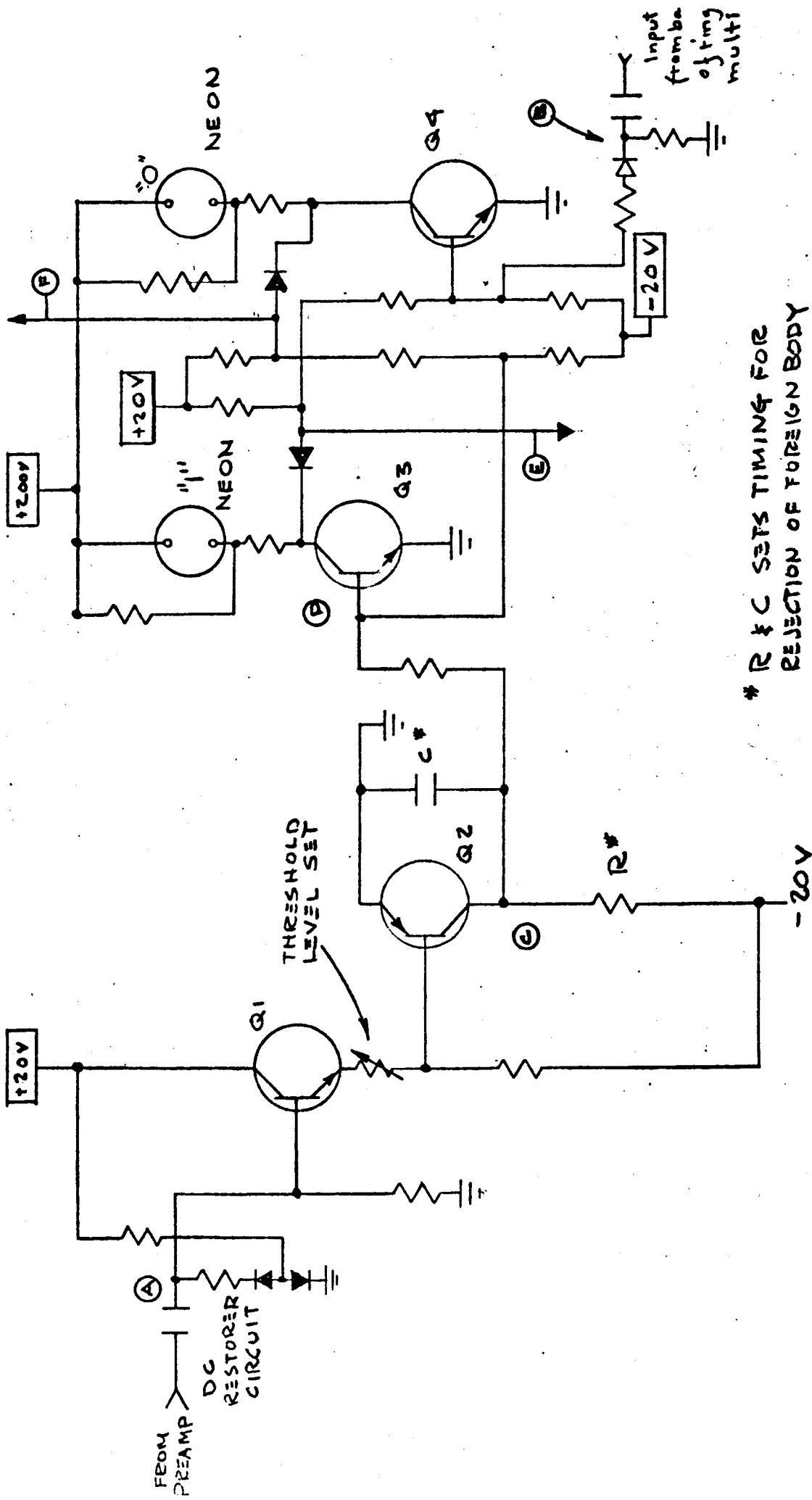
The elimination of spurious foreign bodies of relatively small angular size is accomplished on a time scale by rejection of signal pulses shorter than a pre-established minimum. Rapid recovery is essential so that valid signals occurring shortly after such spurious signals can be distinguished. Such a circuit, used in other systems developed at Barnes, is used in this system and is shown in Figure 5-15.

The preamplifier signal appears at the coupling capacitor (Figure 5-16, waveform A), where the most negative going signal — representing space — is clamped to zero volts. The clamp is shown as a diode clamp circuit, but in final form, it will become a transistor clamp. This will provide better clamping accuracy and noise excursions will be symmetrical around 0 volts. A secondary input will open the clamp circuit when the input signal is positive or grounded, which will minimize overshoot problems in this area.

Transistor Q1 acts as an emitter follower, and the voltage at the base of Q2 is the same as the input A less the 0.1 volt threshold voltage level (and less the transistor potential, but this voltage is compensated for by the transistor potential of Q2). When the space signal is present, the voltage at the base of Q2 is sufficiently negative to keep that transistor in conduction, holding its collector potential near zero volts.

When a signal corresponding to at least 100°K appears at Q1, the base potential of Q2 goes positive just enough to shut off the transistor, and the





20,047

Figure S-15 THRESHOLD CIRCUIT AND ZERO-ONE INPUT

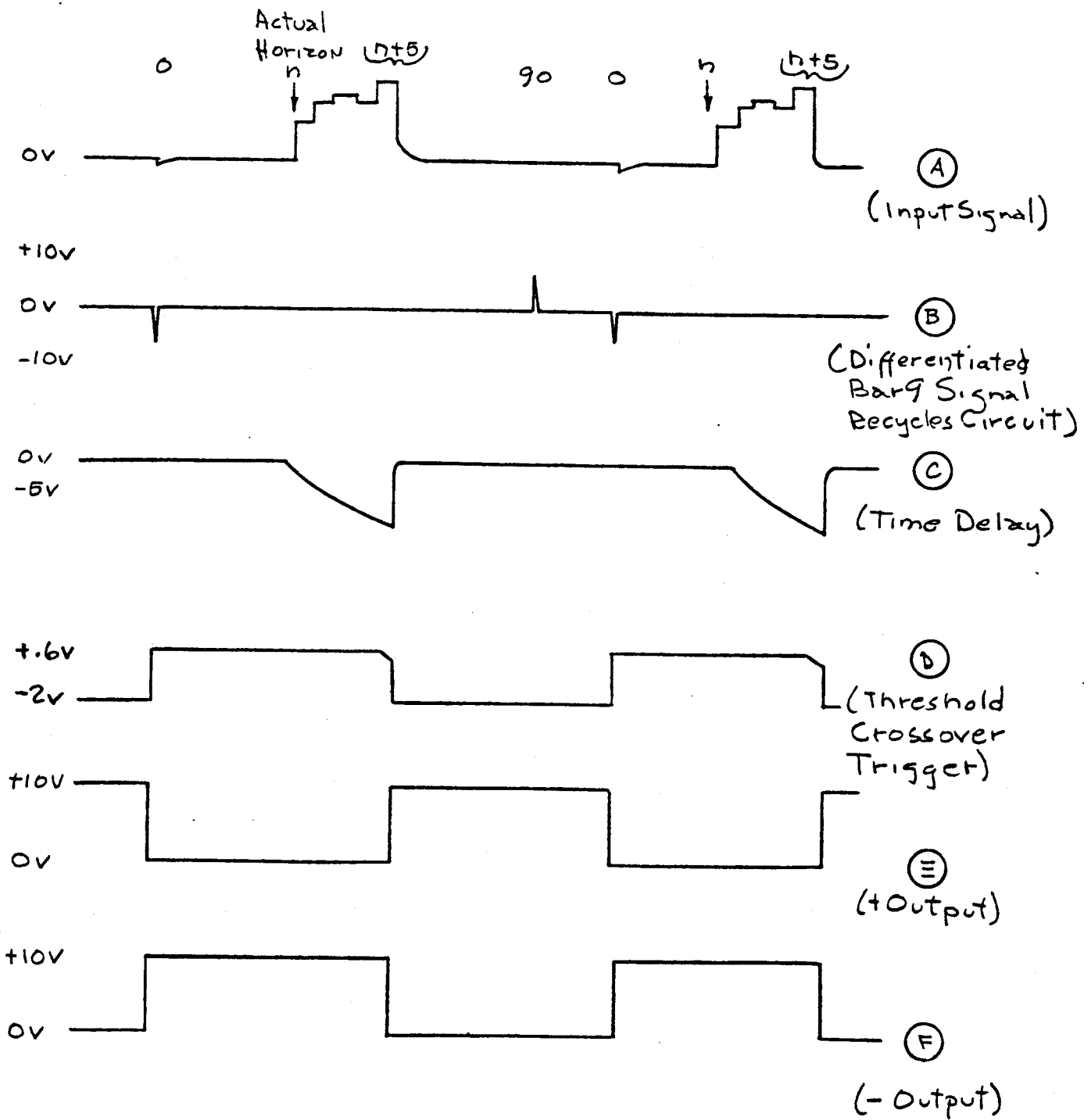


Figure 5-16 Waveshapes, Threshold and Zero-one Circuit 20,048

potential at the collector begins to fall, as shown in waveform C. A potential divider from +20 volts keeps transistor Q3 on until the collector potential of Q2 reaches -8 volts. This means that the signal has remained above 100°K long enough to verify that it is not a spurious body. At this time the voltage at D goes slightly negative, which causes the bistable flip-flop formed by Q3 and Q4 to switch, Q4 turning on and holding Q3 off.

The circuit remains locked in this manner until the negative pulse in waveform B shuts transistor Q4 off, resetting the bistable. Waveforms E and F are the processing outputs of the bistable flip-flop, which are used to determine attitude and altitude.

The bistable is also connected to the "0" and "1" neon lamps, which activate photoresistive cells, grounding the commutator input when the threshold has been crossed. The actual photoresistor circuit is a series-shunt pair, of which one opens (1) and one shorts (0). (Depending on the duty cycle, these neons are on for much longer periods than the high speed commutating lamps, and so three or four lamps may be used in redundancy to improve reliability for this element. The power dissipated by the 0-1 pair is always constant for one of the two is always on.)

The operation of the threshold circuit and 0-1 switch can be best understood by considering a typical scan situation. Figure 5-17 shows the LPHS centering on the moon as a reference body. Head XI scans space, views the earth as a spurious body, crosses the lunar horizon on the cold night side and proceeds past the terminator to the hot day side. Scan XII views the sun and the hot day side.

Figure 5-18 shows the waveforms generated in this situation. The signal produced by the detectors through the commutator is shown for both channels XI and XII. Waveshapes C show the time delay effect, waveshapes E the threshold signal + output, and waveshapes A the preamplifier output showing the action of the 0-1 switch in shorting out signal once horizon threshold has been verified.

The threshold output signals are then fed into the attitude, altitude and alarm readout circuits. The following sections cover the operations performed by these circuits with the illustrated lunar scan conditions as an input.

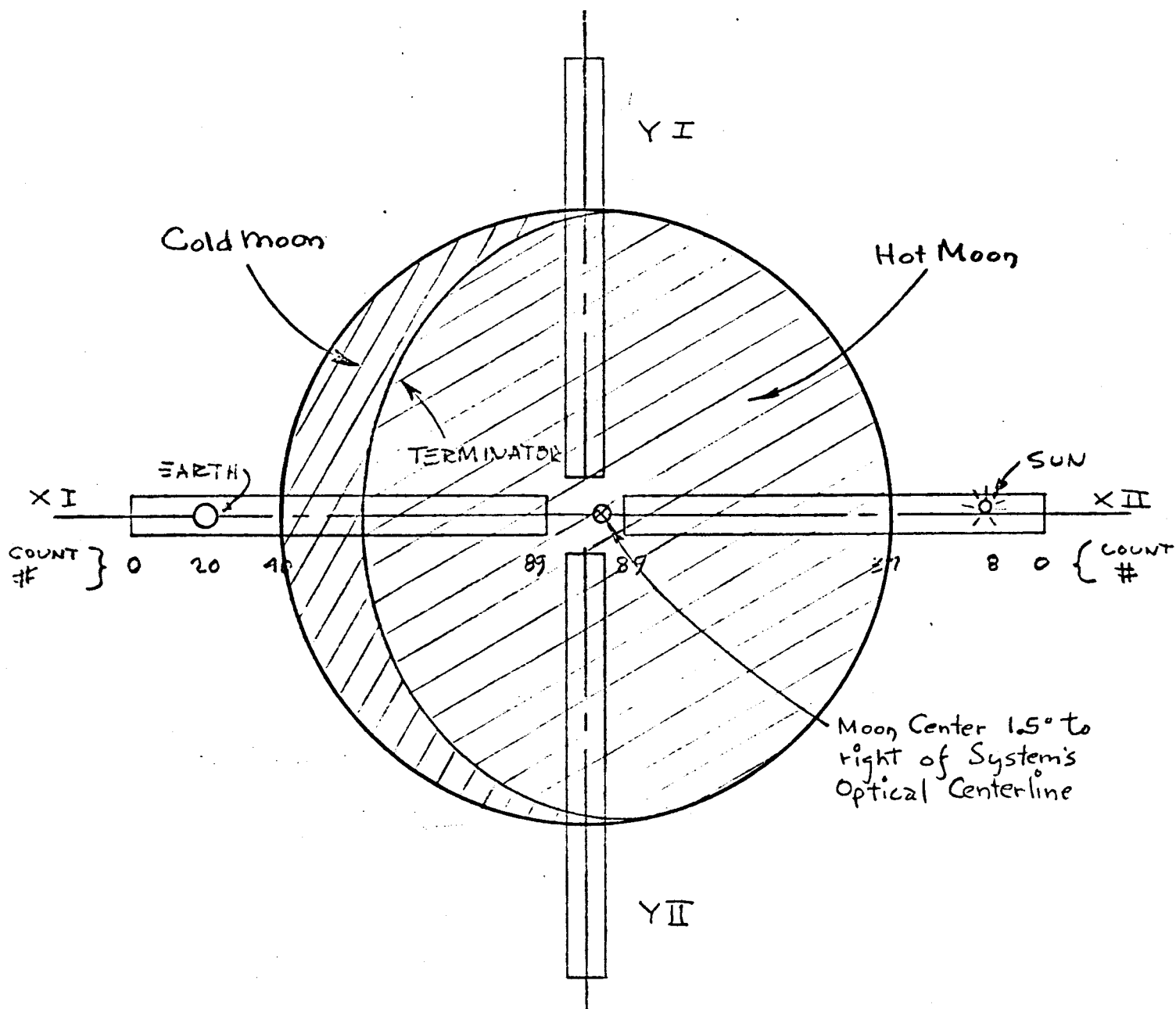


Figure S-17 Lunar Scan

20,049

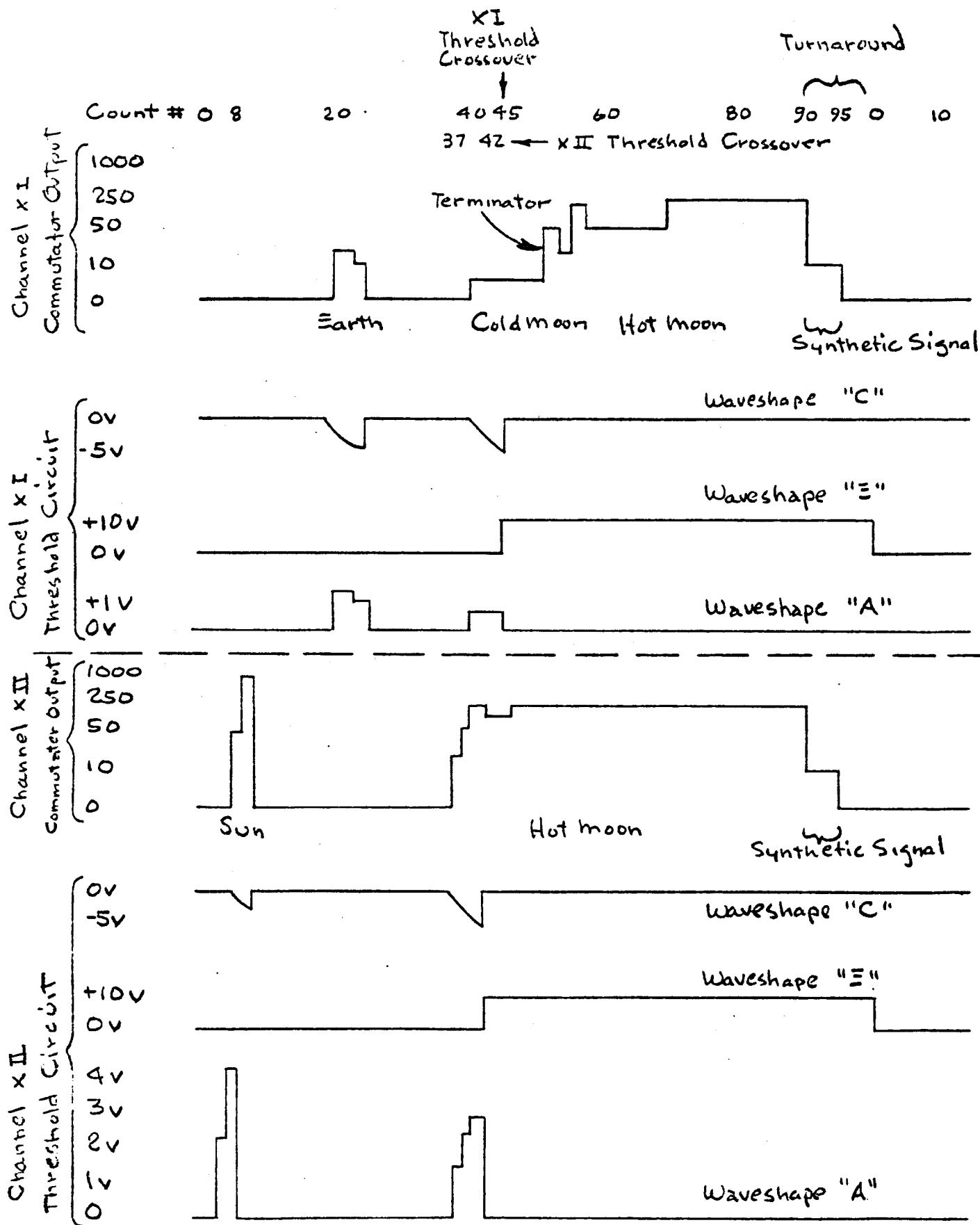


Figure 5-18 Waveshapes: Channels XI & XII, Lunar Scan 20,050

### 5.8 ATTITUDE PROCESSING LOGIC (See Figure 5-19)

The attitude determination is directly obtained as the count difference between horizon crossovers of two opposing heads. Bipolar staircase generators sum clock pulses occurring after the first horizon is crossed and before the second. This sum is held and reads directly as attitude error. When the horizon is crossed during the next cycle, the count is immediately rezeroed, and begins again.

### 5.9 ATTITUDE ZEROING DRIVE CIRCUIT (See Figure 5-20)

This circuit is basically an "or" gate with a differentiator following it. The pulse obtained is limited and both normal and inverse polarity are obtained. Figure 5-21 shows the waveforms.

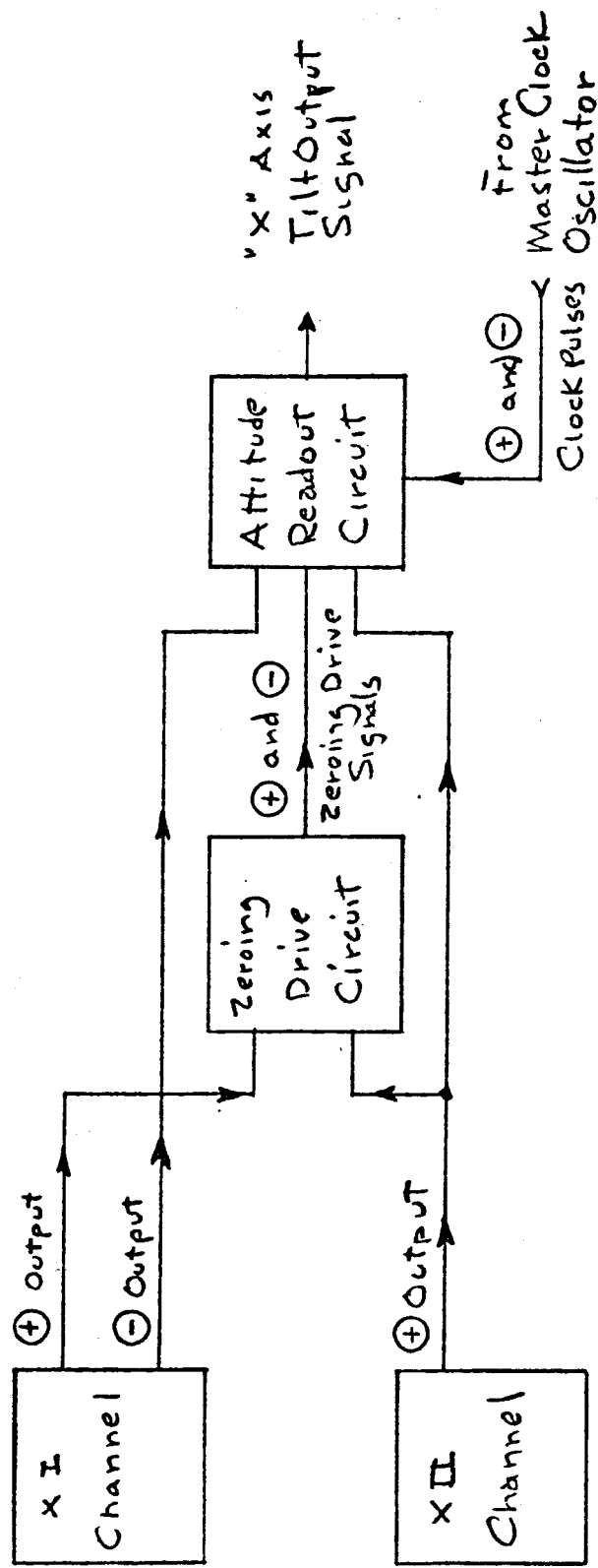
### 5.10 ATTITUDE READOUT CIRCUIT (See Figure 5-22)

Transistors Q1 and Q2 are normally conducting, shorting out plus and minus clock pulses. Normal signals from channel XII and inverted signals from channel XI are added to give the signal shown in waveform A in Figure 5-23. Channel XI crosses the threshold first, turning off transistor Q1, and allowing the positive clock pulses (B) to enter the tunnel diode staircase counter. Here the clock pulses are stored (C) until the second threshold is crossed and transistor Q1 again prevents any clock pulses from entering the counter. A standard emitter follower, Q5, presents the filtered sum of the positive and negative counters as tilt readout (E). In the event that the XII channel crosses threshold first, the negative staircase counter accumulates a negative count which is read out.

Each time the cycle repeats and the threshold is crossed, the readout zeroing drive circuit nulls both tunnel diode staircase counters. In this way, new readout information is generated each cycle.

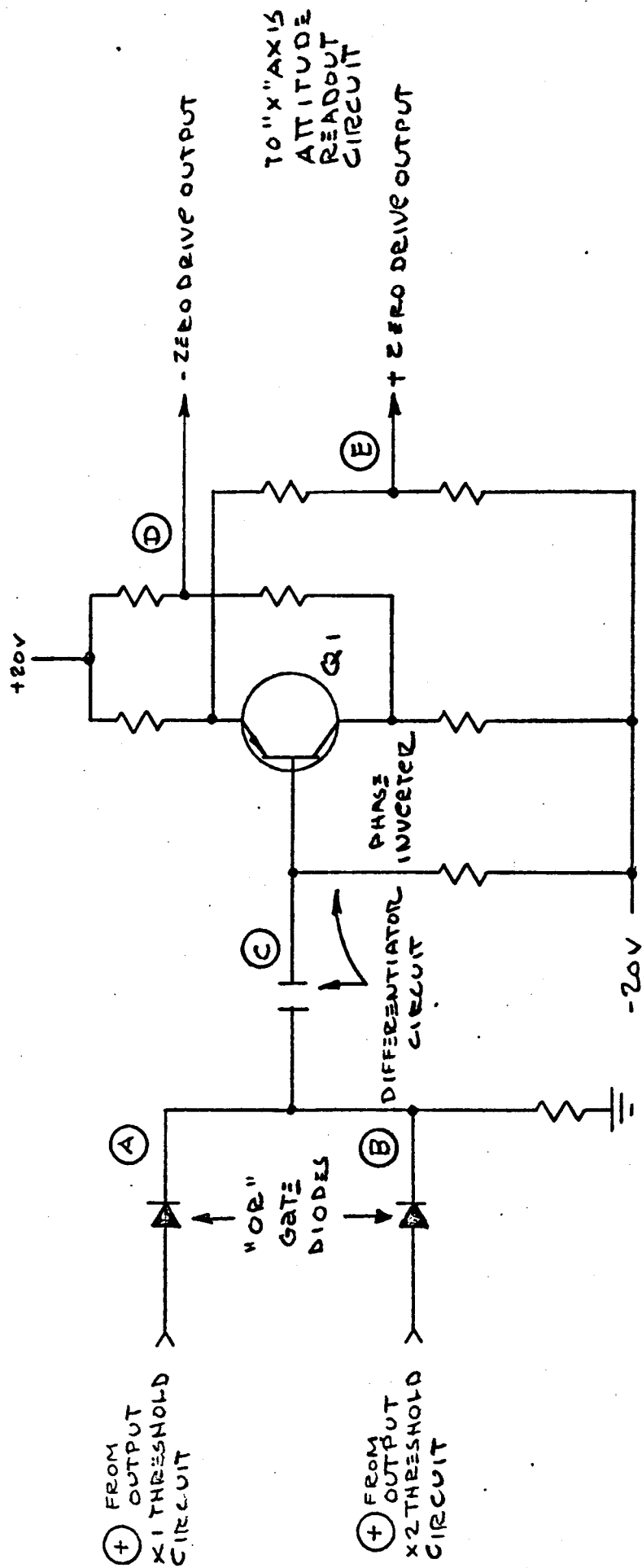
### 5.11 ALTITUDE PROCESSING LOGIC

The altitude processing is somewhat more complicated in nature than the attitude, principally because of the large dynamic range required. Figure 5-24



Note: "Y" axis attitude readout Block Diagram same as for "X" axis

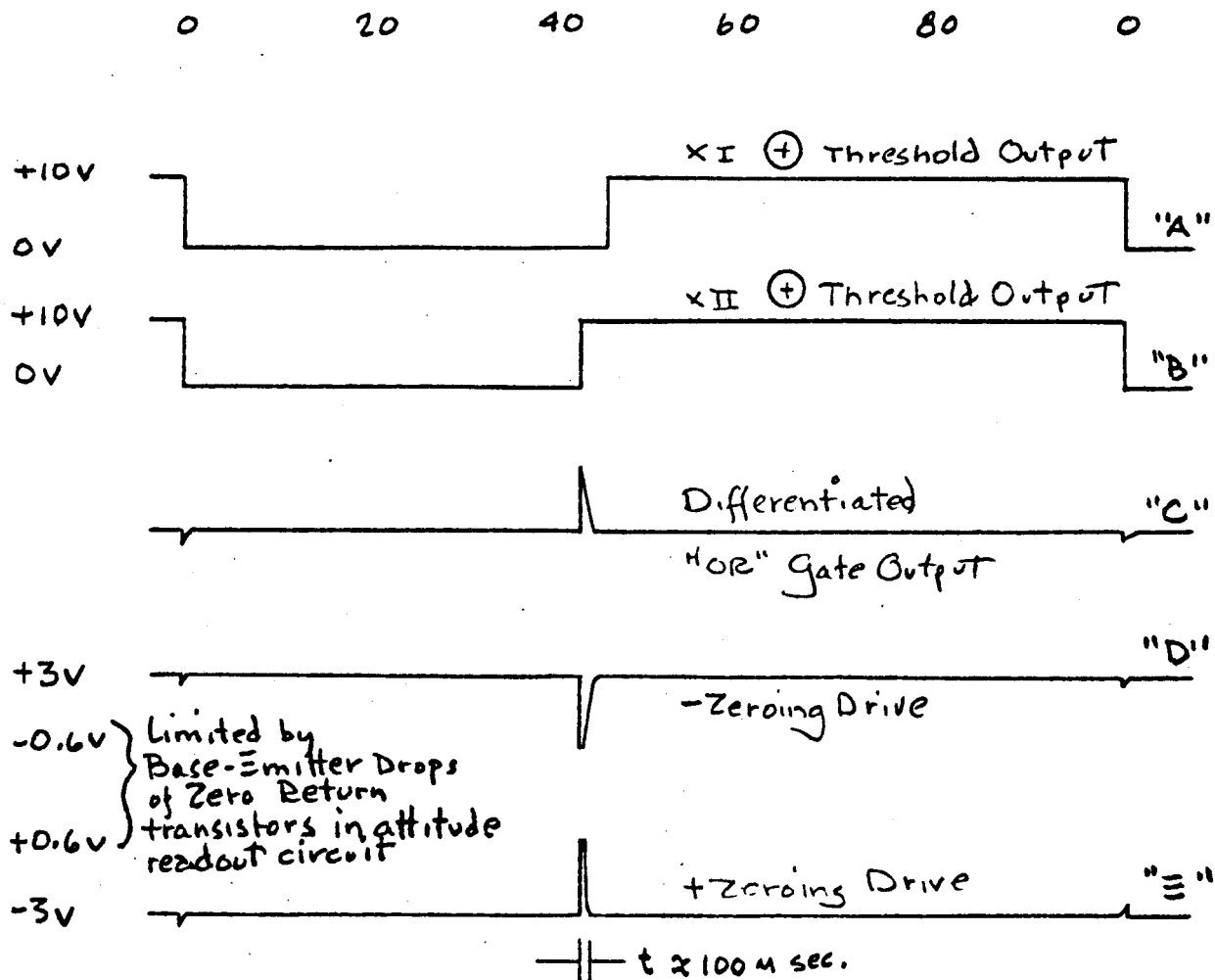
Figure S-19 "X" Axis Attitude Readout Block Diagram <sup>20,051</sup>



Note: "Y" axis zeroing drive circuit same as shown for "x" axis

FIGURE 5-20 ATTITUDE READOUT ZEROING DRIVE CIRCUIT





20,053

Figure 5-24 Waveshapes: Attitude Readout Zeroing Drive Circuit

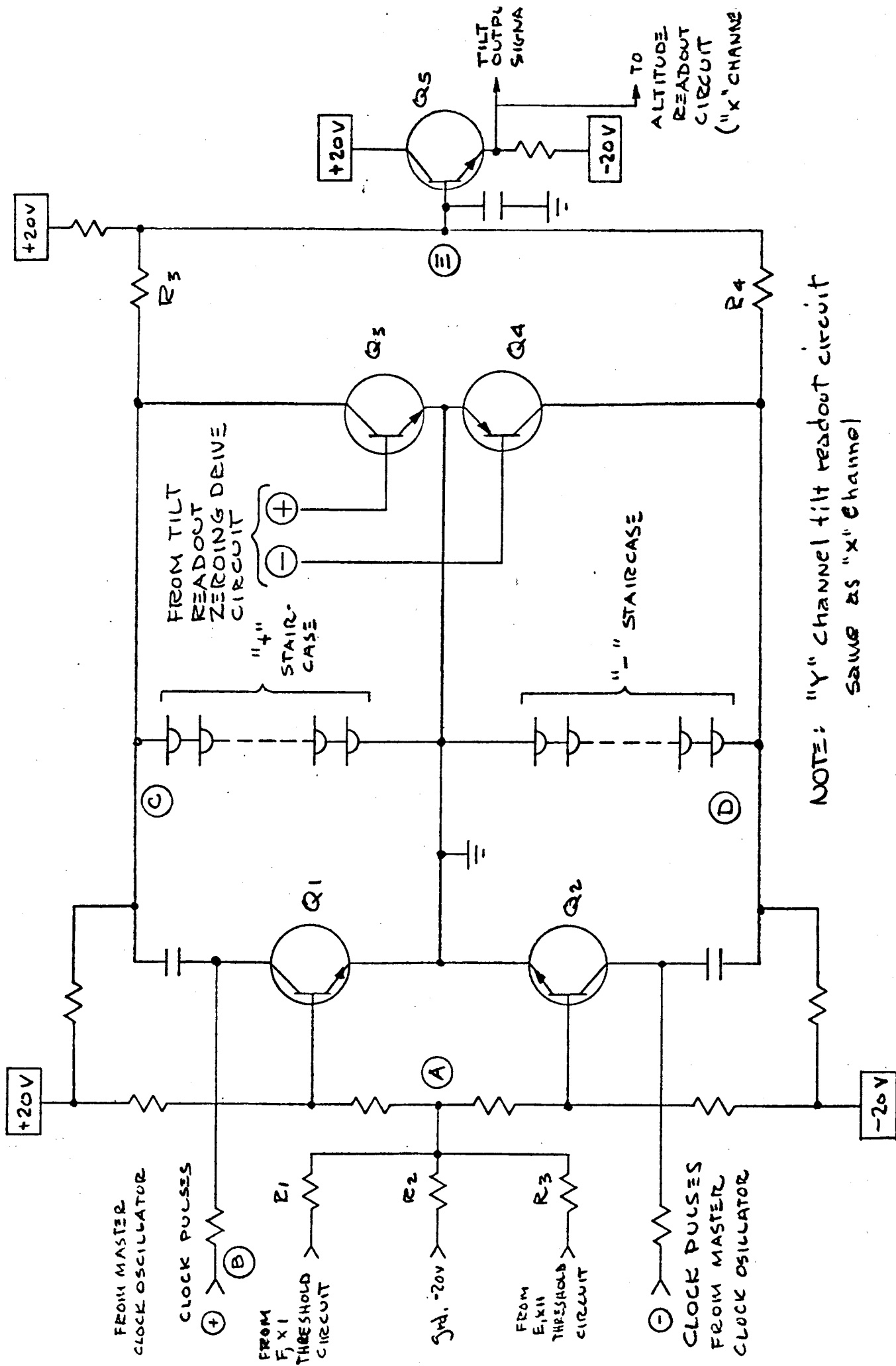
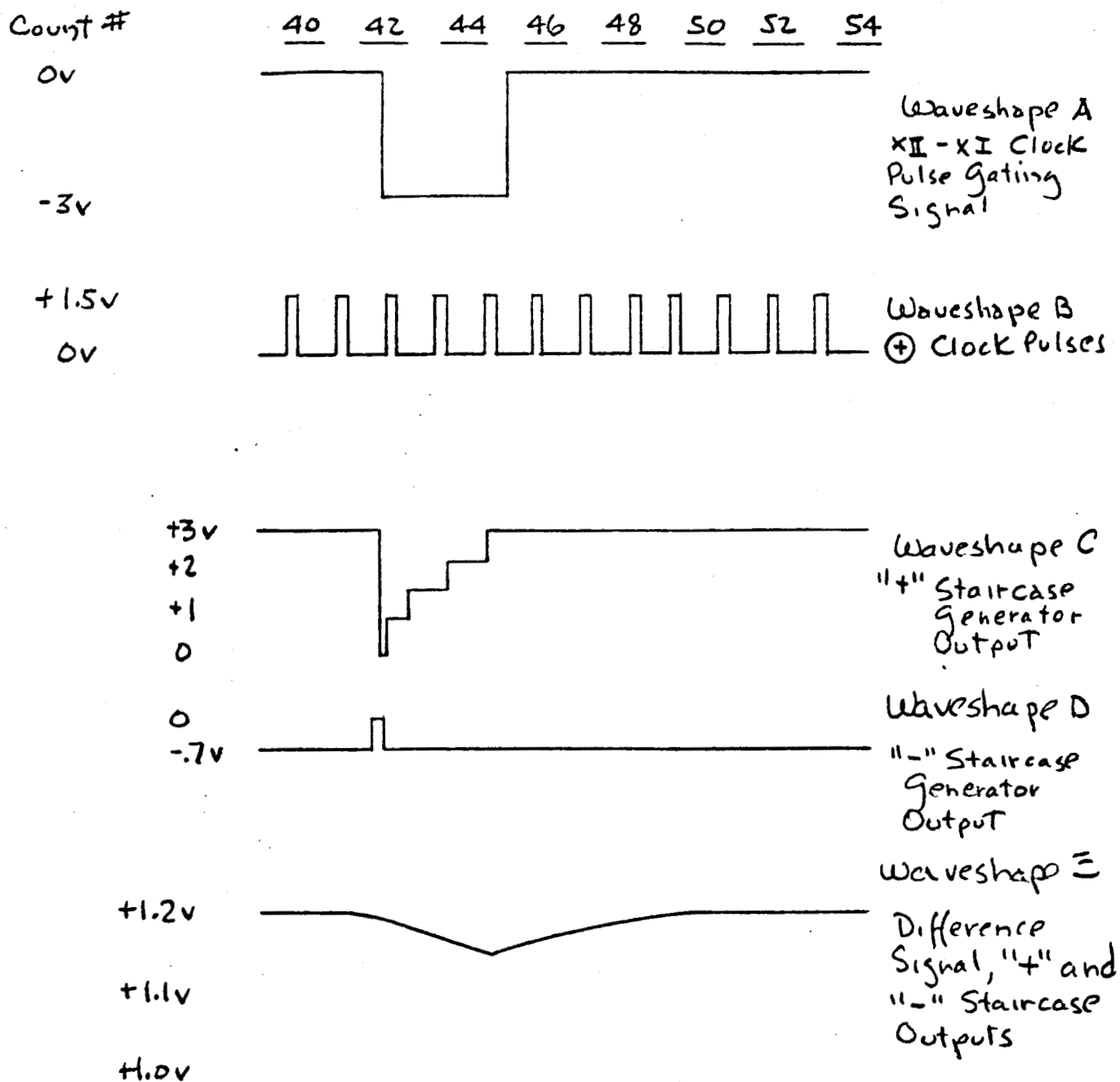


Figure S-22 ALTITUDE READOUT CIRCUIT—"X" CHANNEL

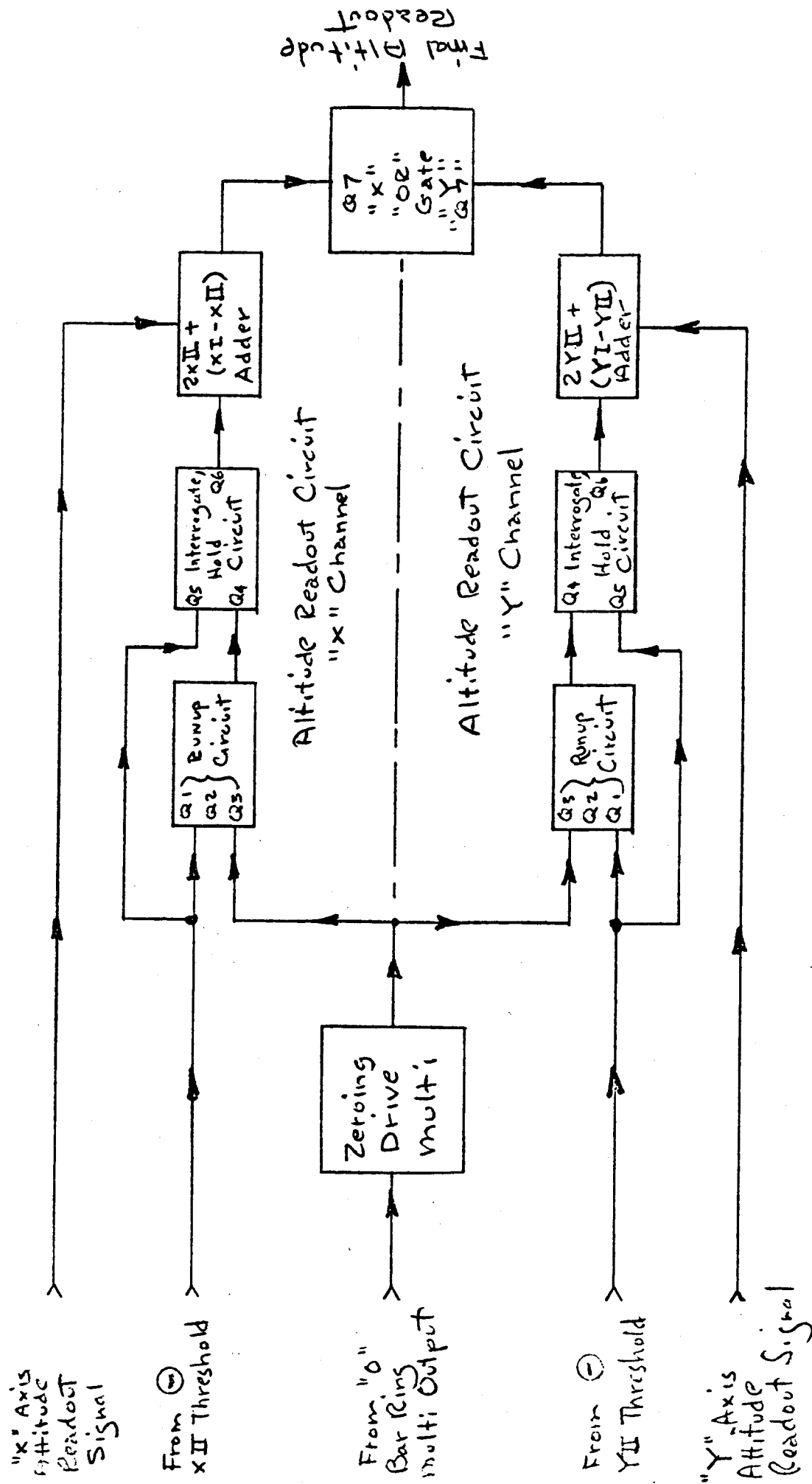
20,054



Note: Scale factor at E equals  $\pm 0.8\text{v/degrees tilt}$

Figure S-23 Waveshapes, X-Channel Attitude Readout Circuit,  
Lunar Scan

20,055



20,036

Figure S-24 Altitude Readout Block Diagram

shows the basic process, in which the time interval from the beginning of the cycle to horizon crossover for channels XII and VII is obtained as a voltage integral. The tilt error signal for X and Y heads is added to their respective time-voltage integrals (using appropriate scale factors), giving the space subtense angle ( $180^\circ$  minus planet subtense angle) as independently measured by the two orthogonal sets of heads. The highest of these summations is read out as the altitude output. (A foreign body near the planet limb in one sensor's field of view gives a smaller sum for that opposing pair of heads.) The counts are zeroed each cycle on the first detector sample.

#### 5.12 ALTITUDE RUNUP ZEROING DRIVE MULTIVIBRATOR

This circuit, shown in Figure 5-25, is a one-shot multivibrator which is triggered by the zero bar of the ring multivibrator. It generates a pulse whose timing corresponds to the first five sample periods, and during its occurrence the altitude readout circuit is zeroed.

#### 5.13 ALTITUDE READOUT CIRCUIT (See Figure 5-26)

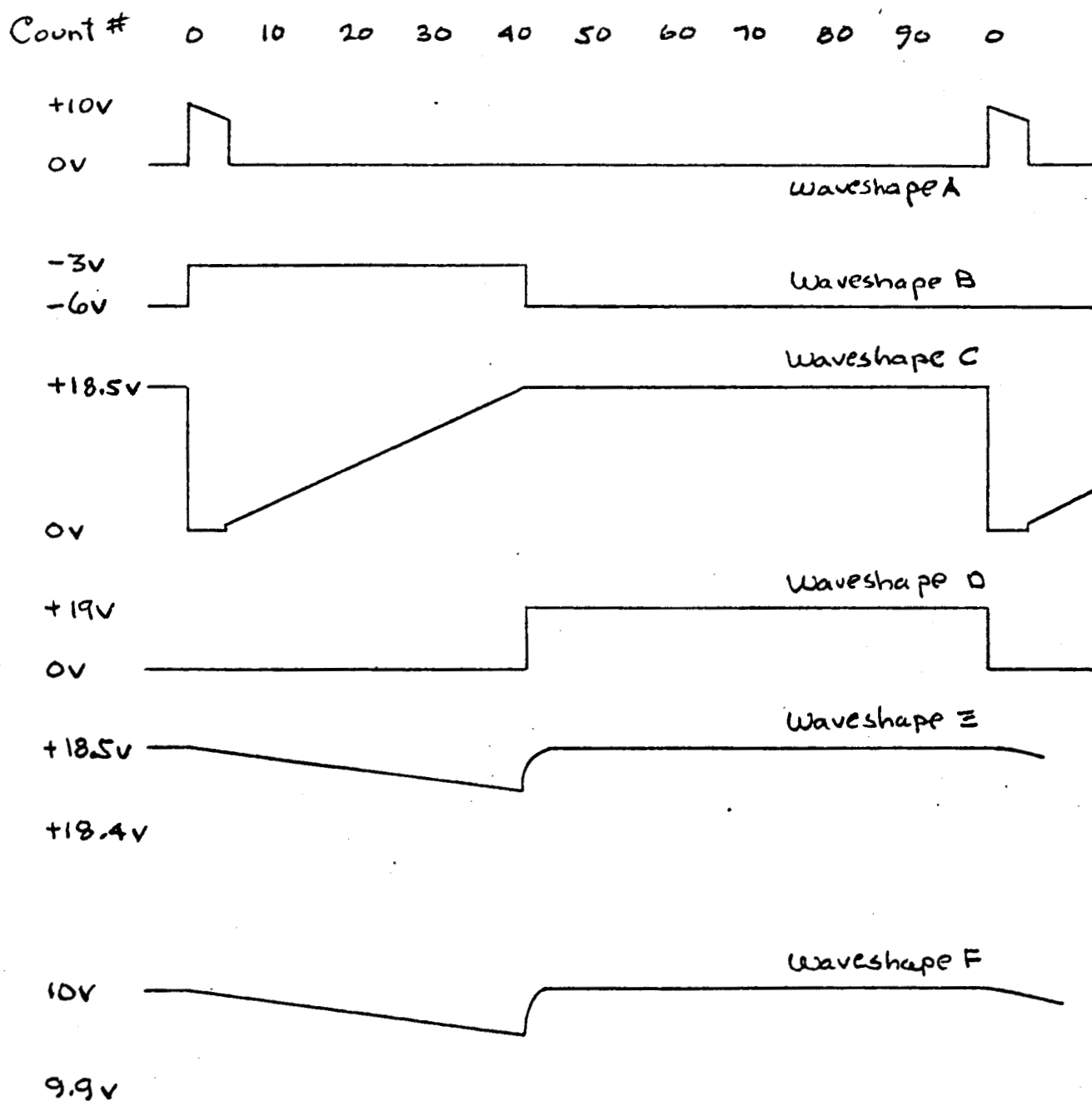
This circuit is a precision integrator which charges capacitor C1 through resistor R1 until threshold crossover is achieved. Transistor Q1 is held at -3 volts by the resistor divider, (see Figure 5-27, waveshape B). When threshold crossover occurs, this voltage drops to -8 volts. Since the zener Z1 firing voltage is less than this, transistor Q1 is cut off, and the voltage on C1 is held, (see waveform C). At the same instant, transistor Q5 is also cut off, and Q4 is driven from the +40 volt supply (D), performing the interrogation function (E). Capacitor C2 filters the signal, and the addition of the tilt signal is performed (F) before the final output stage Q7, which, with the corresponding Y channel output transistor selects the largest signal (most space).

#### 5.14 ALARM OUTPUT

If the planet (space) subtense angles obtained from the X and Y channels are not the same (within two counts), a foreign body is present, or a system malfunction has occurred. In either case, an alarm output is provided.







Note: Output at F equals plus .13 v/element of space scanned. 10 volt output shown corresponds to 77 detectors viewing space.

20,059

Figure 5-27 Waveforms, x Channel Altitude Readout Circuit, Lunar Scan



This output is obtained by taking the difference between the sums of the threshold signals for the X and the Y channels. As shown in Figure 5-28, the first threshold crossover from any of the four heads acts through the "or" gate to zero the alarm integrators. Then the negative Y threshold signals are added to the positive X threshold signals and the combined sum is integrated. This integral is filtered to remove the zero component and becomes the alarm output signal. A new determination is made of the alarm output during each scan interval.

#### 5.15 ALARM OUTPUT CIRCUIT (See Figure 5-29)

This circuit consists of a diode "or" gate, and an inverter which operates a bipolar zeroing drive. A resistive summing network adds the threshold signals. The amplifiers Q1, Q2, and Q3 form an operational integrator, which provides the alarm output. Figure 5-30 shows the waveforms.

It should be noted that the alarm output is only significant when the attitude readouts are within their linear range. In addition, the alarm output must reach plus or minus 4 volts before definite recognition of a spurious body can be determined. The output polarity signifies whether the "X" or "Y" channel readouts are in error due to spurious body presence. If only a go - no go type of output is desired, an over-under comparator circuit set to  $\pm 3$  volts has to follow the alarm output circuit.

#### 5.16 ELECTRONICS RELIABILITY

The following is a breakdown of the total number of transistors used in the system's electronics.

Timing and Commutator Drives	24
Clock - 2	
Ring Multi - 11, (2 required)	
Signal Channel	56
Preamplifier - 5, (4 required)	
Offset Source - 5 (4 required)	
Threshold, "0-1" switch - 4, (4 required)	

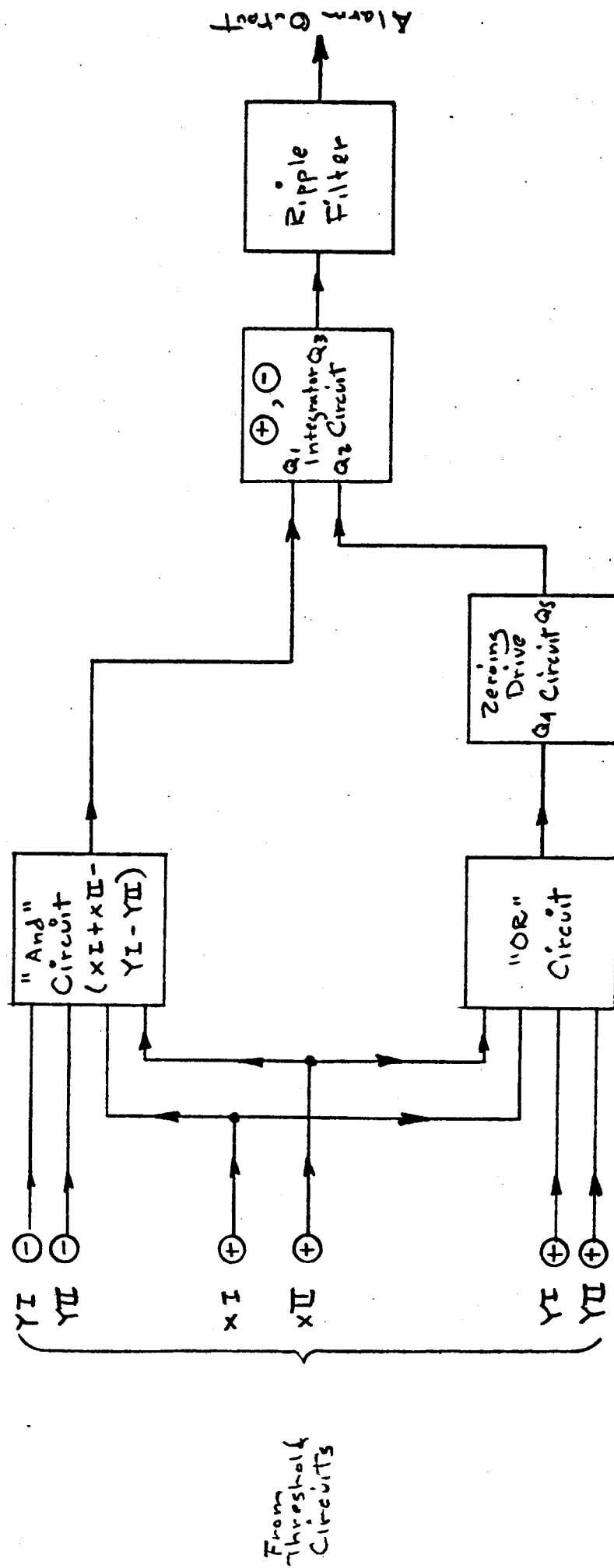


Figure 5-28 Alarm Output Circuit Block Diagram

20,060

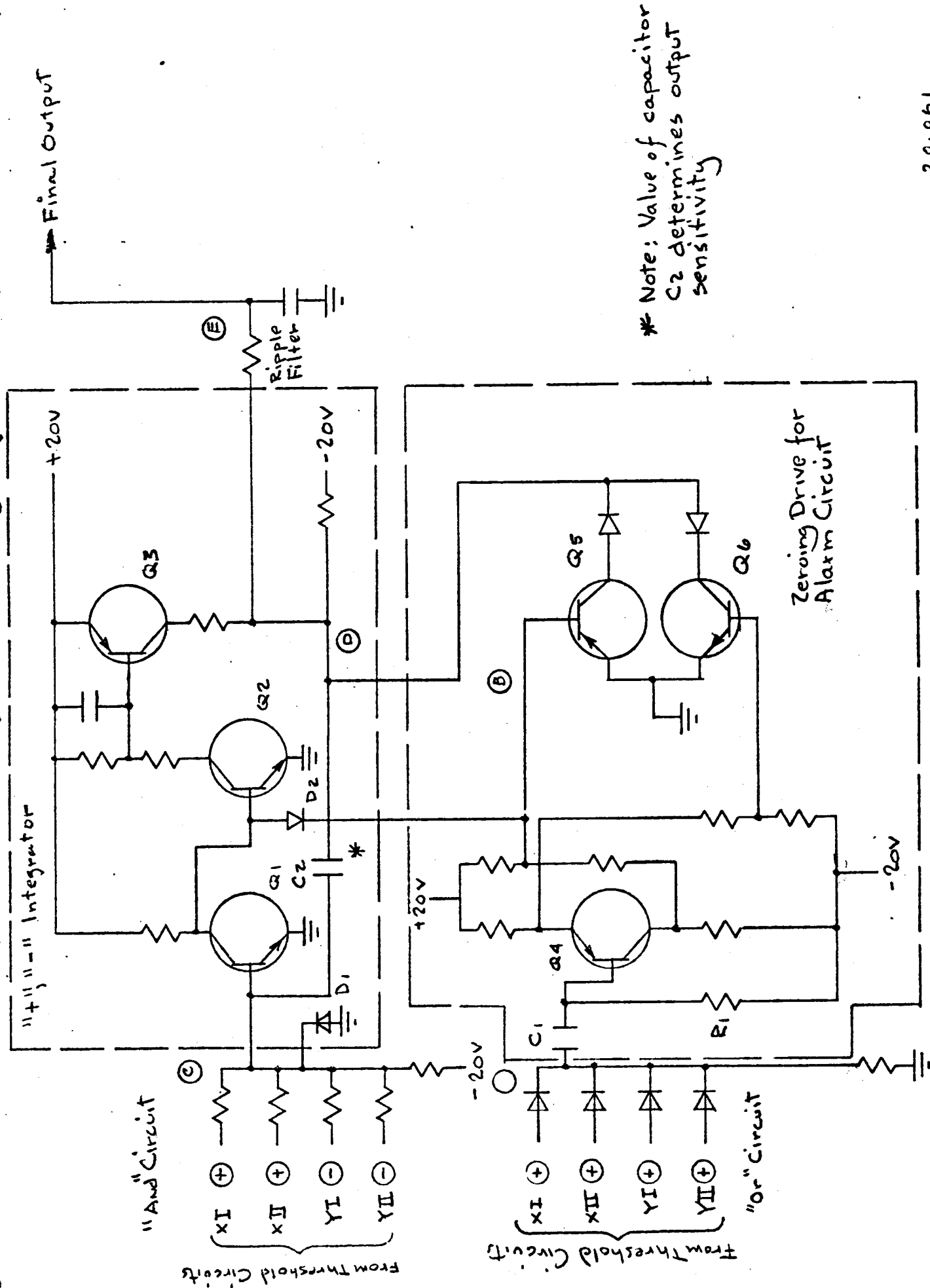


Figure 529 Alarm Output Circuit

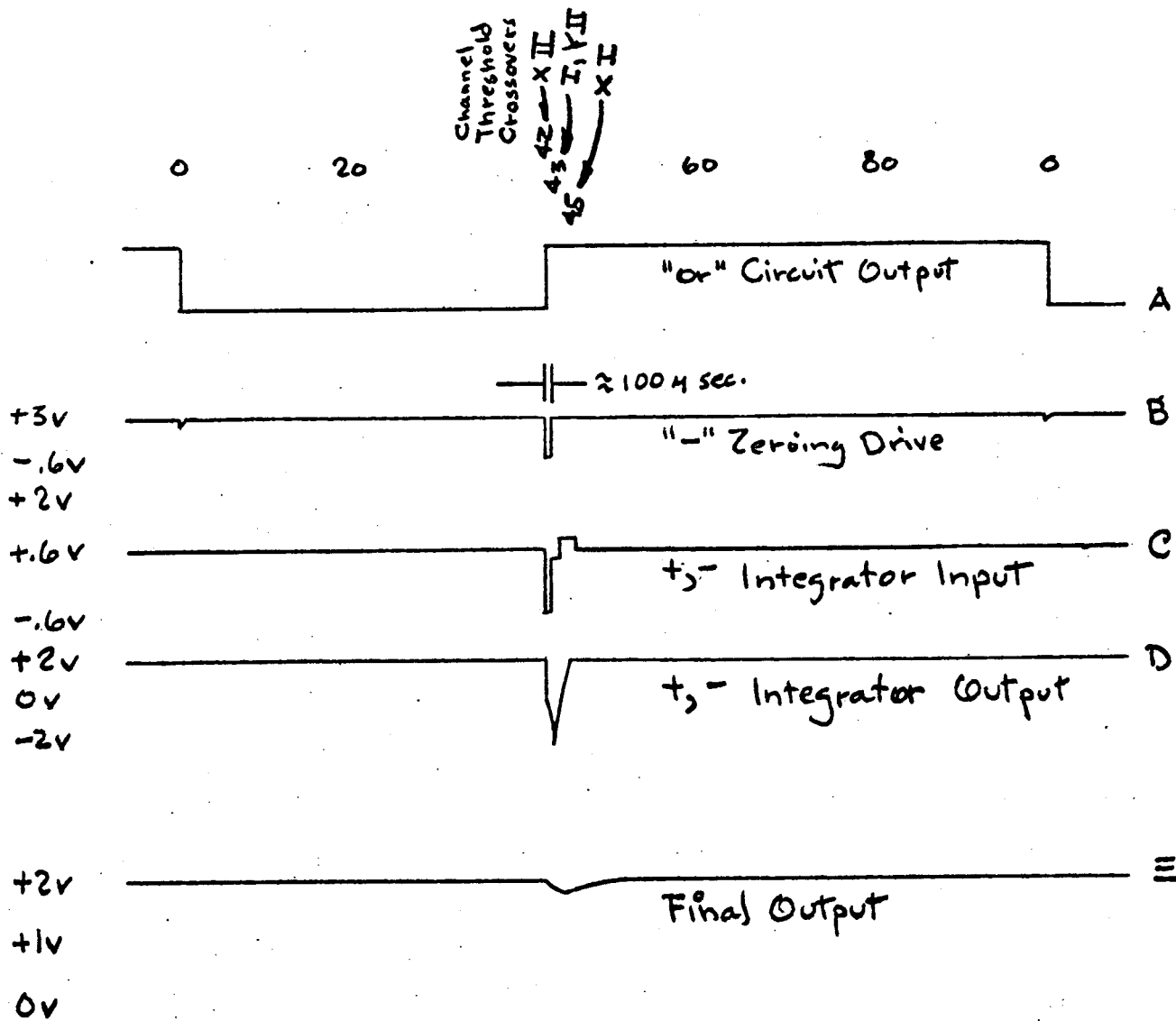


Figure 5-30 Waveshapes, Alarm Circuit 20,062

Attitude Readout	12
Zeroing Drive - 1, (2 required)	
Readout Circuit - 5, (2 required)	
Altitude Readout	16
Zeroing Drive - 2	
Altitude Circuit - 7, (2 required)	
Alarm Output Circuit	6
Power Supplies (+ and - regulation) (approximately)	<u>6</u>
Transistors Total per System =	118

On the average, 3 resistors, 1 capacitor, and 1 diode is used with each transistor. According to the R.A.D.C. components reliability handbook, the failure rate for each transistor (conservatively stressed) is  $0.22 \times 10^{-6}$  failure/hour, and the combined failure rate of the associated resistors, capacitor, and diode are about equivalent.

The mean time to failure of the electronics section of the system can be computed by the following formula:

$$\begin{aligned} \text{System MTBF (years)} &= \frac{1}{F \times N \times 8760 \text{ hrs./year}} \\ &\approx \frac{1}{.44 \times 10^{-6} \times 8760} = 2.6 \text{ years.} \end{aligned}$$

where  $F$  = failures per hour of each transistor and associated components  
and  $N$  = total number of transistors.

The R.A.D.C. handbook gives reliability figures for standard grade Mil specification components. If high reliability parts (similar to Minute Man parts) were used instead, the individual component reliabilities are increased by the following factors.

<u>Component</u>	<u>Reliability Improvement</u>
Transistor	10x
Resistors	2x
Capacitors	5x
Diodes	5x

By using high reliability components, the system's overall electronic reliability MTBF can be extended to approximately 7 years. The system also utilizes thermopile detectors and cadmium selenide cells. Little information is currently available regarding the reliability of these components. However, the overall system configuration is such that single components in these areas can fail without seriously affecting the overall performance.

It is realized that this equipment may be expected to function without maintenance in a space environment for over two years. With this time interval, the probability of success of the system as presented is approximately 70% (using high reliability parts throughout). If better reliability is desired, redundancy should be used wherever necessary to achieve the desired overall probability of success.

One other factor should be considered in regard to reliability. The individual circuits either operate in a zero-one fashion, or are inclosed by negative feedback. For this reason, (except for a few components such as the selected low noise amplifier input transistors), individual component failure must be catastrophic before system failure occurs. Therefore, slow degradation of components due to operation in space vacuum and radiation fields for long periods of time should not affect system performance.

Section 6.0 CONCLUSION6.1 GENERAL SPECIFICATION6.1.1 Scope

This General Specification covers anticipated capabilities of the Lunar and Planetary Horizon Scanner prototype, hereinafter referred to as LPHS, that would be useful for Lunar orbiters as well as other missions, including Voyager terminal guidance and orbiters of Mars and Venus.

6.1.2 Description

The LPHS provides two-axis local vertical position error signals and apparent angular diameter information to be used for range purposes against the following celestial objects in the order of their relative priority: (1) Moon, (2) Mars, (3) Venus, and (4) Earth.

6.1.3 Applicable Documents

No JPL Specifications are included in this General Specification.

6.1.4 Requirements

6.1.4.1 Accuracy and Dynamic Range - The accuracy and dynamic range capability are shown in Table 6-1.

6.1.4.2 Optional Accuracy - The optional accuracy under influence of a disturbing radiant source.

a. If a single foreign radiant source is within  $2^\circ$  of the planet limb being tracked (see Figure 2-3), and is viewed by the system, the accuracy requirements of Table 6-1 are relaxed to  $2.5^\circ$  null stability and 10% range accuracy. In flight, the device yields an alarm output (into a 50K resistive load) when the optional accuracy applies.

6.1.4.3 Acquisition Range - The LPHS shall deliver properly phased error signals or search logic signals when the near planet limb is within  $91^\circ$  of the LPHS mechanical null line of sight in certain configurations, as shown in Figure 2-2.

TABLE 6-1  
ACCURACY VS. RANGE FROM SURFACE\*\*

3σ Tolerance on "absolute"* null stability	.45°	.45°	.45°	.45°	.45°	.45°	.45°	
3σ Tolerance on "absolute" apparent diameter	20%	3.8%	3.6%	2%	1.2%	.3%	6%	
Range from Planet Surface in Planet Radii	50	8.5	8.1	4.1	2.1	.1	.02	0
Apparent Diam. (approximate)	2.2°	11.9°	12.5°	22°	37.6°	130°	157°	180°
Optional Region for future growth potential	Required Region							

\* Absolute null stability is the maximum allowable in-flight angular deviation between "the instrument" electrical null position and its external mechanical reference surfaces. (In contrast with resolution which is the minimum detectable angular change.)

\*\* Sensor heads are assumed tilted down 9° from positions described in the body of this report to reach optional region.



6.1.4.4 Time Constant - The system time constant is .3 seconds when viewing bodies at 120°K, and 1.2 seconds when viewing bodies at 400°K in response to a step function change in angular position from null to  $1.2^\circ + 3\sigma$ . Time constant refers to response within the linear range region only.

6.1.4.5 Error Signal Output - The two axis output error signals are step-analog .6 volt per degree ( $\pm 10\%$ ) with an output impedance of less than 3000 ohms.

6.1.4.6 Apparent Diameter Output - The apparent diameter output is step-analog and is linear. The apparent diameter output will be single valued when the planet is within  $6^\circ + 3\sigma$  null requirement of its external alignment reference null position.

6.1.4.7 Required Power - The following power will be required by the LPHS:

2400 cycle square wave 104 volt peak-to-peak

( $\pm 5\%$  tolerance on the RMS value)

D.C. battery power  $28V_{-4V}^{+6V}$ : 10 watts (In vacuum)

6.1.4.8 Prototype Definition - The LPHS prototype developed under this contract need not be flight configuration.

a. An optical breadboard, neatly packaged, the volume of which should be approximately the same as the expected flight hardware, is visualized as the mechanical configuration of the optical portion of the prototype.

b. An electronic breadboard, neatly packaged, the volume of which is not specified, is visualized as a satisfactory configuration for the electronics portion of this prototype.

c. The electronic and optical breadboards, when properly interconnected, must meet the other accuracy specifications of this General Specification.

#### 6.1.5 Anticipated Specifications for the Follow-On Flight Units

The anticipated specifications for the follow-on flight units include the following requirements:

a. Specification No. 30258, Environmental Specification, Mariner B Flight Equipment.

- b. Specification No. 20061A, JPL Preferred Parts List.
- c. Specification No. 30237, JPL Component Screening Specification.
- d. Continuous unattended operation in flight of three (3) years mean time to failure.
- e. It is unlikely that the follow-on flight hardware will be capable of withstanding heat sterilization of 145°C for twenty-four (24) hours non-operating.

## 6.2 SYSTEM TESTING

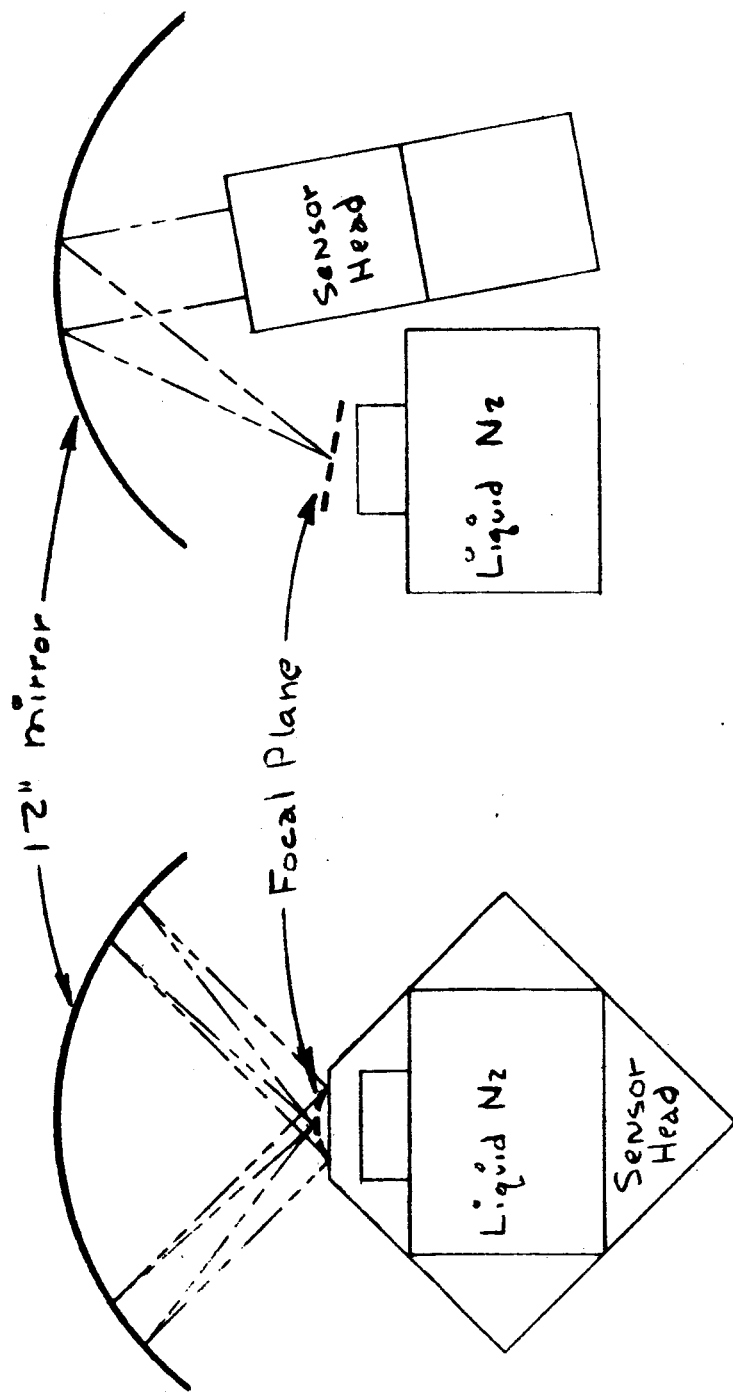
Although important tests will undoubtedly be performed in a vacuum chamber, the system has been designed to operate in normal atmosphere (although slightly more power is required). Because of the need to test operation against cold sources, a simple simulator will be constructed which will permit the sensor to look directly at the surface of liquid nitrogen as a space reference. Such a simulator is shown in Figure 6-1, and would be minimal to permit preliminary checkout of the LPHS.

## 6.3 ANALOGUE INTERPOLATION

The logarithmic compression necessary in the preamplifier to reduce dynamic range allows the incorporation of a simplified analogue interpolation technique. In this technique, the logarithmic signal from the first detector partially viewing planet is subtracted from the logarithmic signal from the next. The antilog of this difference is the percentage of the first detector that actually sees planet. This antilog is finally added to the tilt readouts in correct proportion, giving the interpolated signal.

The technique depends on the infrared uniformity of the planet over a 2° region at the limb. If the planet is not uniform in this region, the accuracy is degraded, but can never become worse than the inherent digital accuracy. The probability of degradation is least on Venus and the Earth, greater on Mars, and greatest on the Moon.

This circuit is easily incorporated into the system as presently envisioned, and its addition is strongly recommended.



20,043

Figure 6-1 Minimal Simulator

#### 6.4 PROBLEM AREAS

Several problems were uncovered in the study which will require further investigation. The preamplifier described in this report has some low frequency instability which is not understood. A somewhat different design is being considered which also permits grounding one side of the detectors and will be easier to evaluate. Basic design criteria are similar for this preamplifier.

A recent report<sup>6</sup> reveals that the Moon may reach 100°K or colder after several days of lunar night. This would make operation exceedingly difficult as originally envisioned, and signal-to-noise improvement is necessary.

A further difficulty has been suggested in the variation of incidence angle on the optical coating. (The Appendix shows the variation of wavelength turn-on with incidence angle.) Investigation shows that an energy transmission variation of +8% occurs from 0° to 45° incidence. This changes to +4% when the sensor goes from +70°C to -40°C. By proper aperture obscuration at the ends of the mirror, this change can be reduced to +1% to -3%. Without further reduction, the +1% variation of the +70°C space radiation offset of -150μV gives an imbalance of -1.5μV over half of the detector array. Likewise, the -3% variation of the -50μV space radiation offset gives +1.5μV over half the detector array.

One additional variation with incidence angle exists in the change in absorption due to path length increase at 45° incidence. This amounts to a .6% decrease in energy transmission, which partially acts as the aperture obscuration described in the preceding paragraph. The Appendix shows the absorption characteristics of silicon.

These variations, though small, are very significant in lunar operation. A short preamplifier time constant allows such small variations to exist along the detector array. However, a long time constant is necessary to eliminate foreign bodies. Clamping techniques appear to offer the best means of solving this problem, as this permits a fast time constant while scanning space, and a slow time constant to allow maximum fidelity in examining possible planetary reference bodies. No processing difficulty is expected in operation on Mars, Venus, or the Earth.

Another significant problem is the possible ionization of the neon lamps in penetrating radiation. Little has been found to indicate how severe such ionization could be, but it is probably restricted to the Van Allen belts. If the effect is only to lower the firing potentials of the lamps, the system will function satisfactorily. If, however, all lamps glow to any extent, system performance will be seriously degraded. In deep space, cosmic rays may produce momentary lamp ionization, but the probability is relatively good that a space viewing element will be activated, which will not produce system error.

#### 6.5 FEASIBILITY

Serious problems remain to be solved in order to achieve operation on the dark side of the Moon. These problems do not appear insolvable, and several techniques are being considered to resolve the difficulties. This will not seriously interfere with the Phase II prototype as presently seen, since this unit does not contain the logic processing.

In the case of Mars, Venus, and the Earth, no difficulty is seen except for possible radiation effects on the commutator lamps. The system appears entirely feasible as presently conceived, and the incorporation of analogue interpolation as a technique is strongly recommended to improve the accuracy to  $0.1^\circ$  on attitude stabilization.

## APPENDIX I

### THERMAL ANALYSIS

#### 1-1 DEFINITIONS (as used in the Handbook of Physics and Chemistry)

##### A. Calorie

The definition of the calorie is the amount of heat required to raise the temperature of 1 gram (1 cc.) of water 1°C.

$$1 \text{ calorie/sec.} = 4.186 \text{ watts}$$

The calorie is a basic unit of heat, and is dimensionally identical (only differing by a multiplier constant) to British Thermal Units.

$$1 \text{ calorie} = .003968 \text{ B.T.U.}$$

##### B. Specific Heat

The definition of a material's specific heat is the number of calories required to raise the temperature of 1 gram of material 1°C. Note that specific heat relates different materials to water on an equal weight basis. To obtain a material's specific heat on a volume basis, it is necessary to multiply the specific heat of a material by the reciprocal of its specific gravity. It is more convenient to utilize the volumetric specific heat of a material in thermal computations because physical structures are generally specified in length dimensions rather than by weight.

##### C. Thermal Conductivity

This is defined as the number of calories per second required through a pair of opposite faces on a 1 cm x 1 cm x 1 cm cube of material to obtain 1°C temperature differential across the cube. Note that the 1°C temperature differential is measured along 1 cm length of caloric flow, and that the calories are flowing through a uniform cross-section of 1 square cm.

#### D. Thermal Resistivity

A material's thermal resistivity is the reciprocal of its thermal conductivity. Dimensionally, the thermal resistivity of a material is the degrees centigrade temperature differential obtained by causing 1 calorie per second to flow along a 1 cm path length through a 1 square cm. crosssection of material. Note that the temperature differential is measured along (and not across) the directions of caloric flow.

#### E. Static Cases

Static cases involve temperature gradients within and caloric flows through a given structure wherein no temperature variations are occurring with time, (i.e.: temperature equilibrium has been achieved). This implies that the same number of calories are flowing into and out of any single section within a given structure. Solutions to thermal problems involving thermal static structures are relatively simple and do not require knowledge of a material's specific heat.

#### F. Dynamic Cases

Under dynamic conditions the temperatures and/or calories throughout a structure are varying in time. Solutions to these types of problems are more involved than for static conditions, and both the specific heat and thermal resistivity of the structure materials being considered must be known to yield solutions.

#### G. Radiation Interfaces

When a structure terminates at an outer boundary that faces space and the radiant watts being absorbed and emitted by the surface are known, the

watts can be converted directly to calories (see IA). Temperature and caloric flow considerations involving the surface can then be treated as if no interface exists, and the actual boundary only implies the dimensional limit of the structure.

## I-2 BASIC SYMBOLS AND FORMULATIONS

- 1)  $Q$  = Calories
- 2)  $h$  = material specific heat per cubic centimeter
- 3)  $c$  = material thermal conductivity per square centimeter area and per centimeter length
- 4)  $r = \frac{1}{C}$  = material thermal resistivity
- 5)  $H = V \times h$  = the total heat mass of a given volume of material  
 $V$  = volume expressed in  $\text{cm}^3$ .

Dimensionally,  $H$  is the number of calories required to raise the temperature of a specified material volume  $1^\circ\text{C}$ .

- 6)  $C = \frac{W \times H}{L} \times c$  = total thermal conductance of a given homogenous section of material.

where  $L$  is the distance in cm. through the material along which a constant amount of calories are flowing each second, and  $W \times H$  is the crosssection through which the calories are flowing. It is necessary to have the crosssection being considered perpendicular to the direction of caloric flow. In addition, the calories flowing into and out of each crosssectional area must be the same.

Dimensionally,  $C$  is in terms of calories per second required to establish a  $1^\circ\text{C}$  differential along a given distance in a given direction through the structure being considered.



7)  $R = \frac{L}{W X_H}$  X r = the total thermal resistance of a given homogenous section of structure.

$R = \frac{1}{C}$ , and therefore the same comments on caloric

flow direction apply for R as for C.

Dimensionally, R is in terms of degrees centigrade temperature difference required between two parts of a structure to produce a caloric flow of 1 calorie/second through the structure.

### I-3 STATIC CASE THERMAL COMPUTATIONS

Formulas (6) and (7) can be used in static case computations to determine caloric flows through and temperature differences across homogenous, uniform crosssectional area structure sections. A complex structure can generally be broken down into individual sections that have uniform homogenous crosssections. If necessary, approximations can be made of complex crosssections to yield an average uniform area. If the temperature differential across an individual section is known, then multiplying "C" in formula (6) by the  $\Delta T$  gives the calories through the section. Similarly, if the calories through a structure section is known, multiplying "R" in formula (7) gives the  $\Delta T$  across the section with the known caloric flow.

The summation of the temperature differentials caused by a known caloric flow through adjacent sections that comprise the structure yields the over-all temperature differential across the structure. Similarly, the summation of all caloric flows through sections between separated structure areas yields the total caloric flow between the areas being considered.

With the foregoing, a general statement can be made. If the various caloric flows into and out of a complex structure are known and one point on the structure provides a temperature reference, then all temperatures and caloric flows throughout the structure can be determined.

The thermal solution of a static complex structure requires repetitious computations involving formulas (6) and (7), and additional computations involving radiation interfaces. For this reason, use is made of thermal work sheets to simplify the computations made in report sections 4.6.2 and 4.6.3. The individual computations are numbered in the order of their occurrence, as results of individual structure section computations are sometimes used to determine temperature differentials across or caloric flows through adjacent sections. The dimensions of the numbers used in each individual computation is given at the head of each column, and the text calls out the final result.

#### I-4 DYNAMIC CASE THERMAL COMPUTATIONS

Dynamic case thermal formulations are more complex to derive than those for static cases. Only one dynamic condition is covered in this report. This deals with the temperature differentials throughout a structure driven from one area, which causes all points in the structure to change temperature at an equal and uniform rate. In the situation covered, the varying temperature is introduced at the ends of the bridge that supports the thermopile detector array, and computations are made of the distribution of temperatures along the bridge and the maximum degrees per hour temperature rates that the system will accommodate without affecting performance. Various shaped bridge structures were analyzed and the optimum shape and characteristics are indicated in the text.

One term of importance in dynamic thermal analysis is diffusivity, symbolically represented by "k", which is the ratio of a materials thermal conductivity divided by its volumetric heat mass. In similar shape structures and dynamic thermal conditions, the temperature differential between two points is inversely proportional to the diffusivity of the structure's material. The best diffusivity figure is obtained with silver, and second best are copper and aluminum. Magnesium and Beryllium have both relatively poor diffusivities. When, as in this system, easy machinability, light weight and high diffusivity are all important, aluminum appears most desirable as a choice of structure material.

It is easiest to understand the dynamic case thermal equation presented in section 4.6 by the following example -- assume a bar of material with a uniform cross section of 1 square cm. and a length of 10 cm. - let both the thermal resistivity and volumetric heat mass of the bar material be equal to unity. Then assume that one end of the bar is caused to continuously increase in temperature at a rate of 1°C per second, and the other bar end is "space" terminated. If the bar were in vacuum, and its outer surfaces were 100% reflecting, then the only source of calories to the space terminated end of the bar would be through the bar itself. The last cm. of length on the bar would require 1 calorie per second (thermal heat mass = 1) to change temperature at a 1° per second rate. This one calorie/sec. would flow through 9 cm. of bar length from the driven end to within 1 cm. of the space terminated end.

The next cubic cm. adjacent to the last cm. at the bar end also requires 1 calorie per second to change temperature at a  $1^\circ/\text{second}$  rate. Therefore, to supply calories to this next to the end cubic cm., one additional calorie must flow through the first 8 cm. of bar length each record.

Continuing the foregoing to cover the entire length it is obvious that with the conditions stated, the difference in calories/second entering and leaving each cubic cm. along the bar length is 1, and that the total calories entering the bar's thermally driven end is  $10/\text{second}$ , and leaving the space suspended end is 0. A more general statement of the foregoing is that for a constant  $1^\circ/\text{sec.}$  bar temperature rate of change, the number of calories/sec. passing through a crosssection at a point along the bar's length is directly proportional to the thermal heat mass between that point and the space suspended bar end. From this, the gradient at any bar point can be obtained as the forementioned heat mass multiplied by the bar material's thermal resistivity. (Note that thermal resistivity equals 1 divided by thermal conductivity, and therefrom comes the necessity of maximum diffusivity for minimum gradient in dynamic cases.) The gradient at the bar's space end is zero, and is maximum at the driven end.

To obtain the difference in temperature between any two points on the bar, it is necessary to integrate the gradients between the two points. Then, by knowing what temperature is produced between two points on a specified bar driven at a specified rate, it is possible to compute the inverse relationship, (i.e. what temperature rate of change will produce a specified temperature difference), which is the ultimate desired information.

The following thermal formulations develop the general dynamic single end driven bar case. Although these formulations are evolved from the previously covered constant crosssectional area bar description, they are also valid for any bars where the bar's crosssectional area can be expressed as a function of position along the bar.

#### DYNAMIC CASE FORMULATIONS - GENERAL.

Extended bar, one end driven at a constant temperature rate, other end space terminated.

$$1) V = \text{Volume} = L \times W \times H$$

$$2) A = \text{Crosssectional area} = W \times H$$

where  $L = X = \text{dist. in cm. from space suspended bar end}$

$$W = \text{constant} = 1$$

$$H = f(x)$$

$$\text{if we let } L = \int_0^x dx + c_1$$

then

$$3) V(x) = \int_0^x f(x) dx + C_1$$

and

$$4) A(x) = f(x)$$

with a  $\frac{dT}{dt} = 1^\circ\text{C/sec.}$

$$5) \frac{dT}{dx} = \text{temperature gradient at point "x" on bar}$$

$$= r h \frac{V(x)}{A(x)} = \frac{h}{c} \frac{V(x)}{A(x)} = \frac{1}{k} \frac{V(x)}{A(x)}$$

where  $r$ ,  $h$ , and  $c$  are as defined in Section I-2 for the

bar material used, and  $k = \frac{c}{h} = \text{material diffusivity.}$

6) 
$$\int_0^x \frac{dT}{dx} = \text{temperature difference between the space}$$
  
 suspended end of bar and point "x" on bar,  

$$= \frac{1}{K} \int_0^x \frac{V(x)}{A(x)} + C_2$$

7) to determine  $\frac{dT}{dt}$  ("M") required to achieve X  
 temperature difference between the space suspended end  
 of the bar (x=0) and some point x (x=n) on the bar.

$$\Delta X = M \int_0^{x_n} \frac{dT}{dx} = \frac{M}{K} \int_0^{x_n} \frac{V(x)}{A(x)} + C_2$$

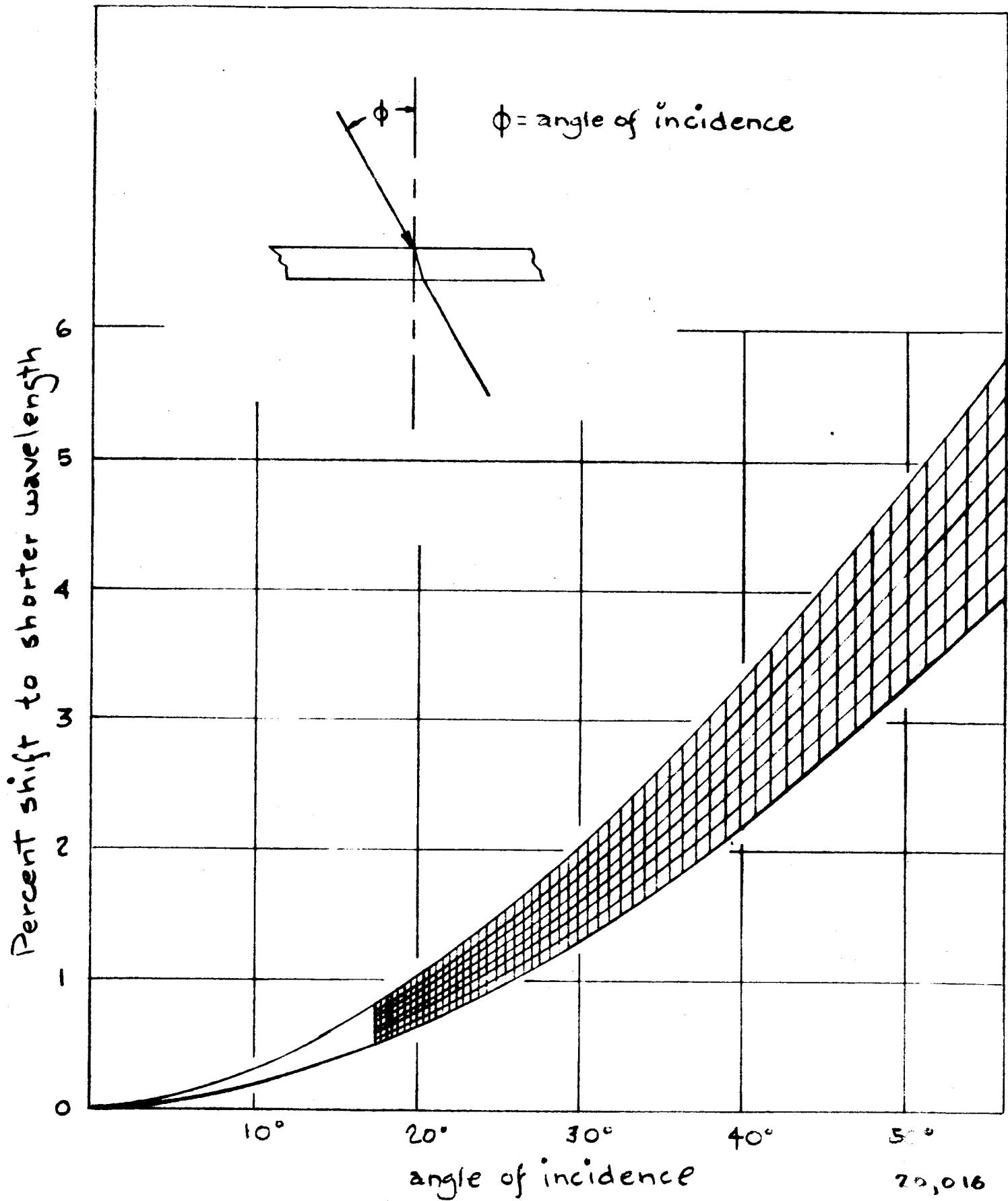
or 
$$\frac{1}{M} = \frac{1}{\Delta X K} \int_0^{x_n} \frac{V(x)}{A(x)} + C_2$$

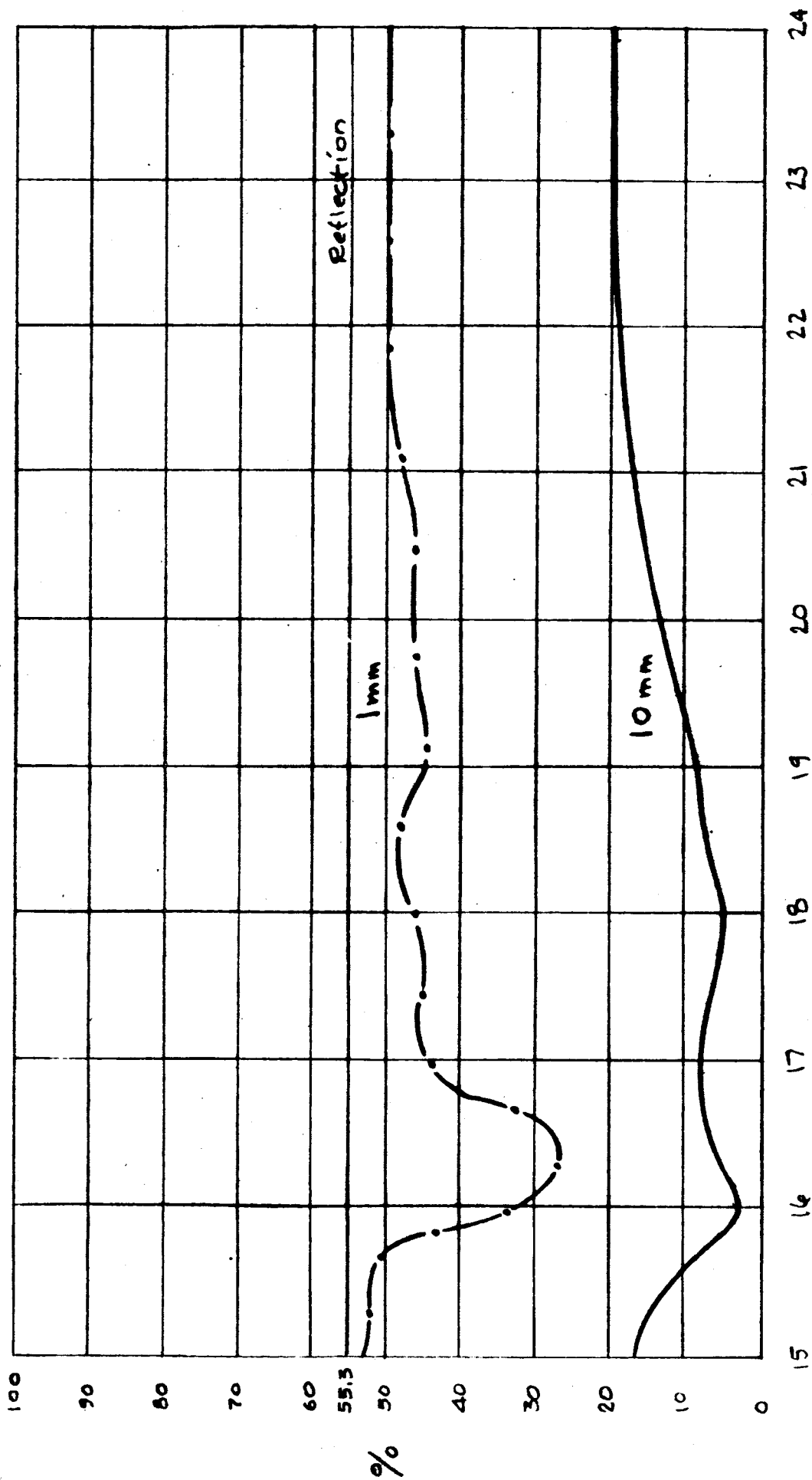
The previous formulas assume that each crosssectional area considered is perpendicular to the direction of caloric flow, and that the distribution of calories is uniform in each crosssection at any instant of time. Appropriate corrective approximations should be used if these restrictions are not satisfied.

Table 4.1 in Section 4.6.4 covers various bar shapes, and analyzes their gradients and temperature differentials. As the bar shapes become more complex, the corresponding integrals that show crosssectional area and the double integral functions that provide the temperature difference between points on the bar become increasingly more difficult to determine and evaluate. If it is felt, however, that sufficient shapes have been covered to show that the one that is to be used is optimum.

# APPENDIX

## A-1 Wavelength Shift as a Function of Angle





A-2 Percent Transmission of Silicon  
λ Microns

201017



## BIBLIOGRAPHY

1. Physics and Astronomy of the Moon, by Zdenek Kopel, Academic Press, New York, 1962.
2. The Atmosphere of Mars and Venus. National Research Council, Space Science Board, Ad Hoc Panel on Planetary Atmospheres, Washington, 1962.
3. Behavior of Materials In Space Environments, by L. D. Toffe and J. B. Rittenhouse, Jet Propulsion Laboratory Technical Report No. 32-150, November 1, 1961.
4. Space Materials Handbook, Edited by C. G. Goetzal and J. B. Singletary, Lockheed Missiles & Space Company, January 1962.
5. Computation of Spherical-Mirror Systems by Means of Finite-Difference Equations, Louis P. Raitiere, Journal of the Optical Society of America, Vol. 42, No. 12, pp. 960-965, December 1962.
6. Stellar and Planetary Observations at 10 Microns, by B. C. Murray and R. L. Wildey, California Institute of Technology, Pasadena, California, September 21, 1962, Submitted as a note to the Astrophysical Journal.